ICENS 10TH INTERNATIONAL CONFERENCE ON ENGINEERING AND NATURAL SCIENCE
October 02-06 2024 Sarajevo (Hybrid Event)

FLOWER BIOLOGY AND BREEDING SYSTEM OF GLYCYRRHIZA ICONICA HUB.-MOR. (FABACEAE)

Burcu Yilmaz Citak[a*], Betül Kabalcı[a]

[a]University of Selçuk

*burcuyilmaz@selcuk.edu.tr

Abstract:

Natural selection, mediated by pollinators, has led to the evolution of a significant diversity of floral adaptations and reproductive strategies in flowering plants. Together with post-pollination processes like incompatibility systems, the structure and operation of sexual units dictate patterns of pollen reception and dispersal, which in turn dictate the reproductive fitness of plants. Because of their small populations and limited ranges, rare and endemic species place a premium on reproductive biology. Glycyrrhiza iconica is an endemic species lives in a small habitat growing aid of stolones with conservation interest for which little information is available. The goal of this research was to examine the flower biology and breeding system of G. iconica and evaluate the effects of herbivory, pollination services, and reproductive traits on this species' ability to reproduce. Only known one natural population were selected to study flower lifespan, floral rewards and sexual functioning and to determine the reproductive system, pollen limitation and herbivory of sexual structures were quantified. G. iconica produces brief-lived, nectar-free flowers in inflorescences that have multiple blooms open at once. Despite the fact that stigmatic receptivity and pollen germinability peaked at the same time, the flowers are protandrous. Pollination experiments demonstrated the self-compatibility and potential for spontaneous selfing of G. iconica. Additionally, pollen limitation was noted on both a quantitative and qualitative level. Eventually, it was discovered that pesticides, which severely harmed the sexual structures, also had an impact on the success of reproduction. The implications of the acquired findings for the dynamics of populations of G. iconica are examined.

Keywords: Pollen limitation, Protandry, Leguminosae, liquorice

ICENS 10TH INTERNATIONAL CONFERENCE ON ENGINEERING AND NATURAL SCIENCE
October 02-06 2024 Sarajevo (Hybrid Event)

FLOW DISTRIBUTION AT LATERAL DIVERSIONS

Firat Gumgum[a*]

[a]Dicle University

*firatgumgum@dicle.edu.tr

Abstract:

Diversion channels are constructed to redirect water from its natural course for purposes such as irrigation, flood control, hydroelectric power generation, wastewater management, water supply for urban and industrial use. They must be carefully designed to ensure the efficient distribution of water resources and sediment. The flow distribution at the bifurcation zone constitutes the major problem of the flow division. Numerous researchers contributed to the phenomenon by studying it experimentally and/or numerically and obtained statistical relationships to estimate the flow distribution at the junction. This abstract summarizes the earlier results of a numerical campaign that aims to obtain discharge distribution curves at lateral diversions with various angles and channel width ratios. The lengths of the main channel extension and the diversion channel were 2.6 m and the upstream length of the main channel was 2 m. Both channels were 0.30 m wide and controlled by weirs of the same height downstream. The diversion angles 30, 45, 60, 75 and 90° were tested. The model was validated with the experimental velocity field and discharge data obtained from the literature. The change in the diversion angles does not influence the main channel upstream flow parameters. The flow depths slightly increased, and Froude numbers significantly decreased in the main channel extension. The diversion angle did not play a crucial role under the tested flow parameters, i.e., the discharge of 4 L/s, flow depth of 0.048 m and Froude number of 0.40 at the main channel upstream. The flow parameters at the diversion channel downstream were in the order of those in the main channel extension. The amount of the diverted discharge increased with the decrease in the diversion angle, as expected.

Keywords: open channel diversions, discharge distribution, lateral intakes

ICENS 10TH INTERNATIONAL CONFERENCE ON ENGINEERING AND NATURAL SCIENCE
October 02-06 2024 Sarajevo (Hybrid Event)

NOVEL LEATHER PRODUCTION SYSTEM: VACUUM OPERATED DRUM FOR CHROMIUM TANNING PROCESS

Ersin Önem[a*], Ali Yorgancioglu[a], Behzat Oral Bitlisli[a], Onur Yilmaz[a], Ugur Cavdar[b], Yalcin Yilmaz[a]

[a] Ege University
[b] Izmir Demokrasi University

*ersin.onem@ege.edu.tr

Abstract:

During leather production based on chemical modification of collagen protein, high volumes of water and various chemicals are used. During production, high volumes and pollution loads of wastewater are released. Therefore, converting raw skins into high value-added products with the least possible use of water and chemicals is of great importance for the protection of natural resources and the environment for sustainability of leather industry.
Chemical modification processes in leather production are carried out in process tanks called ""drums"" under normal atmospheric pressure and accompanied by mechanical effect. With the help of high volume of water and mechanical effect contained in these reaction vessels, the substances first penetrate into the skin section and then bind to the reactive groups of collagen protein. However, chemicals used in traditional systems carried out under normal atmospheric pressure have difficulty in penetrating the skin, uptake of chemicals is not complete and high volume of water is required as a carrier.
In our work to bring solutions to these problems; it is aimed to design special production recipes under low atmospheric pressure by creating a controlled vacuum in leather production cabinet, to reduce the rates of water and chemicals and to shorten the processing times, to determine the properties of finished leather and wastewater and to produce optimized recipe designs and products through optimization methods. The system is placed under controlled vacuum and aimed to open collagen fiber bundles faster and more effectively, thus to use low volumes of water and chemicals as carrier medium, to penetrate easier/faster the chemicals between the opened fiber bundles, and to significantly reduce the pollution load in wastes. Our study was carried out on the tanning process, important in terms of ecological, economic and engineering applications for leather production, and satisfactory results were obtained towards sustainable future.

Keywords: leather, vacuum, sustainable, eco-friendly

SUSTAINABLE DESIGNED LEATHER PRODUCTION RECIPES ACCORDING TO THE CHARACTERISTIC PROPERTIES OF MONGOLIAN SHEEPSKINS

Ersin Önem[a*], Ali Yorgancioglu[a], Udval Lodoi[b], Turmunkh Togmid[b], Behzat Oral Bitlisli[a], Huseyin Ata Karavana[a], Mehmet Mete Mutlu[a], Sugarsuren Enkhbaatar[b]

[a] Ege University
[b] Mongolian University of Science and Technology

*ersin.onem@ege.edu.tr

Abstract:

Mongolian sheepskins were targeted to create sustainable tanning recipes. Mongolian leather sector comprises factories involved in processing and exporting of untreated animal materials, leather and fur garments, and is one of the leading economic sectors in the country. The main problem is that although the country has traditional skills in leather goods manufacture and ample labour, skills for operating modern leather goods are lacking with very limited institutional support services. In order to remain internationally competitive in the long-run, these industries need to move toward production of more sophisticated products, higher added value, and quality levels conforming the international standards. Tanneries use and pollute large quantities of water, contaminate fertile soil, and tannery workers often suffer from diseases caused by chemicals. The lack of pollution control regulations may deprive tanneries of significant export opportunities and business partnerships with foreign companies due to consumer concerns to environmental issues. Turkish leather manufacturing sector is old, well-established industry with a technical infrastructure. According to the records and documents, Turkish leatherwork dates back to 2,400 years ago. Turkey, with the advantages of geographical location and the production of the accumulation of many years, have created the infrastructure and technologies to produce garment, fur and shoe leathers.

Our study aimed to well characterize Mongolia's rich natural resources (animal asset) in a correct way, to make it ready for leather production with high efficiency and to turn it into finished products with environmentally friendly systems. Mongolian sheepskins were produced according to the empirical ways in Mongolia and produced with the sustainable designed recipes. Before and after tanning operations, characteristic properties of the skins were put forward. Thus, quality and environmental comparisons between the procedures were emerged and discussed. Higher quality leathers and reduced waste pollution loads were obtained via sustainable ways.

Keywords: leather, sustainable production, recipe design, tanning

ICENS 10TH INTERNATIONAL CONFERENCE ON ENGINEERING AND NATURAL SCIENCE
October 02-06 2024 Sarajevo (Hybrid Event)

CO-EVAPORATION AND FLASH EVAPORATION TECHNIQUES PRODUCTION METHOD COMPARISON FOR SEMITRANSPARENT LEAD FREE MA3BI2I9 PEROVSKITE ABSORBER

Asuman Koçu[a*], Gökhan Yılmaz[a]

[a] Burdur Mehmet Akif Ersoy Üniversitesi

*asumankocu20@gmail.com

Abstract:

The rapid progress in the efficiency of solar cells, especially the increase in the efficiency of next generation perovskite solar cells (from ~3% to ~26%), has attracted the attention of scientists working in this field[1]. However, there are two main problems with high efficiency perovskite solar cells. The first one is the instability of the solar cells and the second one is the toxicity caused by lead (Pb) in the absorption layer[2-3]. Scientists are in search of elements that can replace Pb in perovskite absorption layers and increase stability. Therefore, instead of Pb, bismuth (Bi) was chosen for the best candidate. Scientists prefer to produce perovskite solar cells based on chemical solutions due to production costs and ease of applicability, but problems arise in the morphology of the thin films produced and in the structure due to the solvents used. The production of perovskite absorption layers with vacuum-based evaporation systems, enables the production of thin films with homogeneous and repeatable. In vacuum-based evaporation systems, compounds can be evaporated with more than one source. Instead, producing compounds in a common crucible by flash evaporation in a single step will prevent the problems that may arise from co-evaporation. In this study, thin films in the form of (CH3NH3)3Bi2I9 used as absorption layer in perovskite solar cells were manufactured by co-evaporation and flash evaporation. XRD, SEM and UV-Vis measurements were used for structural, morphological and optical analysis of the grown thin films. The flash evaporation method enables the use of semi-transparent MA3Bi2I9 solar cells in tandem and transparent cells. In addition, MA3Bi2I9 thin films produced by flash evaporation method have the potential to be used in electronic circuit elements requiring medium temperature such as diodes or field effect transistors due to the improved phase stability.

Keywords: perovskite absorber layer, co-evaporation, flash evaporation, degradation, instability

OPTIMIZING ACADEMIC PUBLICATIONS: AN ALTERNATIVE APPROACH TO JOURNAL MANAGEMENT AT THE UNIVERSITY OF TETOVO

Puhiza Iseni[a*], Suela Rushiti[a], Agon Memeti[a], Florinda Imeri[a]

[a]Univerisity of Tetovo

*puhiza.iseni@unite.edu.mk

Abstract:

The transition from traditional to electronic systems in academic publishing has revolutionized information management practices, particularly in developing countries. This shift has led to the widespread adoption of digital formats for scientific research journals, including emails, websites, and server-stored databases, thereby rendering traditional printed journals obsolete. In response, electronic journal management systems have emerged as essential tools for institutions and organizations, facilitating seamless data integration and management.

Motivated by this transformative trend, our study, titled “Optimizing Academic Publishing: A Case Study of Electronic Journal Management at the University of Tetovo”, investigates this phenomenon within the specific context of the University of Tetovo. Through comprehensive research, comparison and verification methods, our study aims to analyze the electronic journal management practices at the University of Tetovo. Employing a web-based system, we seek to evaluate software design, assess resource availability and develop a functional website. Leveraging ASP.NET Core technology in the C# programming language, coupled with Microsoft SQL Server Management for database storage and employing HTML, CSS, and JavaScript for design, our approach aims to optimize journal management processes.

Our study underscores the critical importance of electronic systems in modern academic publishing. By enabling efficient data creation, maintenance, and organization within institutions, these systems facilitate streamlined workflows, ultimately enhancing the scholarly publishing landscape.

Keywords: academic, journal, University of Tetovo, electronic journal management

ICENS 10TH INTERNATIONAL CONFERENCE ON ENGINEERING AND NATURAL SCIENCE
October 02-06 2024 Sarajevo (Hybrid Event)

ENHANCING CULINARY CREATIONS: A SERVICE-ORIENTED APPROACH TO RECIPE APP DEVELOPMENT

Puhiza Iseni[a*], Suela Rushiti[a], Agon Memeti[a], Florinda Imeri[a], Shkurte Luma-Osmani[a]

[a]Univerisity of Tetovo

*puhiza.iseni@unite.edu.mk

Abstract:

This paper outlines the development of a recipe app rooted in Service-Oriented Architecture (SOA) principles, aiming to meet the rising demand for digital culinary solutions. Motivated by the absence of a dedicated culinary app in our local community, we embarked on this innovative journey to enable users to seamlessly explore, create, and share culinary creations within a digital space. By integrating advanced frontend and backend technologies, our app offers scalability, adaptability, and personalized user interactions. Our platform bridges the gap between culinary enthusiasts and diverse culinary experiences, to revolutionize the culinary landscape. We aim to foster creativity, community engagement, and culinary exploration on a global scale. Future endeavors involve continuous improvements based on user feedback and technological advancements, enhancing user experiences, and fostering culinary innovation.

Keywords: Recipe app, Service-Oriented Architecture (SOA), Culinary exploration, Digital solutions, Culinary innovation, User satisfaction

ICENS 10TH INTERNATIONAL CONFERENCE ON ENGINEERING AND NATURAL SCIENCE
October 02-06 2024 Sarajevo (Hybrid Event)

CARBON DIOXIDE'S IMPACT ON TRI-CULTURED MICROALGAE GROWTH IN AIR-LIFT PHOTOBIOREACTOR

Ugur Tepe[a], Bahar Aslanbay Guler[a], Zeliha Demirel[a*], Esra Imamoglu[a]

[a] Ege University

*zelihademirel@gmail.com

Abstract:

Photosynthetic microorganisms such as microalgae and cyanobacteria, which inhabit freshwater, marine, soil ecosystems, and extremophile environments, synthesize organic chemicals through photosynthesis. These substances have recently attracted more attention due to their potential applications. To lower costs, save labor and space, and boost biomass yield, an alternate approach would be to use one PBR, two microalgae, and one cyanobacterium culture. This study examined the production of phycobiliproteins (phycoerythrin, phycocyanin, and allophycocyanin), astaxanthin, and total carotenoid concentration in the consortium of Chlorella vulgaris, Haematococcus pluvialis, and Arthrospira platensis. Throughout the nine-day batch culture, the growth conditions were maintained at 22 ± 2°C with the light intensity of 400 µE m−2 s−1 at the aeration rate of 1 L min-1 (air) and 1 L min-1 (air+1.5% carbon dioxide) in modified water (pH=8.5) medium in an air-lift photobioreactor (PBR). In the different air conditions, inoculation ratios (5:1:1) of two algae and cyanobacterium were carried out. After the batch production procedure was completed, the biomass productivity, total carotenoid, phycobiliprotein, and astaxanthin were measured. As a result, the total carotenoid content of the tri-cultivation was achieved the highest concentration of the air aeration. Phycobiliprotein and astaxanthin concentrations, however, were 19.203±0.432 mg g-1 and 2.878±0.015 mg g-1 at the aeration rate of 1 L min-1 containing carbon dioxide respectively.

Keywords: Microalgae, cyanobacterium, total carotenoid, phycobiliprotein, astaxanthin

ICENS 10TH INTERNATIONAL CONFERENCE ON ENGINEERING AND NATURAL SCIENCE
October 02-06 2024 Sarajevo (Hybrid Event)

MICROALGAE, CYANOBACTERIUM, TOTAL CAROTENOID, PHYCOBILIPROTEIN, ASTAXANTHIN

Yılmaz Yilmaz[a*], Serhat Demir[a], Ferhan Öztürk[b]

[a]Karadeniz Technical University
[b]CW-ENERGY

*yilmazyilmaz@ktu.edu.tr

Abstract:

Cold-formed steel (CFS) sections are increasingly used, but face buckling problems due to their thin sections. Investigation of this behaviour by experimental and numerical studies is difficult and time consuming. This study aims to predict the bearing capacity of CFS sections of different slenderness using advanced machine learning (ML) models. A detailed finite element model, including material nonlinearity and geometric imperfections, was used to perform 2240 finite element analyses and a dataset containing 2240 data points and nine features was generated. Five machine learning models - Support Vector Regression (SVR), Random Forest (RF), Multilayer Perceptron (MLP), Gradient Boosting Regressor (GBR) and Extreme Gradient Boosting (XGB) - were applied to predict the load bearing capacity. Cross-validation and hyperparameter tuning optimised the models. The results showed that all models were effective and the MLP model obtained the best predictions with an accuracy of ± 4.26 kN, which is less than 4% of the average load carrying capacity. Flange length and section thickness were found to have the most significant effect on the load bearing capacity.

Keywords: cold-formed steel, buckling, finite element analysis, machine learning

ICENS 10TH INTERNATIONAL CONFERENCE ON ENGINEERING AND NATURAL SCIENCE
October 02-06 2024 Sarajevo (Hybrid Event)

PROCESS SIMULATION OF 1,4-CYCLOHEXANEDIMETHANOL PRODUCTION FROM WASTE PETS

Berk Esin[a*], Gulhayat Nasun-Saygili[a]

[a]Istanbul Technical University

*esinbe@itu.edu.tr

Abstract:

Dramatically increasing polyethylene terephthalate (PET) usage due to their cheapness, durability, and lightweight, can cause environmental pollution, so the importance of recycling facilities is increasing. Tertiary recycling, one of the PET recycling methods, is the chemical process of converting used PETs into smaller molecules. This method is more expensive than secondary recycling, but it is more sustainable than the others. Solvolysis is the process of degrading PET into its monomers and/or oligomers using water or solvents like methanol, glycol, etc. Glycolysis, one of the tertiary recycling methods, is the process of breaking down into bis(2-hydroxyethyl) terephthalate (BHET) monomers and oligomers with glycols. Catalyzed glycolysis is the more common method to produce BHET monomer. Without any catalyst, the glycolysis reaction is so slow, and a complete production yield is not achievable. 1,4-cyclohexanedimethanol (CHDM) is one of the important chemicals used in various commercial polyesters. It is used for producing more chemical-resistant and durable polyesters. One of the ways to produce CHDM is the hydrogenation of BHET. The efficiency of CHDM production depends on temperature, pressure, and catalyst selection.

This study focuses on the design of a process for CHDM production via hydrogenation of BHET obtained from waste PET glycolysis via Aspen Plus simulation program. The main purpose of this project is to investigate the feasibility of the process that produces CHDM by recycling PET. The annual plant capacity is determined by recycling 7920 tons of PET corresponding to producing 4999 tons of product with 97.07% CHDM purity. For 10 years project life, the net present value (NPV), the discounted cash flow rate of return (DCFROR), and discounted payback period (DPBP) are found as $4.39 million, 16.14%, and 3.8 years, respectively. The overall proposed project is expected to be profitable and environmental friendly.

Keywords: Waste, PET, CHDM, Recycle, Simulation, Design

ICENS 10TH INTERNATIONAL CONFERENCE ON ENGINEERING AND NATURAL SCIENCE
October 02-06 2024 Sarajevo (Hybrid Event)

INVESTIGATION OF SEATBELT ANCHOR POINT LOCATION EFFECTS ON OVERALL STRENGTH OF PASSENGER SEATS DEVELOPED FOR HIGH COMMERCIAL VEHICLES UNDER UN ECE-R14 REGULATIONS

Çağla Doygun[a*]

[a]Assan Hanil Automotive and Trade Inc

*cagla.doygun@assanhanil.com.tr

Abstract:

With the increasing demands for more practical interior designs, automotive industry has evolved in so many ways to enhance the end user's accessibility. In recent years, most OEM's have switched to different seating configurations in terms of anchor point fix location, number of seatbelt points, folding, retracting and reclining capabilities. This research paper investigates the strength characteristics of two high commercial vehicle passenger seat designs under UN ECE-R14 loading conditions for M3 and N3 type of vehicles. The study compares a passenger seat with a fixed top anchor point to a foldable seat with an anchor point on the car body. It focuses on torsional moments on seat recliners, one-dimensional stresses, and axial and shear forces on floor beams. Using finite element analysis, the structural responses of each seat were simulated.

The passenger seat with a fixed anchor point on the seat itself offers versatility and space-saving benefits on the inside of car body and this extra door post area might be beneficial for the vehicle manufacturer for customization in terms of extra storage.

According to the study, the foldable seat showed enhanced stability in handling torsional moments due to its even stress distribution across the recliner mechanism from the left-hand side to the right. The foldable seat offered space-saving benefits on the free space of truck cabin but occupied a space on door post and faced higher shear forces, relying heavily on body's structural integrity.

Overall, the research highlights the trade-offs between flexibility and strength in seat design under regulatory conditions. The findings provide valuable insights for engineers in automotive, guiding future innovations to enhance safety and functionality in vehicle seating systems.

Keywords: Automotive Seating Systems, UN ECE Regulations, Structural Integrity, Truck Cabin Interior, HCV Interior Trim

ICENS 10TH INTERNATIONAL CONFERENCE ON ENGINEERING AND NATURAL SCIENCE
October 02-06 2024 Sarajevo (Hybrid Event)

THE EFFECTS OF USING GMT COMPOSITE MATERIAL IN THE HEADREST PART OF A COMMERCIAL VEHICLE SEAT

Esat Egemen Yüksel[a*], Muhammet Akinci[a]

[a]Assan Hanil Automotive and Trade Inc

*egemen.yuksel@assanhanil.com.tr

Abstract:

The automotive industry is constantly exploring new material solutions to achieve sustainability and light-weighting goals. Various optimization studies are carried out within the context of lightweight studies in the automotive industry. Apart from the optimization studies, the most preferred method for weight reduction in the automotive industry is material alteration.. In this context, using of glass mat reinforced thermoplastic (GMT) materials in vehicle seats is a noteworthy area. The primary benefit of using GMT in headrests is its lightweight nature. Compared to metal, GMT significantly decreases the overall weight of the seat assembly, contributing to improved fuel efficiency and lower emissions. Additionally, GMT provides excellent impact resistance and energy absorption properties, which are vital for passenger safety. These characteristics align well with the European Regulation ECE-R17, which sets standards for the safety and performance of headrests. In this study, metal headrest of a truck seat material, replaced with GMT headrest, and the weight of headrest has been reduced from 660gr to 490gr. ECE-R17 Frontal Impact, Headrestraint Moment and Headrestraint Impact analyses perform on the seat model to improve this change and compare the performance requirements with the metal part. As a result of these analyses, it was seen that the GMT model successfully completed the analyses requirements.

In conclusion, the conversion of seat headrests from metal to GMT represents a promising advancement in automotive design, offering a balance of safety, efficiency, and comfort. With careful compliance to ECE-R17 standards, this shift can significantly enhance both vehicle performance and passenger safety.

Keywords: Glass Mat Thermoplastic (GMT), CAE Analysis, Automotive

ICENS 10TH INTERNATIONAL CONFERENCE ON ENGINEERING AND NATURAL SCIENCE
October 02-06 2024 Sarajevo (Hybrid Event)

EFFECTS ON THE MECHANICAL AND CORROSION PROPERTIES OF LA, TI AND ZR ADDITION ON THE MODOFICATION OF SECONDARY A356 ALLOY

Simge Gençalp İrizalp[a*], Handenur Karaoğlu[a], Burçak Kardelen Köroğlu[b]

[a]Manisa Celal Bayar University
[b]CMS Jant ve Makina San A.Ş. ArGe Merkezi, Çiğli, İzmir

*simge.gencalp@cbu.edu.tr

Abstract:

The aim of this study is to achieve energy savings and reduce the carbon footprint by recycling the widely used A356 aluminum alloy in the casting industry. Aluminum is one of the industrial metals that significantly contributes to greenhouse gas emissions and is energy-intensive to produce from ore. Annually, 1.1 Gt (gigatons) of carbon dioxide is emitted from the primary production of aluminum, with each ton of metal generating approximately 12–16.5 tons of greenhouse gases. The substantial differences in greenhouse gas and energy consumption between primary and secondary synthesis have made aluminum alloys a crucial topic for sustainable metallurgy research, as they are a key pillar of the circular economy. This study focuses on the precipitation reactions caused by the addition of trace elements to address impurities related to scrap. Elements such as lanthanum (La), zirconium (Zr), and titanium (Ti) were added for modification, and their effects on the microstructure and mechanical properties were examined. The goal is to promote the design and production of secondary aluminum alloys with the highest possible scrap ratios by using lower-quality scrap and scrap types while modifying both alpha-aluminum grains and intermetallics with rare alloying elements. The chemical composition of the secondary A356 aluminum used in this study was modified with additions of 0.1% La, 0.05% La + 0.15% Ti, 0.05% La + 0.1% Zr, 0.3% La, 0.1% La + 0.2% Zr, and 0.1% La + 0.2% Ti. The microstructures of the developed alloys were examined using optical microscopy, the micro hardness of the phases was measured with a Vickers indenter, and tensile tests were conducted. Additionally, the materials were immersed in a corrosion solution containing NaCl and HCl, and corrosion results were evaluated through weight loss measurements. The study demonstrates that the addition of lanthanum and titanium together improved mechanical properties and refined the grain structure. However, these modifications did not improve corrosion resistance. These modifications, particularly the grain size reduction during casting, enhanced properties such as strength and ductility. The grain size reduction increased the surface area, potentially accelerating corrosion reactions. The increase in grain boundary area made the alloy more susceptible to oxidation and pitting corrosion, leading to a deterioration in corrosion behavior. Lanthanum and titanium formed secondary phases in the alloy, which tended to accumulate at

the grain boundaries, potentially creating active sites for corrosion cells and accelerating corrosion through the formation of micro-galvanic couples in these regions. The study continues to be developed with detailed characterization work in this direction.

Keywords: Aluminum-silicon alloy, Rare earth intermetallics, microstructure, mechanical properties, corrosion properties

ICENS 10TH INTERNATIONAL CONFERENCE ON ENGINEERING AND NATURAL SCIENCE
October 02-06 2024 Sarajevo (Hybrid Event)

PERFORMANCE ANALYSIS OF CORROSION SEGMENTATION WITH U-NET-BASED DEEP LEARNING MODELS

Yılmaz Yilmaz[a*], Safa Nayır[a]

[a]Karadeniz Technical University

*yilmazyilmaz@ktu.edu.tr

Abstract:

The automotive industry is constantly exploring new material solutions to achieve sustainability and light-weighting goals. Various optimization studies are carried out within the context of lightweight studies in the automotive industry. Apart from the optimization studies, the most preferred method for weight reduction in the automotive industry is material alteration.. In this context, using of glass mat reinforced thermoplastic (GMT) materials in vehicle seats is a noteworthy area. The primary benefit of using GMT in headrests is its lightweight nature. Compared to metal, GMT significantly decreases the overall weight of the seat assembly, contributing to improved fuel efficiency and lower emissions. Additionally, GMT provides excellent impact resistance and energy absorption properties, which are vital for passenger safety. These characteristics align well with the European Regulation ECE-R17, which sets standards for the safety and performance of headrests. In this study, metal headrest of a truck seat material, replaced with GMT headrest, and the weight of headrest has been reduced from 660gr to 490gr. ECE-R17 Frontal Impact, Headrestraint Moment and Headrestraint Impact analyses perform on the seat model to improve this change and compare the performance requirements with the metal part. As a result of these analyses, it was seen that the GMT model successfully completed the analyses requirements.
In conclusion, the conversion of seat headrests from metal to GMT represents a promising advancement in automotive design, offering a balance of safety, efficiency, and comfort. With careful compliance to ECE-R17 standards, this shift can significantly enhance both vehicle performance and passenger safety.

Keywords: corrosion, deep learning, semantic segmentation, U-Net, GUI

SYNTHESIS AND IN SILICO STUDIES OF NOVEL 1,2-DIARYLINDOLIZINE DERIVATIVES AS POTENT LIPOPROTEIN-ASSOCIATED PHOSPHOLIPASE A2 INHIBITORS

Nikita Kuznetsov[a*], Daniil Rusanov[b], Samet Alexander[a]

[a]N.D. Zelinsky Institute of Organic Chemistry
[b]City University of Hong Kong

*caltechbuddy@gmail.com

Abstract:

Lipoprotein-associated phospholipase A2 (Lp-PLA2) is a promising therapeutic target for the treatment of atherosclerosis [1], Alzheimer's disease, and diabetic macular edema [2]. Several therapeutics targeting Lp-PLA2, such as Darapladib [3], Rilapladib [4], and ATL-801 [5], have been explored in clinical trials. However, many of these studies were discontinued due to various challenges, including lack of efficacy, diverse side effects (e.g., diarrhea, liver function abnormalities), and high development costs.
Recently, it has been demonstrated that indole and indolizine derivatives exhibit significant inhibitory activity against Lp-PLA2 [6]. Consequently, developing novel Lp-PLA2 inhibitors incorporating these accessible moieties presents a promising approach to novel drug candidates with improved cost efficiency and structural feasibility.
In this study, we designed a small library of 16 1,2-diarylindolizines with various substituents and conducted in silico studies to investigate their noncovalent inhibition of Lp-PLA2, comparing them with a known inhibitor, the benzenesulfonamide derivative. The 1,2-diarylindolizines were synthesized using a green and robust protocol involving a [3 + 2] cycloaddition reaction between pyridinium ylides and α-nitrostilbenes. Structure-activity relationship (SAR) analysis using molecular docking tools identified three lead compounds with docking scores comparable to the benzenesulfonamide derivative, positioning them as potent Lp-PLA2 inhibitors.

Keywords: Indolizines, Lp-PLA2, atherosclerosis, Alzheimer's disease, [3 + 2] cycloaddition

ICENS 10TH INTERNATIONAL CONFERENCE ON ENGINEERING AND NATURAL SCIENCE
October 02-06 2024 Sarajevo (Hybrid Event)

HYDRAULIC REBOUND STOPPER AFFECT FOR PASSENGER CARS ON SHOCK ABSORBER

Semih Çalli[a*], Abdurrahım Arkan[a]

[a]Maysan Mando

*scalli@maysanmando.com

Abstract:

The vehicles driving on the road, road-related impacts affect the chassis. These impacts should not be transmitted to the cabin. The That absorbs these impacts between the chassis and cabin is the shock absorber. The shock absorber does this damping by converting motion energy into heat energy. During this energy conversion, the hydraulic flow inside the shock absorber is limited by piston valve. The valve damping force is adjustable according to vehicle type for the passive Shock Absorbers and occurs reaction forces during driving. However, the damping force must be variable in order to meet driving dynamics and driver expectations that change over time. Active shock absorbers are used to provide this variability. However, active shock absorbers are more costly and more difficult to implement. For this reason, different technologies such as hydraulic rebound stopper and hydraulic compression stopper are used in passive shock absorbers to ensure the variability of force. In this study, comparative numerical data were obtained by applying the hydraulic rebound stopper system to the shock absorbers used in small family cars and lower middle-class cars. In road conditions where the reaction force of the valve against the hydraulic fluid is not sufficient, the hydraulic rebound stopper is activated by creating extra force. With this extra force, disturbing vibrations to the vehicle and the driver are dampened, increasing driving safety and comfort.

Keywords: Shock absorber, Hydraulic rebound stopper, Hydraulic flow, Piston Valve

ICENS 10TH INTERNATIONAL CONFERENCE ON ENGINEERING AND NATURAL SCIENCE
October 02-06 2024 Sarajevo (Hybrid Event)

EFFECT OF GAS PRESSURE ON CAVITATION AT SHOCK ABSORBER USED PASSENGER CAR

Ramazan Ferik[a*], Semih Çallı[a]

[a]Maysan Mando

*ramazanfrk16@gmail.com

Abstract:

Shock absorber is one of the main parts of suspension system. Road bumps or vehicle vibrations accumulate energy in the spring. The shock absorber absorbs this energy. It is an important part to guarantee comfort and safety. connects to the axon at the bottom and to the upper tower at the top. Roughness from the road moves the wheel in a vertical direction. the upper part, movement is undesirable. This is important for comfort. The difference in speed between the upper and lower connection generates energy. The kinetic energy here is absorbed by the shock absorber by converting it into heat energy. Valve system inside the shock absorber provides this transformation. The valves limit the oil flow, generating heat energy. The oil flows through small channels in the valves. Cavitation may occur in these channels during rapid velocity changes. Cavitation is an undesirable situation in the shock absorber and when it occurs, the shock absorber cannot produce reaction force and cannot perform its function. Gas is added into the shock absorber to prevent the low pressure that occurs here. The high pressure created by the gas prevents cavitation that may occur in the oil. It can be seen from the graphs during the force test if cavitation occurs. In this study, cavitation under different gas pressures was investigated. These values were determined as 0, 1, 2, 3 and 4 bar. At the end of the test, the effect of gas pressure on cavitation was analysed by comparing the graphs. As a result, the optimum gas pressure was determined as 3 bar.

Keywords: Shock Absorber, Hydraulic Fluid, Pressure, Cavitation

ICENS 10TH INTERNATIONAL CONFERENCE ON ENGINEERING AND NATURAL SCIENCE
October 02-06 2024 Sarajevo (Hybrid Event)

NUMERICAL SIMULATION OF MASS TRANSFER MECHANISM OF STRATOSPHERIC SOLAR POWERED TELECOMMUNICATION BALLOONS

Öznur Kayhan[a*]

[a]Gebze Technical University

*okayhan@gtu.edu.tr

Abstract:

Stratospheric balloon systems, which have the ability to fly for long periods of time such as months or even a year in 20 km or higher layers of the atmosphere, have been an elusive goal to achieve in recent years. It is critical issue to solve the energy problem of stratospheric balloon to operate at target altitudes for extended durations. As an ideal alternative, solar power units are supplied to the balloons by mounting them on the balloon's envelope and classified as solar powered balloons. This method can cause the buoyant gas inside the balloon to overheat and pressurize, leading to further gas leakage from the balloon's polymeric material. In this investigation, the mass transfer model of a solar-powered zero-pressure balloon has been built up and simulated in Fortran via iterative techniques for the first time in literature. The simulation has been run for solar powered balloon flight under one of the cities of Turkey's real atmospheric conditions including solar radiation flux and wind velocities. The temperature variation of interior helium and mass transfer coefficient and diffusivity with thermal effect have been observed and compared with the unpowered balloon in summer atmospheric conditions. The maximum temperature, mass transfer coefficient and diffusivity of the interior helium for solar powered and unpowered balloon is obtained as 350.51 K, 1.54 x 10-2 m/s, 0.83x10-8 m/s2 and 310.49 K, 1.48x10-2 m/s, 0.78x10-8 m/s2 respectively. This results will be helpful to design the solar powered balloon systems to stay at higher altitudes for longer durations.

Keywords: Mass Transfer, Diffusion, Solar Energy, High Altitude, Zero Pressure Balloons

IS PLANT-BASED MILK A FUNCTIONAL BEVERAGE?

Rabia Serpil Günhan[a*]

[a]Konya Technical University

*rsgunhan@ktun.edu.tr

Abstract:

Increasing demand for healthy food alternatives has a significant impact on the beverage market. The search for functionality in beverages makes plant-based milks gain importance in the food industry in the world and in our country. Cows' milk is highly valued for its high content of nutritional components such as protein, minerals, fat and sugar. However, plant-based milks are an alternative for person who are lactose intolerant, worried about calories, or allergic to animal milk. They come in varieties such as soybean, oat, almond, coconut, hemp seed. Plant milks are beverages obtained by dissolving cereals, semi-cereals, legumes, oil seeds, nuts in water and then homogenizing the liquids. The level of components such as carbohydrate, protein and fat content of plant-based milks varies according to the processing technique used. The nutritional properties of different plant-based milks also vary greatly. Plant-based milks are especially preferred for vegan diets, while they are beverages with lower protein quality and sweetened with added sugar compared to cow's milk. In order to obtain a product with a nutritional content close to cow's milk, plant-based milks need to be enriched (e.g. by the addition of proteins, enzymes...). It can be a functional beverage alternative, especially when cow's milk needs to be replaced in the diet due to health problems. Processing methods based on consumer preferences and functional properties are very important in the development of plant-based milk. In this review, the importance of plant-based milk, nutritional profiles, processing steps, its place in the functional beverage market and differences with cow's milk are explained.

Keywords: Vegetable Milk, Cows' milk, Functional Beverage

ICENS 10TH INTERNATIONAL CONFERENCE ON ENGINEERING AND NATURAL SCIENCE
October 02-06 2024 Sarajevo (Hybrid Event)

THE IMPORTANCE OF SUMAC SOUR

Rabia Serpil Günhan[a*]

[a]**Konya Technical University**

*rsgunhan@ktun.edu.tr

Abstract:

In the course of healthy life, topics such as the type of foods we consume, their preparation, processing and how we should consume them has gained importance. One of the functional products with increasing importance and awareness is sumac sour. Sumac sour is obtained from sumac fruit containing phenolic compounds, flavonoids, organic acids, tannins, essential oil, anthocyanins and their derivatives. Sumac plant is used in food, pharmaceutical and dye industries due to its bioactive compounds and various phytochemical components such as phenolic compounds. It has high medicinal and nutritional value. It has bioactivities such as antifibrogenic, antifungal, anti-inflammatory, antimicrobial, antimutagenic, antioxidant, antitumorigenic, antiviral, cytotoxic and hypoglycemic. Sumac sour is produced in the traditional method by soaking the sumac (Rhus coriaria) fruit in water, straining the fruit and concentrated the extract in the sun. It is an aqueous extract of sumac fruits. Sumac sour is used to add a sweet/sour flavor to various dishes and salads. Beyond flavoring, it has a strong antioxidant and antimicrobial effect, which allows it to be used as a natural preservative to extend the shelf life of foods. The use of natural preservatives against synthetic preservatives ensures healthy production and consumption. The aim of this review is to emphasize the importance of sumac syrup and to provide awareness to our nutrition and the innovative change and development of the food industry.

Keywords: Sumac, Sumac sour, Functional Food

ICENS 10TH INTERNATIONAL CONFERENCE ON ENGINEERING AND NATURAL SCIENCE
October 02-06 2024 Sarajevo (Hybrid Event)

INVESTIGATION OF THE EFFECTS OF DIFFERENT RETANNING AGENTS USED IN SPLIT SUEDE PRODUCTION ON PHYSICAL AND SURFACE PROPERTIES OF LEATHER

Cengizhan Demir[a*], Ersin Önem[a]

[a]Ege University

*ersin.onem@hotmail.com

Abstract:

Retanning agents are among the most important production inputs used in determining the touch properties of leather products and giving them characteristic features. In addition to giving the leather properties such as fullness and tightness, they play a role in the appearance of suitable surface touch/velvet effects to be obtained for the production of split suede leathers.
In the study, different retanning agents were used in the retanning stage of leather production and their various effects on suede leathers were investigated. The main objective was to improve the surface properties, appearance and touch of suede leathers.
The different retanning agents used in production recipes are as follows:
- Aluminum sulphate
- Phenolic syntan
- White syntan with bleaching properties
- Sodium aluminum silicate
- Zeolite

Among the results obtained, aluminum sulfate provided optimum results that can be preferred for suede leathers due to its feature of being a cheap retanning agent that is frequently used in the industry. Consistent and repeatable results in suede leathers will enable the production of aesthetically pleasing split suede products. This will translate into significant potential to increase customer and consumer orientation and increase market share for suede leather.

Keywords: Leather, suede, split hide, surface properties

ICENS 10TH INTERNATIONAL CONFERENCE ON ENGINEERING AND NATURAL SCIENCE
October 02-06 2024 Sarajevo (Hybrid Event)

INVESTIGATION OF THE EFFECTS OF DIFFERENT VEGETABLE TANNIN COMBINATIONS ON PHYSICAL PROPERTIES OF LEATHER

Emre Başaran[a*], Ali Yorgancioglu[a]

[a]Ege University

*aliyorgancoglu@hotmail.com

Abstract:

Vegetable tannins have been used in leather processing since Neolithic times and are an important alternative for chrome-free and metal-free leather production. These natural substances play a critical role in imparting various properties to leather. In particular, they contribute to the natural appearance, fullness and tightness of the leather. However, at the same time, the specific color tone of the grain is transferred to the leather. This poses major problems in industrial production, especially for businesses working in pastel and light tones.

A tannin or combination of tannins, even when used at the same concentration, can produce different skin colors depending on the amount of consumption and other factors. This is further complicated by the use of different combinations of vegetable tannins in industrial production. In addition, it is stated that in vegetal production enterprises, unexpected dark shades are obtained in some leathers and changes in these shades can be seen in each batch production. Although different combinations are used to adjust the color tone, the desired fullness, hardness and toughness of the leather may vary. In addition, some vegetable tanned leathers may have problems such as discoloration and darkening due to waiting after production.

The focus of this work is an optimization study with combinations of vegetable tannins. This study aims to achieve stable and reproducible color properties, especially in light-toned leathers.

Mimosa, quebracho, tara and chestnut tannins were used as vegetable tannins in the study. Cattle skins were used as leather material. The most successful combination was found in the trials with mimosa and kebrako tannins. The stable and reproducible color characteristics and shrinkage temperature results obtained in the study for light toned leathers are satisfactory.

Keywords: Leather, vegetable tannins, heavy leather, color, shrinkage temperature

ICENS 10TH INTERNATIONAL CONFERENCE ON ENGINEERING AND NATURAL SCIENCE
October 02-06 2024 Sarajevo (Hybrid Event)

WIRE SELECTION FOR DISSIMILAR WELDING BETWEEN G24MN6+QT3 AND S355J2+N STEELS BY GMAW

Ali Akay[a*], Fatih Güven[a]

[a]Birikim Mühendislik ve Endüstriyel Yüklenim A.Ş.
[b]Hacettepe University

*fatihguven@hacettepe.edu.tr

Abstract:

In this study, the performance of two types of filler wires for the dissimilar welding of G24Mn6+QT3 cast steel and S355J2+N structural steel was investigated. The plates were joined with ER70S-6 and ER110S-G fillers by GMAW, which is widely used in the industry. The tensile strength of the welded joint, the impact toughness of the weld zone and the hardness values were investigated. In terms of tensile strength, both wires were successful and the welded joint was fractured from the base metal on the S355J2+N side. The yield strengths of were more than 400 MPa and the tensile strengths were more than 550 MPa for both filler types. When the toughness values of the heat-affected-zones (HAZs) were compared, no difference was observed. However, the weld seam toughness values were 33J and 108J on average for ER110S-G and ER70S-6 wires, respectively. ER70S-6 wire gave better results for toughness. Considering that they have sufficient tensile strength, ER70S-6 wire would be more suitable for joining these two metals.

Keywords: MAG, ER110S-G, ER70S-6, Tensile strength

ICENS 10TH INTERNATIONAL CONFERENCE ON ENGINEERING AND NATURAL SCIENCE
October 02-06 2024 Sarajevo (Hybrid Event)

FERTILIZATION ZONES GENERATION USING SATELLITE IMAGINARY

Štefan Horvat[a*], Damjan Strnad[a], Matej Brumen[a], Domen Mongus[a]

[a]University of Maribor

*stefan.horvat@um.si

Abstract:

One of the main goals of precision agriculture is to maximize crop yields, which requires the efficient utilization of fertilizers. This paper presents an automated procedure to generate a vector layer of zones that require different intensities of fertilization based on the value of the vegetation index obtained from Sentinel-2 imagery. After obtaining imagery, a histogram is created, where the number of bins determines the number of fertilization zone classes. Using the marching squares algorithm, the final vector layer is produced and exported to the GeoPackage format which can be utilized on modern agricultural equipment. This approach offers a scalable solution for the generation of the fertilization zones and was tested on terrain in conjunction with agricultural advisors. It represents an important step towards more sustainable farming practices.

Keywords: Fertilization, Precision agriculture, Prescription maps, Remote sensing

ICENS 10TH INTERNATIONAL CONFERENCE ON ENGINEERING AND NATURAL SCIENCE
October 02-06 2024 Sarajevo (Hybrid Event)

HUMAN IMPACT ON RIVER POLLUTION IN ADJARA: WATER QUALITY ASSESSMENT

Guram Darchidze[a*], Gela Kifiani[a]

[a]Georgian Technical Univercity

*darchidz1995@gmail.com

Abstract:

Human impact has extended to water resources, making the study of these resources and their sustainable use crucial for a country's development. Adjara, one of Georgia's most scenic and strategically important regions due to its location, rich biodiversity, and tourism potential, contains over 400 small and medium-sized rivers. Many of these rivers are significantly affected by human activities, both chemically and biologically, leading to pollution of the water.

The practical importance of this work lies in assessing the level of human-induced pollution through surface water quality monitoring, laboratory analyses, and river basin inspections in Adjara. Based on these findings, recommendations will be made to address existing pollution sources and prevent future contamination, ultimately benefiting both the local population and national interests. This research will also serve as a foundation for creating a database on the condition of rivers in Adjara.

The Autonomous Republic of Adjara was selected for this study, as the main pollution factors and sources in several rivers are being examined for the first time, and their causes identified. Sixteen independent rivers with distinct catchment areas were chosen for pollution analysis using laboratory methods.

This article highlights the research process, focusing on one of the selected rivers with a major watershed in the Adjara region.

Keywords: river, pollution, water source, E. coli, river contamination

ICENS 10TH INTERNATIONAL CONFERENCE ON ENGINEERING AND NATURAL SCIENCE
October 02-06 2024 Sarajevo (Hybrid Event)

DEVELOPMENT OF SMART TEST CASE GENERATION AND SELECTION TOOL

Eda Nur Ayan[a*], Ugur Yayan[a]

[a]Eskısehir Osmangazi Unıversıty

*edanurayan430@gmail.com

Abstract:

Bu çalışma, Meta'nın LLaMA (Large Language Model Meta AI) modelini kullanarak yazılım test süreçlerini otomatikleştirmek ve optimize etmek amacıyla AI tabanlı bir yazılım geliştirmeyi hedeflemektedir. Ana hedef, genellikle zaman alıcı, hataya açık ve yazılım geliştirme sürecinde gecikmelere ve yetersiz test kapsamına yol açan manuel testlerin verimsizliklerini ele almaktır. Test senaryolarının otomatik olarak üretilmesi ve en uygun olanlarının seçilmesi yoluyla bu araştırma, test kapsamını genişletmeyi, test prosedürlerini hızlandırmayı ve ilgili maliyetleri azaltmayı amaçlamaktadır.

Araştırma dört aşamalı bir metodoloji izlemektedir. İlk olarak, yazılım belirli bir programlama dilindeki verilen kaynak koda dayalı test senaryolarını otomatik olarak üretir. İkinci aşamada, üretilen senaryolar yazılım gereksinimlerine göre optimize edilir, böylece kapsamlı bir test stratejisi sağlanır. Üçüncü olarak, optimize edilmiş test senaryoları için otomatik test kodu üretilir. Son olarak, ön ve sonrası optimizasyon süreçleri karşılaştırılarak test süresi ve kapsamındaki iyileşmeler analiz edilir.

Ön bulgular, LLaMA modelinin kapsamlı dil işleme yeteneklerinin, geleneksel manuel yöntemlerden daha kapsamlı test senaryoları üretebildiğini göstermektedir. Örneğin, AI tarafından üretilen senaryolar, manuel olarak oluşturulanlara kıyasla %30 daha fazla test vakasını kapsamaktadır. Ayrıca, senaryo üretme süresi yaklaşık %50 oranında azalırken, kritik hataları tespit etme doğruluğu %20 oranında artmıştır. Bu bulgular, AI destekli test senaryo üretiminin ve optimizasyonunun kalite güvence prosedürlerinin verimliliğini ve etkinliğini önemli ölçüde artırabileceğini öne sürmektedir.

Sonuç olarak, bu çalışma, Meta'nın LLaMA modelinin test otomasyon sürecine entegrasyonunun daha güvenilir ve ölçeklenebilir yazılım projeleri sağladığını göstermektedir. Test senaryolarının otomatikleştirilmesi ve optimize edilmesi, yazılım testini daha verimli hale getirerek daha geniş bir potansiyel sorun yelpazesini ele alma yeteneğini geliştirmektedir.

Keywords: Artifical Intelligence, Test Scenario Generation, Optimization, LLaMA, Software Testing

DEVELOPMENT OF AI-BASED SOFTWARE FOR GENERATING AND SELECTING TEST SCENARIOS: UTILIZATION OF META'S LLAMA MODEL

Eda Nur Ayan[a*], Ugur Yayan[a]

[a]Eskısehir Osmangazi Unıversıty

*edanurayan430@gmail.com

Abstract:

This study aims to develop an AI-based software solution for automating and optimizing software testing processes using Meta's LLaMA (Large Language Model Meta AI) model. The main goal is to address the inefficiencies of manual testing, which is often time-consuming, error-prone, and leads to delays and inadequate test coverage in the software development process. By automatically generating and selecting the most suitable test scenarios, this research seeks to expand test coverage, accelerate testing procedures, and reduce associated costs.

The research follows a four-stage methodology. First, the software automatically generates test scenarios based on the given source code in a specific programming language. In the second stage, the generated scenarios are optimized according to software requirements, ensuring a comprehensive testing strategy. Thirdly, automated test code is produced for the optimized test scenarios. Finally, the pre- and post-optimization processes are compared to analyze improvements in test duration and coverage.

Preliminary findings indicate that the LLaMA model's extensive language processing capabilities allow for the generation of more comprehensive and faster test scenarios compared to manual testing processes. AI-generated test scenarios cover 35% more test cases than those from manual processes, and the scenario generation time has been reduced by 60%. Additionally, the accuracy in detecting critical errors with these scenarios has increased by 25%. These results suggest that AI-assisted test scenarios can significantly enhance efficiency and accuracy in quality assurance processes.

In conclusion, this study demonstrates that integrating Meta's LLaMA model into the test automation process provides more reliable and scalable software projects. Automating and optimizing test scenarios makes software testing more efficient, improving the ability to address a broader range of potential issues.

Keywords: Artifical Intelligence, Test Scenario Generation, Optimization, LLaMA, Software Testing

ICENS 10TH INTERNATIONAL CONFERENCE ON ENGINEERING AND NATURAL SCIENCE
October 02-06 2024 Sarajevo (Hybrid Event)

OPTIMIZATION OF A 33-BUS POWER DISTRIBUTION SYSTEM USING ARTIFICIAL HUMMINGBIRD ALGORITHM FOR POWER LOSS AND VOLTAGE STABILITY ENHANCEMENT

Nisa Nacar Çikan[a*]

[a]**Cukurova University**

*nacarnisa@gmail.com

Abstract:

This paper presents an optimization study on the 33-bus power distribution system using a reconfiguration technique to enhance system performance. The optimization process employs two objective functions: minimizing active power losses and improving voltage stability through the reduction of the voltage stability index. The Artificial Hummingbird Algorithm (AHA), a novel metaheuristic approach, is adopted due to its efficiency in handling complex optimization problems. The proposed methodology is applied to both single-objective and multi-objective scenarios to comprehensively evaluate the system's performance. Results demonstrate significant improvements in power loss reduction and voltage stability enhancement, underscoring the effectiveness of the AHA in optimizing reconfigured power distribution networks.

Keywords: Reconfiguration, Power Distribution Networks, Metaheuristic Algorithm, Power Loss Minimization

SIMULTANEOUS ALLOCATION, SIZING, AND POWER FACTOR OPTIMIZATION OF WIND TURBINES AND EV CHARGING STATIONS IN POWER DISTRIBUTION NETWORKS

Murat Cikan[a*]

[a]**Cukurova University**

*mcikan@cu.edu.tr

Abstract:

This study explores the application of the Runga-Kutta Algorithm (RKO), a cutting-edge metaheuristic search technique, for the simultaneous allocation, sizing, and power factor optimization of wind turbines in power distribution systems. The research also involves the concurrent allocation of three 5 MW electric vehicle (EV) charging stations, integrated alongside the wind turbine installations. The objective is to minimize power loss while ensuring the efficient integration of renewable energy sources and EV charging infrastructure. The proposed RKO-based approach is evaluated for its effectiveness in optimizing component placement and enhancing overall system performance under dynamic load conditions. Simulation results indicate that the RKO algorithm offers a robust and efficient method for reducing power loss, making it a promising tool for future energy distribution system optimization.

Keywords: Dg Allocation, Meta-heuristic Search Algorithm, Electric Vehicle (EV) Charging Stations, Runge-Kutta Algorithm

ICENS 10TH INTERNATIONAL CONFERENCE ON ENGINEERING AND NATURAL SCIENCE
October 02-06 2024 Sarajevo (Hybrid Event)

OPTIMIZATION OF PV, CAPACITOR BANK, AND EV CHARGING STATION ALLOCATION IN A 33-BUS POWER DISTRIBUTION SYSTEM USING THE SLIME MOULD ALGORITHM

Nisa Nacar Çikan[a*]

[a]**Cukurova University**

*nacarnisa@gmail.com

Abstract:

This study presents a comprehensive approach to the optimal allocation and sizing of photovoltaic (PV) systems and capacitor banks in a 33-bus power distribution system, focusing on enhancing system performance. Simultaneously, the allocation of PV systems, capacitor banks, and electric vehicle (EV) charging stations is addressed to optimize system efficiency. The primary objectives include minimizing active power losses and improving the voltage profile across the network. To solve this complex optimization problem, the Slime Mould Algorithm (SMA), a cutting-edge metaheuristic technique, is employed as an advanced tool for distributed generation (DG) allocation. SMA's robust search capability and adaptability make it well-suited for addressing the multi-objective nature of this study, delivering optimized results that balance system losses and voltage stability. The proposed method demonstrates significant potential for improving the efficiency and stability of modern power distribution networks.

Keywords: Electrical Vehicle Charging Stations, Slime Mode Algorithm, DG Allocation

ICENS 10TH INTERNATIONAL CONFERENCE ON ENGINEERING AND NATURAL SCIENCE
October 02-06 2024 Sarajevo (Hybrid Event)

MAXIMUM POWER POINT TRACKING (MPPT) IN PHOTOVOLTAIC SYSTEMS USING THE SLIME MOULD ALGORITHM UNDER UNIFORM AND PARTIAL SHADING CONDITIONS

Murat Cikan[a*]

[a]**Cukurova University**

*mcikan@cu.edu.tr

Abstract:

This study explores the application of the Slime Mould Algorithm (SMA), an advanced metaheuristic technique, for maximum power point tracking (MPPT) in photovoltaic (PV) systems. The focus is on a configuration involving three solar panels connected in both series and parallel arrangements, operating under uniform and partial shading conditions. Accurate detection of the maximum power point (MPP) is critical to improving the efficiency of PV systems, especially when subjected to varying irradiance levels. The proposed SMA-based MPPT method is evaluated for its effectiveness in handling the non-linear characteristics and power fluctuations inherent in partial shading. Comparative analysis is performed to assess its performance against traditional MPPT algorithms in terms of convergence speed, accuracy, and robustness. The results highlight the potential of the SMA to optimize energy extraction under diverse shading scenarios, offering a promising approach for enhancing PV system efficiency.

Keywords: MPPT, Partial Shading Condition, PV, Meta-heuristic serach algorithm, Slime Mould Algorithm

ICENS 10TH INTERNATIONAL CONFERENCE ON ENGINEERING AND NATURAL SCIENCE
October 02-06 2024 Sarajevo (Hybrid Event)

PERFORMANCE OF SUSTAINABLE SELF-COMPACTING MORTAR INCLUDING VARIOUS TYPES OF MINERAL ADDITIONS

Boukhelkhal Aboubakeur[a*], Muhammet Akinci[a]

[a]University of Laghouat

*a.boukhelkhal@lagh-univ.dz

Abstract:

This experimental work aims to produce a sustainable self-compacting mortar (SCM) by replacing a proportion of ordinary Portland cement with silica fume (SF), natural pozzolana (PZ) and calcareous tuff (CT). Mixtures including various percentages of SF (5%), PZ (5 and 15%) and CT (10 and 20%) were prepared and tested. Two tests were realized slump flow and V-funnel time at fresh state. Compressive strength and ultrasonic pulse velocity were performed at 3, 28 and 56 days.
The results showed that the addition of SF slightly increases the fluidity SCM. Similar effect was observed in mixture including 5% of PZ but increasing the substitution level of PZ improved the fluidity of SCM. calcareous tuff has a negative effect on the fluidity of SCM. Regarding the results of compressive strength at 3, 28 and 56 days, in general the use of mineral additions was found to reduce the compressive strength at 3 days but the rate of reduction decreases at 28 days, while at 90 days mixtures made with SF and PZ exhibited similar higher compressive strength as compared to reference mixture which may due to the pozzolanic reactivity of these materials. The values of ultrasonic pulse velocity showed that all mixtures have a good quality, exception for mixture with 20 TC in which the mortar quality is relatively lower.

Keywords: Self-compacting mortar, sustainable mortar, mineral additions, strength, performance

EFFECT OF LOCAL NATURAL POZZOLANA ON FLUIDITY AND COMPRESSIVE STRENGTH OF SELF-COMPACTING CONCRETE

Rima Hibat Errahmane Cherifi[a*], Boukhelkhal Aboubakeur[b], Mohamed Omrane[a]

[a]University of Djelfa
[b]University of Laghouat

*a.boukhelkhal@lagh-univ.dz

Abstract:

By offering outstanding workability and excellent performance without the need for vibration, the invention of self-compacting concrete (SCC) has revolutionized modern constructions. However, its disadvantages are the significant dependency on cement and the greater expense and environmental impact compared to traditional concrete. Self-compacting concrete (SCC) usually necessitates a greater amount of cement than traditional concrete in order to achieve its desired flow characteristics and strength. One of the solutions to reduce the significant CO2 emissions from cement production is to develop alternative products that can replace cement with varying percentages. This paper will examine the practical uses of including pozzolana in self-compacting concrete, specifically highlighting its impact on the fluidity and compressive strength as key indicators of concrete quality at fresh and hardened state. Four mixtures have been tested, one as reference mixture and includes only Ordinary Portland cement (OPC), and three including different proportions of natural pozzolana (5, 10 and 15%). The fluidity was asseses by measuring the slump flow of fresh SCC. Compressive strength was measured at 28 days. Experimental results demonstrate that replacing part of cement by natural pozzolana caused a reduction in the fluidity of SCC but all resulted are accepted according to EFNARC recommendations. The use of natural pozzolana was found to slightly reduce the 28 days compressive strength. SCC mixture made with 15% of PZ has a compressive strength of 47 MPa, which is very close to that of control mixture (48 MPa).

Keywords: Natural pozzolana, self-compacting concrete, fluidity, compressive strength

Full-text articles

ICENS 10TH INTERNATIONAL CONFERENCE ON ENGINEERING AND NATURAL SCIENCE
October 02-06 2024 Sarajevo (Hybrid Event)

Flower Biology and Breeding System of Glycyrrhiza iconica Hub.& Mor. (Fabaceae)

Burcu Yılmaz Çıtak[1], Betül Kabalcı[2]

Abstract

A broad scale of floral adaptations and reproductive strategies have evolved in flowering plants as a consequence of natural selection acting through pollinators. Reproductive biology is significant to endemic and rare species because of their limited and small populations and restricted ranges. Glycyrrhiza iconica is an endemic species lives in a small habitat growing with stolones with conservation interest for which little information is available. The goal of this research was to examine the flower biology and breeding system of G. iconica and evaluate effects of herbivory, pollination services, and reproductive traits on this species' ability to reproduce. Only known one natural population were selected to study flower lifespan, floral rewards and sexual functioning and to determine the reproductive system, pollen limitation were quantified. G. iconica produces short-lived, nectar-free flowers in inflorescences with several blooms opening simultaneously. Flowers are protandrous even if stigmatic receptivity and pollen germinability peaked at the same time. Furthermore, a quantitative and qualitative analysis revealed pollen restriction. It was eventually shown that pesticides, which seriously damaged sexual structures, affected the success of reproduction. Examined are the consequences of the obtained results for the dynamics of G. iconica populations.

Keywords: Biodiversity, Endemic, Leguminosae, Liquorice, Protandrous

1. INTRODUCTION

Türkiye is one of the most important countries from the plant genetic diversity in point of the wild and cultivated form of crops. The genetic diversity is maintained ex situ or in situ [1]. Fabaceae family of flowering plants, which includes about 19,500 species divided into 751 genera, is regarded as the third largest flowering plant family. This large family has exhibited a high degree of species diversity and evolutionary success in a variety of global ecosystems, including stony grasslands, deserts, seashores, alpine and arctic meadows [2,3]. There are more than 30 species of *Glycyrrhiza* genus extensively spread worldwide. It was the most prescribed herb in Ancient Egyptian, Roman, Greek, East China, and the West from the Former Han era [4]. There are 6 species distributed in Türkiye (Table 1). One of the most preferred study materials is *G. glabra* has been the type in the *Glycyrrhiza* genus. According to other studies, the chromosome number of the *Glycyrrhiza* genus is stated as 2n = 16. Additionally, there is no comprehensive study on the systematics of this genus. *Glycyrrhiza iconica* which is distributed Konya/Sarayönü in a narrow area edge of fields and roadsides, is in the CR category according to the IUCN. The species is a perennial herbaceous plant with a creeping stem (Figure 1), is 20-30 cm tall and blooms in June-July [5]. Although flowering was observed in the plant, no fruits or seeds were observed. Pollination and fertilization are absolutely necessary for fruit formation. The first condition for these events to occur is that the flower organs develop flawlessly and produce abundant amounts of pollen with a high level of vitality [6]. When the pollen of the *G. iconica* species was examined in the previous study, it was determined that the pollen was 70% amorphous. As a result of palynological, morphological and molecular studies, it was determined that the species may be a hybrid species since it is closely related to *Glycyrrhiza aspera* and *Glycyrrhiza glabra* [5].

Tables 1: *Glycyrrhiza* species found in Türkiye

Species Name	Turkish Name	Endemism	IUCN Category
Glycyrrhiza aspera	Küçük meyan	-	DD
G. asymmetrica	Türk meyanı	Endemic	VU
G. echinata	Pıtırak meyanı	-	-

[1] *Corresponding author: Burcu Yılmaz Çıtak, Selçuk University, Faculty of Science, Department of Biology, 42130, Selçuklu/Konya, Türkiye.* burcuyilmaz@selcuk.edu.tr

[2] *Betül Kabalcı, Selçuk University, Institute of Science, Department of Biology, 42130, Selçuklu/Konya, Türkiye.* kabalcibetul4@gmail.com

G. flavescens *G. flavescens subsp. antalyensis* *G. flavescens subsp. flavescens*	Sarı meyan Antalya meyanı Sarı meyan	- Endemic Endemic	NT CR -
G. glabra	Meyan	-	-
G. iconica	Konya meyanı	Endemic	CR

Figure 1. The general views of *G. iconica* and stem of stolons

Our study aimed to evaluate the cause of the pollen abnormality of the *G. iconica* species within the scope of plant embryology, in term of the amount of pollen on the anther tissue, pollen and stigma viability, germination success of pollen grains possible defects in the tapetum tissue and presence or absence of potential pollinators in the environment that help pollination.

2. MATERIALS AND METHODS

2.1. Material Collection and Determination of the Amount of Pollen Grains

Buds and flowers of *G. iconica* were collected and buds were transferred to 70% alcohol and stored at+4ºC. Unopened buds were used for determination of amount of pollen in the anther. With aid of a clean needle buds were opened and the pollen grains poured onto the slide. Pollen grains were treated with %96 Ethanol and prepared glycerin-gelatin slides. Then pollen grains were counted one by one under a light microscope.

2.1.1. Pollen Viability Test

TTC solution was used for pollen viability test. TTC solution was added to the removed pollen. Pollen grains stained dark red were considered alive, those stained light pink were considered semi-alive and those not colored at all were counted as non-living (Figure 2).

Figure 2. (a) Alive (b) Semi-alive**, (c)** Non-living

2.2. Stigma Viability Test

Macherey-Nagel Peroxtesmo Ko peroxidase test paper were used for controlling the viability of stigmas. If a blue spot appears as a result of applying a little pressure to the stigma, it is understood that the stigma is active (Figure 3).

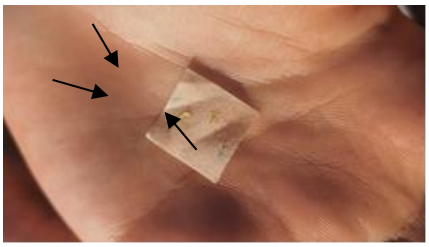

Figure 3. An active stigma on peroxidase test paper.

2.3. Pollen Germination Rate

To determine the pollen germination rate a medium containing 1% agar, 15% sucrose and 50 ppm boric acid was prepared. Pollen grains were planted in the prepared medium and incubated at 25ºC for 24 hours.

2.4. Examination of Tapetum Cell

Flower buds were dehydrated and were saturated with paraffin. Then 20 µm sections were taken and the sections were dyed safranin-fast green and best sections examined under a microscope.

3. RESULTS AND DISCUSSION

In present study, the reproductive biology of *G. iconica*, a local endemic species in Konya, was investigated. It was determined that the species was represented by 4000 individuals in its distribution area. Flowering specimens of plants were observed in 30 of these 4000 individuals and no fruit or seed formation was seen in all individuals. In our studies on reproductive biology, the pollen viability rate was determined to be 90%. However, stigma viability tests have shown that stigmas remain alive for 3-4 days. For this reason, we believe that the number of individuals of the species has decreased. Pollen and stigma viability rates were revealed for the first time in this study.

The total pollen produced by an anther was recorded by calculating the number of pollen obtained from each anther. Accordingly, it was determined that *G. iconica* produced pollen between 203-1067. Since there is no reproductive biology study on the *Glycyrrhiza* genus in the Fabaceae family, it is not possible to make a comparison. For this reason, it was reported that each anther produced 1247 pollen grains in the pollen counts made in the *A. argeus* species for the genus *Astragalus*, which is in the same family [7]. It was determined that this number was quite low in *G. iconica*. We believe that this situation limits the reproduction of the species.

As a result of the pollen germination experiments, no pollen tube development was observed under in vitro conditions. It is thought that this situation is parallel to the short vitality of the pollen grains or the insufficient pollen content.

Anthers contain pollen sacs, which gather pollen and provide nutrients for pollen grain development [8]. Defects in anthers can adversely affect pollen growth. The anther wall comprises the epidermis, endothecium, middle layer, and tapetum being the innermost layer. Tapetum plays unique roles in secreting callose and sporopollenin [9]. In general, the development of tapetal cells is initiated at floral stage 8/anther stage 4 and can be divided inti three stages, including tapetum differentiation, cell binucleation, and tapetum programmed cell death [10,11]. In *G. iconica*, the developmental stages of anther were determined no well-differentiated. And also, the endothecium layer were not in anther sections (Figure 4).

Identification of pollinators is important in pollination biology research, which is an important step in conservation biology studies. The possible pollinator of the individuals we examined could not be identified during field observations. The dense vegetation with plants such as *Centaurea solsitialis* subsp. *solsitialis*, *Consalida orientalis*, *Onobrychies sp.*, *Vicia faba* in the area where Konya licorice is distributed makes it very difficult for pollinators to land on the flowers of the plant. *Coccinella septempunctata* larvae and *Labidostomis longimana* species that land on the plant and take off have been seen.

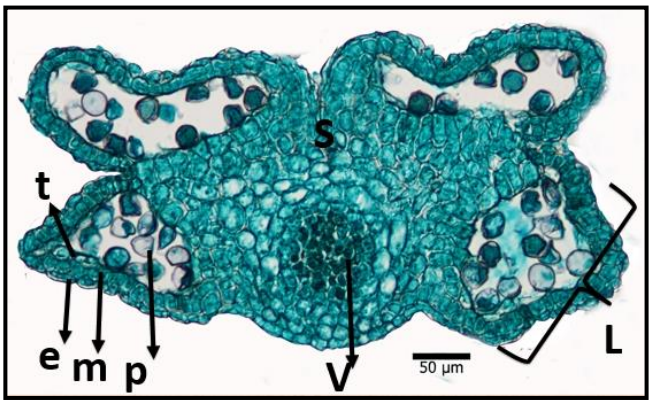

Figure 4. The cross section of anther of *G. iconica*. **L**: locus, **v**: vascular bundle, **t**: tapetum, **e**: epidermis, **m:** middle layer, **s**: septum, **p**: pollen grain.

4. CONCLUSION

It has been determined that the pollen and stigma vitality of *G. iconica* is strong, but the inability of the sexual organs to pollinate at compatible times reduces the chance of generative reproduction of the species. The fact that the number of insects visiting the plant is very low creates a limitation in terms of pollination occurring through insects. The disruption of the sequence of anther development stages has negative effects on pollen development of the species. This study should be supported by further genetic studies and pollinator observations.

ACKNOWLEDGEMENTS

The authors would like to thank a lot the foundation The Scientific And Technological Research Council Of Turkey (project number 1919B012311107) and Financial Unit of Selçuk University (project number 24701067) because of their financial supports.

REFERENCES

[1]. [1]. A. Tan, "Türkiye Geçit Bölgesi Genetik Çeşitliliğinin In Sıtu (Çiftçi Şartlarında) Muhafaza Olanakları", Anadolu Ege Tarımsal Araştırma Enstitüsü Dergisi, vol. 19(1), pp. 1-13, 2009.

[2]. [2]. B. Choi, H. Ohashi, "Generic criteria and an ifrageneric system for Hedysarum and related genera (Papilionoideae- Leguminosae)," Taxon vol. 52, pp. 567–576, 2003.

[3]. [3]. Legume Phylogeney Working Group, "Legume phylogeny and classification in the 21st century: progress, prospects and lessons for other species-rich clades", Taxon vol. 62(2), pp. 217–248, 2013.

[4]. [4]. S. Wahab, S. Annadurai, S.S. Abullais, G. Das, W. Ahmad, M.F. Ahmad, G. Kandasamy, R. Vasudevan, M.S. Ali, M. Amir, "Glycyrrhiza glabra (Licorice): A Comprehensive Review on Its Phytochemistry, Biological Activities", Clinical Evidence and Toxicology, Plants (Basel) vol. 10(12), pp. 2751, 2021.

[5]. [5]. Ö., Çetin, "Türkiye'de Yayılış Gösteren Glycyrrhiza L. (Fabaceae) Cinsinin Revizyonu" Doktora Tezi, Selçuk Üniversitesi, Fen Bilimleri Enstitisü, Konya. 2015.

[6]. [6]. S. Eti, "Bazı Meyve Tür ve Çeşitlerinde Değişik in vitro Testler Yardımıyla Çiçek Tozu Canlılık ve Çimlenme Yeteneklerinin Belirlenmesi", Çukurova Üniversitesi Ziraat Fakültesi Dergisi, vol. 6(1), pp. 69-80, 1991.

[7]. [7]. B. Atasagun, "Endemik Astragalus Argaeus Boiss. & Balansa, Astragalus stenosemioides D.F.Chamb & V.A. Matthwes, Onobrychis argaeae Boiss. & Balansa'nın Biyoteknolojisi ve Koruma Biyolojisi", Doktora Tezi, Erciyes Üniversitesi, Fen Bilimleri Enstitisü, Kayseri. 2018.
[8]. [8]. U. Zajączkowska, B. Denisow, B. Łotocka, A. Dołkin-Lewko, M. Rakoczy-Trojanowska, "Spikelet movements, anther extrusion and pollen production in wheat cultivars with contrasting tendencies to cleistogamy", BMC Plant Biology, vol. 21, pp. 1-15, 2021.
[9]. [9]. Z. Chang, M. Jin, W. Yan, H. Chen, S. Qiu, S. Fu, X. Tang, "The ATP-binding cassette (ABC) transporter OsABCG3 is essential for pollen development in rice", Rice, vol. 11, pp. 1-15, 2018.
[10]. [10]. P.M. Sanders, A.Q. Bui, K. Weterings, K.N. McIntire, Y.C. Hsu, P.Y. Lee, M.T. Truong, T.P. Beals, R.B. Goldberg, "Anther developmental defects in Arabidopsis thaliana male-sterile mutants", Sex. Plant Reprod., vol. 11, pp. 297–322, 1999.
[11]. [11]. R.J. Scott, M. Spielman, H.G. Dickinson, "Stamen Structure and Function", Plant Cell., vol. 16, pp. S46–S60, 2004.

ICENS 10TH INTERNATIONAL CONFERENCE ON ENGINEERING AND NATURAL SCIENCE
October 02-06 2024 Sarajevo (Hybrid Event)

Effect of the Diversion Angle at Lateral Diversions: A Numerical Study

***Firat Gumgum*[1]**

Abstract

Earlier results of the numerical work on the effect of the diversion angle at lateral diversion were introduced in this study. The scope of the study includes submerged flows in open channels with rigid-bed. The simulations were performed using the LES turbulence model in Flow-3D Hydro. The findings were presented and discussed briefly.

Keywords: division of flow; diversion angle; open channel bifurcation.

1. INTRODUCTION

Diversion channels are constructed to redirect water from its natural course for purposes such as irrigation, flood control, hydroelectric power generation, wastewater management, water supply for urban and industrial use etc. Design of these channels requires utmost attention to ensure the efficient distribution of water resources and sediment. The flow distribution at the bifurcation zone constitutes the major problem of the flow division. A wide range of experimental and numerical studies have contributed to the phenomenon by proposing empirical and theoretical models to estimate the flow distribution at the junction. These studies were mostly conducted in an equally wide, T-linked channel system to simplify the problem. Very few studies concern the angle of the diversion channel, θ, and the ratio of the width of the diversion channel, b, to the width of the main channel, B. To extend the scope of the studies concerning the effect of θ at lateral diversions, a numerical campaign was performed with using Flow-3D Hydro, and earlier results were presented in this study.

2. THE MODEL

The channel system was modelled according to the experimental device of [1]. Their experiments were conducted in a T-Linked channel system where the main channel (hereafter, MC) and the diversion channel (hereafter, DC) were 4.6 m and 2.6 m long, respectively. Both channels were 0.3 m wide, and the DC was connected to the MC at a distance of 2 m from the upstream end. The same dimensions were adopted in the model, but the length of the DC was chosen to be 3.6 m to ensure the development of uniform flow downstream of this channel. Two weir crests having a height of 0.025 cm were added at the end of both channels, as in the prototype. Different from the diversion angle ($\theta = 90°$) used in [1], $\theta = 30$, 45, 60 and 75° were also tested by keeping b the same. In this case, the width of the diversion entrance became $b' = b\sin\theta$.

The computational domain was bounded with a single uniform mesh block for each channel having the same length of 0.005 m in each direction. A fixed discharge of $Q_1 = 4$ L/s was introduced to the upstream boundary of the MC at a flow depth of $d_1 = 0.048$ m, in accordance with the work of [1]. The downstream boundaries of the channels were defined as “outlet pressure”, allowing the fluid to leave the domain. Overlapping boundaries of the mesh blocks, i.e., at the DC entrance, were automatically defined as “symmetry”, and other boundaries were set to “wall”. A simple sketch of the model is given in Figure 1.

[1] *Corresponding author: Dicle University, Department of Civil Engineering, 21280, Sur/Diyarbakir, Turkey.* firat.gumgum@dicle.edu.tr

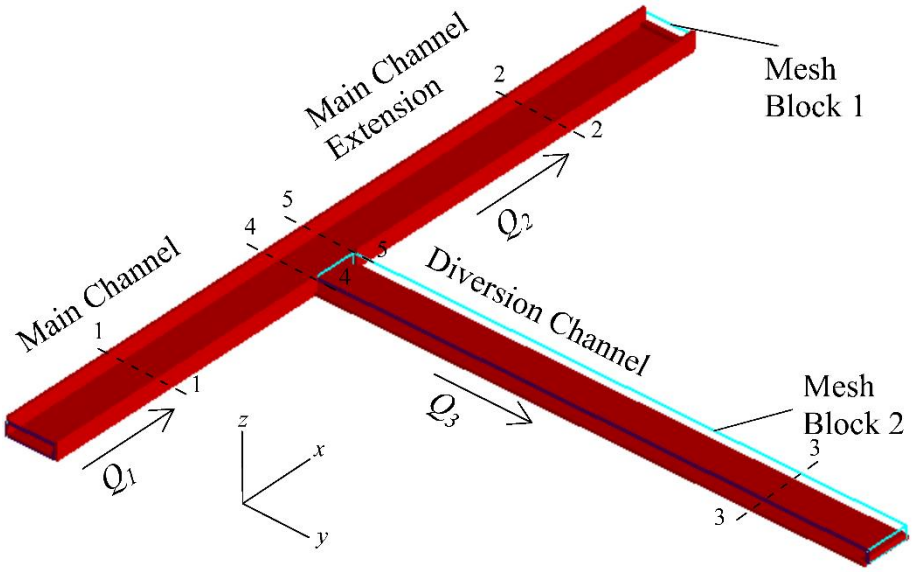

Figure 1. General view of the model and the control sections

As shown in Figure 1, the flow parameters were assessed at five different control sections: i) section 1-1 corresponds to the approach flow conditions, ii) section 2-2 and 3-3 corresponds to the downstream of the MC extension and DC, respectively, where the flow is free from bifurcation and tailwater effects and can be considered as one-dimensional, iii) sections 4-4 and 5-5, respectively, are at the "just" upstream and the "just" downstream corners of the DC. Accordingly, the flow parameters corresponding to these sections are indicated by the first digit of the section in subscript form, i.e., F_3 is the Froude number at section 3-3.

2.1. Governing Equations

Flow-3D Hydro software uses the VOF (Volume of Fluid) method and solves the three-dimensional continuity (Eq. 1) and Navier-Stokes equations (Eq. 2) simultaneously. Considering the complexity of three-dimensional flow structures in the bifurcation zone, LES turbulence model was chosen. Several studies [2]-[4] suggest that the LES turbulence model captures the three-dimensional properties of the flow more accurately than RANS models such as k-ω, k-ε or RNG, at the expense of simulation time.

$$\frac{\partial}{\partial x_i} u_i A_i \tag{1}$$

$$\frac{\partial u_i}{\partial t} + \frac{1}{V_f}\left(u_j A_j \frac{\partial u_i}{\partial x_j}\right) = -\frac{1}{\rho_f}\frac{\partial P}{\partial x_i} + G_i + f_i \tag{2}$$

Where u_i is the velocity component in direction i; A_i is the fractional area open to flow in direction i; V_f is the fractional volume open to the flow; ρ_f is the density of fluid; P is the pressure; G_i is the body accelerations; f_i is the viscous accelerations.

LES model requires a length scale (L) of the mesh grid to compute the eddy viscosity that represents the effects of turbulence too small to compute [5]:

$$L = \left(\delta_x \delta_y \delta_z\right)^{1/3} \tag{3}$$

where δ_x, δ_y and δ_z are the dimensions of the grid cells on x, y and z directions, respectively. The kinematic eddy viscosity (ν_T) of LES turbulence model is defined as:

$$\upsilon_T = {c_s}^2 \sqrt{2e_{ij}e_{ij}} \tag{4}$$

The Smagorinsky coefficient, c_s, was taken as 0.05. e_{ij}, the strain rate tensor, is computed from:

$$e_{ij} = \frac{1}{2}\left(\frac{\partial u_i}{\partial x_j} + \frac{\partial u_j}{\partial x_i}\right) \tag{5}$$

Finally, ν_T is incorporated into the dynamic viscosity (μ) to be used in the momentum equations:

$$\mu = \rho_f(\nu + \nu_T) \tag{6}$$

where and ν is the kinematic viscosity of the fluid.

2.2. Validation of the Model

The model was validated with velocity and discharge data from [1]. The velocities measured by [1] in the DC and the computed velocities are given in Figure 2a at y/b = 1.5 and z = 9 cm, in Figure 2b at y/b = 1.5 and z = 4 cm, in Figure 2c at y/b = 2.5 and z = 9 cm, at y/b = 2.5 and z = 4 cm, where (x, y, z) = (0, 0, 0) corresponds to the bottom of the upstream corner of the DC and v is the velocity component in y direction.

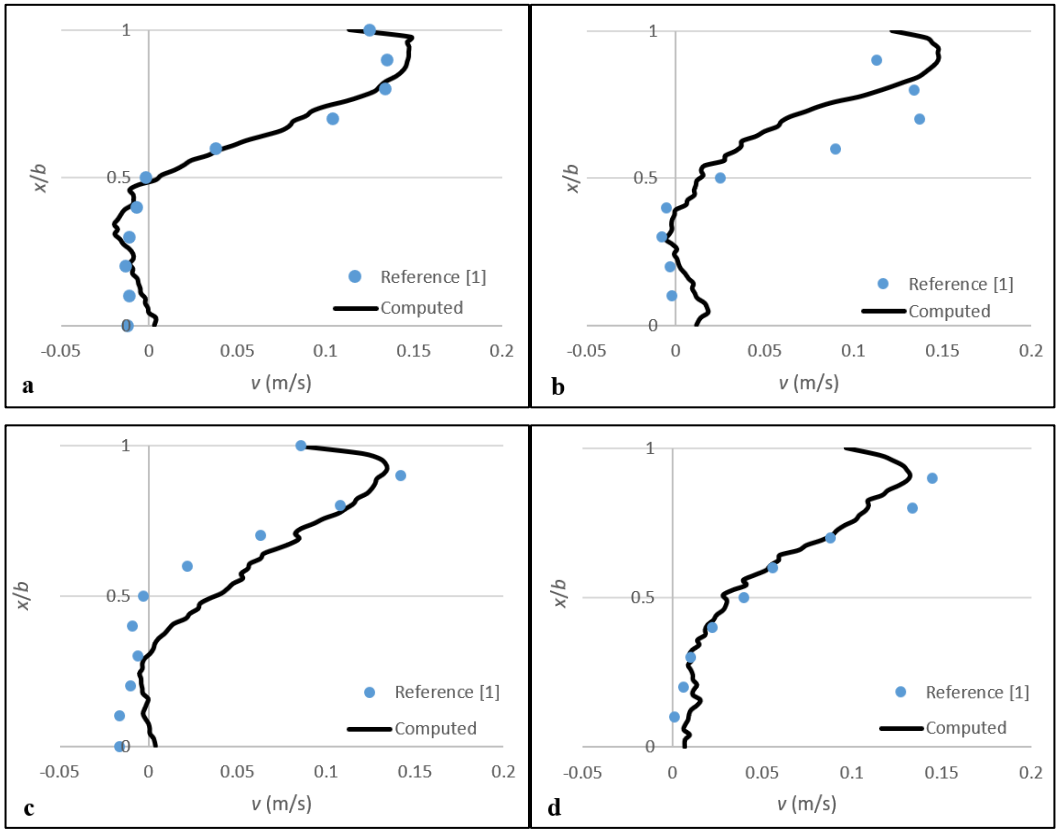

Figure 2. The velocities measured by [1] in the DC and the computed velocities at y/b = 1.5 and z = 9 cm, in Figure 2b at y/b = 1.5 and z = 4 cm, in Figure 2c at y/b = 2.5 and z = 9 cm, at y/b = 2.5 and z = 4 cm

The computed velocities in Figures 2a to 2d were obtained from the time-average of 100 seconds of data after the flow fully developed throughout the channel system. As can be seen from the figures, the computed velocities fairly agree with the measurements of [1]. Additionally, discharge ratio $Q_r = Q_3/Q_1$, upstream flow aspect ratio $A_r = d_1/b$ and upstream Froude number F_1 were measured by [1] as $Q_r = 0.5$, $A_r = 6.69$, $F_1 = 0.4$ and they were computed as $Q_r = 0.44$, $A_r = 6.25$, $F_1 = 0.4$. It can be concluded that the computations of the numerical model are reasonably accurate.

3. RESULTS AND DISCUSSIONS

The time-averaged flow depths are presented in Figure 3a to 3d for θ = 90, 75, 60 and 45°. The figures also include the boundaries of the recirculation zones (white line) at water surface where the flow velocity is zero. In any case, flow depths slightly decreased towards section 4-4. Between sections 4-4 and 5-5, in the inner half of the MC, flow depths further decreased for some distance then increased and reached the maximum at the downstream corner of the DC. This high pressure zone is also known as the stagnation zone [2]. The flow depths at this point were higher for higher values of θ. In the outer half of the MC, between the same sections, flow depths always increased and eventually became uniform in the MC extension. Flow depths further decreased in the DC upstream and slightly increased towards section 3-3. This increase became more pronounced as θ decreased. Hence, the uniform flow depth in the MC extension, d_2, was always the highest and the uniform flow depth in the DC, d_3, was always the lowest. This is coherent with the findings of [3] and [4]. It can also be seen from the figures that variation of θ did not visibly affect the flow depths in the MC upstream but d_2 slightly decreased with θ.

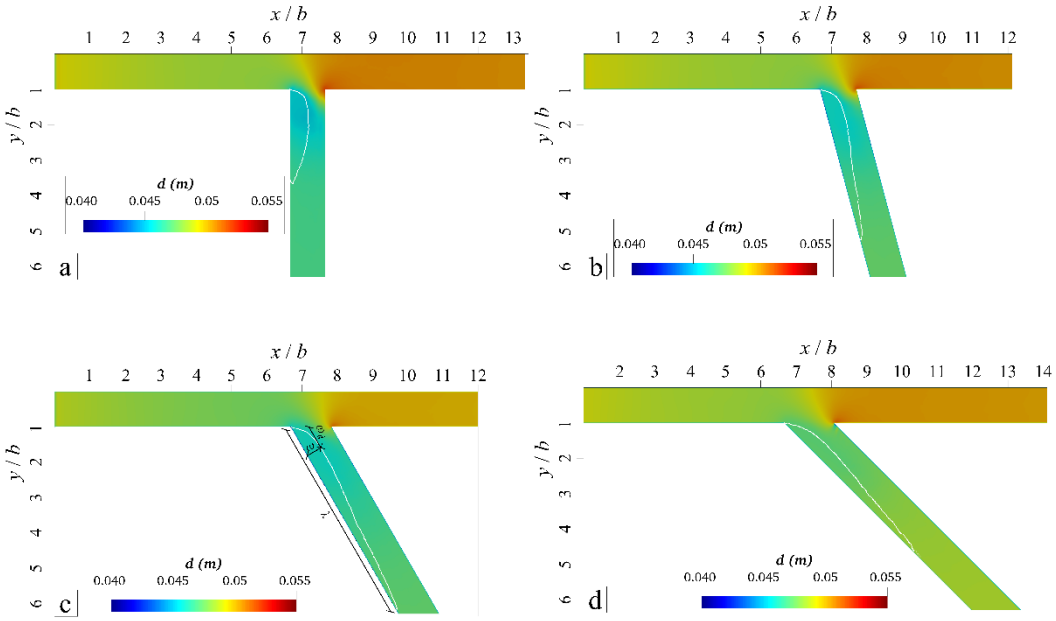

Figure 3. The time-averaged flow depths in the channel system for a) θ = 90°, b) θ = 75°, c) θ = 60° and d) θ = 45°.

The size of the recirculation zone (RZ) at water surface is defined with its maximum width, ω, and its length, λ (Figure 6c). These values were normalized with b, together with the distance from the maximum width of the RZ to the entrance of the DC, ω_d, and presented in Table 1 for θ = 90, 75, 60 and 45°.

Table 1. The normalized values of ω, λ and ω_d for θ = 90, 75, 60 and 45°.

θ (°)	ω/b	λ/b	ω_d/b
90	0.52	2.63	0.70
75	0.49	4.40	0.70
60	0.45	5.97	0.74
45	0.41	5.13	0.86

From Table 1, the maximum width of the RZ was greatest for θ = 90° and it decreased with θ, which is consistent with the findings of [5]. The length of the RZ significantly increased with θ until θ = 60° and then decreased by 14% for θ = 45°. The

greatest value of ω_d was registered for θ = 45° and it decreased with θ. [6] reported $\omega_d/b \approx 0.5$ for T-linked channels (θ = 90°) whereas it was found 0.7 in the present study.

The variation of Q_r values and Froude numbers in sections 1-1, 2-2, 3-3, 4-4 and 5-5 for θ = 90, 75, 60, 45 and 30° are plotted in Figure 4a and 4b. Q_r tends to decrease with θ but slightly in the simulation range, i.e., it decreased by ≈7% when θ = 90°, compared to θ = 30°. However, a small inconsistency appears for θ = 60°, the confirmation of which will be made in future. As it can be seen from Figure 2b, Froude number in section 4-4, F_4, was the greatest among those in other control sections, regardless of θ. Likewise, F_3 was registered to be the smallest. A weak trend of decrement in F_4 with respect to θ can be seen from the figure but Froude numbers in control sections changed insignificantly with θ. This change is expected to be more pronounced for higher Froude numbers.

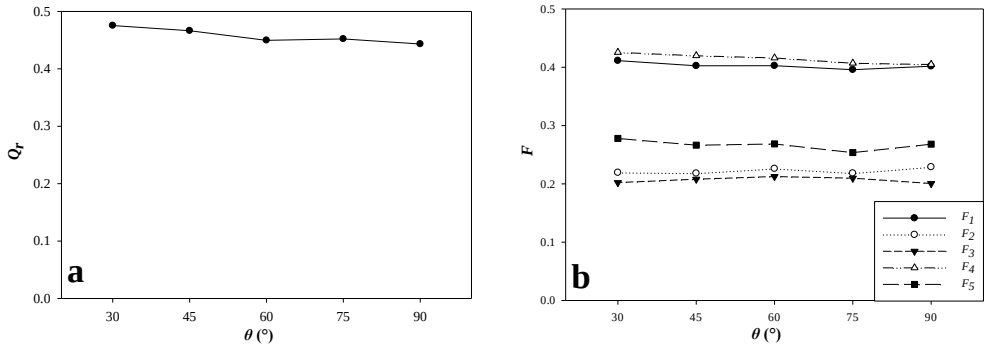

Figure 4. The variation of a) Qr values, b) Froude numbers in sections 1-1, 2-2, 3-3, 4-4 and 5-5 for θ = 90, 75, 60, 45 and 30°

The results of the simulation where θ = 90° were tested with the equations in the literature that estimate Q_r in case of submerged flows, namely, Eq. (7) of [6] and Eq. (8) of [7]:

$$\frac{F_2^{4/3}}{1+2F_2^2} = \frac{F_1^{4/3}Q_{r*}^{4/3}}{1+2F_1^2\left[\frac{1}{6}+\frac{5}{6}Q_{r*}+\frac{F_1^2}{40}(1-Q_{r*})\right]} \tag{7}$$

$$Q_r = \alpha ln\left[\frac{\beta\left[exp\left(\frac{1}{\alpha}\right)-1\right]\left[\frac{B_r F_3}{F_2}\right]}{\left[exp\left(\frac{1}{\alpha}\right)-1\right]+\beta\left[\frac{B_r F_3}{F_2}\right]}+1\right] \tag{8}$$

where $Q_{r*} = 1 - Q_r$, B_r is the ratio of the channel widths and it is equal to 1 here, and α and β are 1.012 and 0.941. Q_r value computed as 0.443 for θ = 90°, and it was calculated as 0.386 and 0.444 from the Eq. (7) and Eq. (8), respectively. Hence, Eq. (8) performed remarkably on estimating Q_r.

4. CONCLUSIONS

In this brief study, preliminary results of simulations of open channel bifurcations with different θ values are presented. Future work will include different flow conditions and channel width ratios for the same values of θ. The present findings are mostly consistent with the literature and some small inconsistencies will be analyzed further.

REFERENCES

[1]. Momplot, G. Lipeme Kouyi, E. Mignot, N. Rivière, and J. L. Bertrand-Krajewski, "Typology of the flow structures in dividing open channel flows," *J. of Hydraul. Res.*, vol. 55, no. 1, pp. 63-71, 2017.

[2]. W. Rodi, "Comparison of LES and RANS calculations of the flow around bluff bodies," *J. Wind Eng. Ind. Aerod.*, vol. 69-71, pp.55-75 July-Oct. 1997.

[3]. G. Kirkil, S.G. Constantinescu, and R. Ettema, "Coherent structures in the flow field around a circular cylinder with scour hole," *J. Hydraul. Eng.*, vol. 134, no. 5, pp. 572-587, May. 2008.
[4]. H. Li, S. Balachandar, and J. Sansalone, "Large-eddy simulation of flow turbulence in clarification systems," *Acta Mech.*, vol. 232, no. 4, pp. 1389-1412, Feb. 2021.
[5]. N. S. L. Rao and K. Sridharan, "Division of flow in open channels," *Water and Energy International*, vol. 24, no. 4, pp. 393-407, 1967.
a. S. Ramamurthy, D. Minh Tran, and L. B. Carballada, "Dividing flow in open channels," *J. Hydraul. Eng.*, vol. 116, no. 3, pp. 449-455, 1990.
[6]. Ibrahim, N. Riviere, I. Lebouteiller, and E. Mignot, "Discharge Distribution in Open-Channel T-Shape Bifurcations: Effect of a Reduced Side Branch Width," *J. Hydraul. Eng.*, vol. 148, no. 9, 04022015, 2022.

ICENS 10TH INTERNATIONAL CONFERENCE ON ENGINEERING AND NATURAL SCIENCE October 02-06 2024 Sarajevo (Hybrid Event)

OPTIMIZING ACADEMIC PUBLICATIONS: AN ALTERNATIVE APPROACH TO JOURNAL MANAGEMENT AT THE UNIVERSITY OF TETOVO

Puhiza Iseni[1], Suela Rushiti[2], Agon Memeti[3], Florinda Imeri[4]

Abstract

Information management techniques have been completely transformed by the shift in academic publication from traditional to electronic systems, especially in developing nations. Due to this change, traditional printed journals have become outdated as a result of the widespread adoption of digital forms for scientific research publications, including emails, websites, and server-stored databases. As a result, electronic journal management systems have become indispensable resources for establishments and businesses, enabling smooth data administration and integration.

Our paper, "Optimizing Academic Publishing: A Case Study of Electronic Journal Management at the University of Tetovo," was inspired by this revolutionary movement and looks at this phenomena in the unique setting of the University of Tetovo. Our study intends to assess the University of Tetovo's electronic journal management processes through thorough research, comparison, and verification methodologies. We aim to analyze software design, assess resource availability, and create a working website using a web-based system. Our method uses Microsoft SQL Server maintenance for database storage, ASP.NET Core technology in the C# programming language, HTML, CSS, and JavaScript for design, and all of this to optimize journal maintenance procedures.

Our research emphasizes how crucial electronic systems are to contemporary scholarly publishing. These technologies promote faster workflows, which in turn improve the landscape of scholarly publication by facilitating efficient data creation, management, and organization within institutions.

Keywords: academic; journal; University of Tetovo; electronic journal management

1. INTRODUCTION

The increased use of information and communication technologies (ICTs) has significantly changed the landscape of academic publishing. Electronic formats are progressively taking the place of traditional print publications as the main means of publishing research findings in science. The creation of electronic journal management systems, which are necessary for effectively organizing and distributing material inside academic institutions, has been made necessary by this change. [1]

Digital technology for information processing, storing, and transmission are now more accessible thanks to the internet, which has also promoted more conversations and the sharing of new scientific discoveries. [2] Nonetheless, managing scientific knowledge properly is made more difficult by the exponential rise in electronic publications as well as the ongoing development of electronic journals and learning materials. [1]

1 Corresponding author: Department of Computer Science, Faculty of Natural Sciences and Mathematics, University of Tetovo, North Macedonia, puhiza.iseni@unite.edu.mk

2 Department of Computer Science, Faculty of Natural Sciences and Mathematics, University of Tetovo, North Macedonia, s.rushiti222501@unite.edu.mk

3 Department of Computer Science, Faculty of Natural Sciences and Mathematics, University of Tetovo, North Macedonia, agon.memeti@unite.edu.mk

4 Department of Computer Science, Faculty of Natural Sciences and Mathematics, University of Tetovo, North Macedonia, florinda.imeri@unite.edu.mk

The sheer volume of electronic information and the cyclical nature of electronic publication lifecycles present challenges for conventional internet search services related to scientific information retrieval, even though traditional methods of accessing and storing electronic publications through full-text search interfaces are widely used. It is especially relevant to integrate electronic data, including scientific and instructional material, into a single information environment. [3]

Academic publications have traditionally been the main sources of scientific information, but with the development of the internet, publishers are now more frequently providing online access to academic research materials. This change brings up legal concerns about access assurance and the preservation of digital research resources. One strategy to guarantee access to the most recent scientific knowledge is to implement publishing capabilities internally within institutions. [3]

Our interest in investigating electronic journal management for the paper work was spurred by the abundance of scientific accomplishments and the growth of journals. [3] Considering that thorough implementation according to particular institutional constraints is necessary, we decided to concentrate on the "Scientific Journals of the University of Tetovo" for our research.

The goal is to carry out a thorough investigation into the University of Tetovo's electronic journal administration procedures, with an emphasis on the efficacy and efficiency of handling publications related to scientific research. It also aims to address the underuse of technologies in diverse situations and offer creative solutions. [4]

This paper aims to offer insights and possible solutions for efficiently integrating online technologies into journal administration by combining a review of the literature, an analysis of the University of Tetovo's current webpages, and a look at approaches employed in other institutions. [4]

2. THE CONCEPT OF ELECTRONIC SCIENTIFIC JOURNALS

Periodicals are publications that cover particular themes and are released on a regular basis, whether they are printed or digital. [2] Of the various themes they cover, news, politics, science, sports, fashion, cuisine, travel, and technology are just a few. Essays, images, graphics, and advertising are used to communicate the information. Time, Sports Illustrated, National Geographic, Vogue, The New Yorker, and Forbes are a few of the well-known magazines. [3]

Journals have seen substantial advancements and modifications over the ages. Among the first were magazines like "The Gentleman's Magazine" and "The Tatler," which were established in the eighteenth century and covered a wide range of topics, including politics and literature. [5] In the 19th century, journals rose to popularity and developed into vital forums for knowledge exchange. Around the turn of the 20th century, technological developments in printing and distribution enhanced journal accessibility and readers' overall reading experiences. [3]

In the age of digitization, journals have evolved into electronic versions that appear on websites, mobile applications, and PDFs with ease. Due to the unprecedented levels of accessibility and participation made possible by this development, readers' interactions with journals have undergone a complete transformation. [3]

Scientific research journals were founded during the scientific revolution in the 17th century, and since then, they have been vital to the advancement of knowledge and the creation of peer review guidelines. These periodicals have changed over the past few decades due to the emergence of electronic publishing, which has accelerated their circulation and increased their accessibility. However, there are still issues that need to be resolved, like the requirement for improved content design in addition to greater effect and visibility. [3]

Initiatives like the "Article of the Future" project combine multimedia components like audio and video recordings coupled with a reevaluation of article presentation in an attempt to solve these issues. Altimetry and identifiers like DOIs and ORCIDs have been shown to be useful tools for increasing the visibility and importance of an article. [5]

With the increasing popularity of tablets and smartphones, it is expected that scientific publications would be published more quickly, resulting in more imaginative reading experiences. In an ever-changing landscape, editors and publishers have to keep up with the latest developments while keeping a careful eye on the requirements of authors and consumers. [5]

Through electronic publishing, North Macedonia has a special chance to raise the impact, awareness, and readability of scientific research articles. Further research in this area may yield important insights into the advantages of electronic publishing for the scientific community in North Macedonia.

The initial challenge was locating "electronic scientific research journals," as the study's inclusion criteria could only be fulfilled by electronic papers. Although the literature employs a range of terms, it continues to concentrate on items that are exclusively accessible online. The phrase is now used to describe digital journals that are published online or on the World Wide Web, though it has other meanings as well. [5]

Scientific research papers in electronic format are becoming more and more prevalent; they cover a broad spectrum of subjects and fields and significantly contribute to the worldwide exchange of knowledge.

Prestigious online scientific research journals with a high impact factor and widespread recognition include Science, Nature, Cell, Proceedings of the National Academy of Sciences (PNAS), and The Lancet. By incorporating electronic scientific research journals into the traditional research system, this program aims to ensure that they are visible in library catalogs, cited by scholars, and acknowledged alongside print publications. Important objectives include figuring out how many electronic journals there are, assessing how many are indexed, and estimating how many citations each journal receives. [3]

3. ELECTRONIC DOCUMENT MANAGEMENT SYSTEM (EDMS)

Electronic document generation, storage, retrieval, distribution, and control are all made easier with the help of an EDMS. It is utilized by many different companies to enhance document management and access. By streamlining the processes of creating, storing, evaluating, and distributing articles for scholarly publications, EDMS improves user experience and overall efficiency. [6]

A planned EDMS at the University of Tetovo seeks to enhance the procedures involved in publishing scientific articles. It will make managing articles, coordinating editors, and author-user contact easier. The system will have automated functions, intuitive user interfaces, and compatibility with current standards such as DOI and ISSN. [6]

4. CHALLENGES OF THE JOURNAL MANAGEMENT SYSTEM ON GOOGLE SITE

The University of Tetovo faces a number of challenges when it comes to manually administering its scientific journals, much like many other academic institutions in the Balkan region. Among these difficulties are: [7]

- High Costs and Time Consumption: Both in print and electronic versions, processing and submitting contributions to scholarly publications require a large investment of time and money.
- Lack of Technological Infrastructure: Higher production and publishing expenses result from many universities' lack of the technology infrastructure required to manage and publish scholarly publications.
- Competition from Other periodicals: Without sufficient financial and personnel resources, the university may find it challenging to contend with the fierce competition it encounters from other academic institutions and foreign periodicals.
- High Quality Standards: To maintain neutrality and excellence, scholarly publications demand high-quality articles and stringent evaluation procedures, which take a significant amount of time and money.

As a result, there are several difficulties with the University of Tetova's manual journal administration system, which is made possible by Google Sites. The institution must make an investment in an appropriate technology to provide consolidated information access and streamline journal administration in order to get over these challenges.

5. REQUIREMENTS OF THE SYSTEM

System requirements are essential statements that describe the functions required to meet client expectations; they are essential to the success of the project. They cover both the hardware and software components necessary for system operation, and they are broadly applicable across different domains and specialized systems. [8]

5.1. Functional Requirements

Describe the specific qualities that a system, program, or application has to have in order to achieve its objectives. They are essential in defining the operations and features of the system. For example, without a feature that allows new tasks to be created, a project management tool is inadequate. The functional needs of the system establish its behaviors and capabilities. [8]

This platform offers the following functional requirements:

- Login interface: to access as an administrator to add and update data about journals and editors
- Journal interface: to find all information about the paper works, journal, editors, submission deadline for sending paper works.

5.2. Non-Functional Requirements

Although they have no direct bearing on how the system operates, they have a big impact on usability, security, performance, and availability. They set standards and operating guidelines meant to guarantee user pleasure. Non-functional requirements include, for example: [8]

- Availability: The platform must remain accessible 24/7, with backup measures in place to minimize service disruptions.
- Usability: The platform should possess an intuitive interface, easy navigation and comprehensive instructions to guide users effectively.
- Performance: To ensure continuous, high-speed service, the system must pass performance testing.
- Security: Strong authentication needs to be implemented by the platform.

6. SYSTEM ARCHITECTURE

Three layers make up the hierarchy of the system used to monitor scientific research journals, and each one serves a different function:

- Server Level: The infrastructure needed to host and enable user-to-underground database connections is provided by the server level, the lowest tier of the system architecture. This level includes all of the hardware and software components that are in charge of making sure the system is connected and functions properly. [6]
- Logical System Level: This important interface acts as a mediator between the data and the server. This layer, which was created using ASP.NET Core and the C# programming language, makes it simple for users to communicate with the database. This logical system level organizes SQL queries to obtain, edit, and maintain data stored in the database and effectively manages user-inputted data via HTML forms. Using object classes to create a well-structured table design guarantees efficient data management and organization, which boosts system efficiency and scalability. [9]
- Data Level: The core element of the system architecture, the data level is where a database management system (DBMS) organizes the storing, retrieving, and altering of data inside Microsoft SQL Server databases. Microsoft SQL Server Management is the official database management system (DBMS), providing a comprehensive toolbox and functionalities for creating, managing, and performing a variety of data operations. [6] Through the processes of downloading, storing, updating, and monitoring the data, these techniques guarantee the data's accessibility and integrity within the database environment. [9]

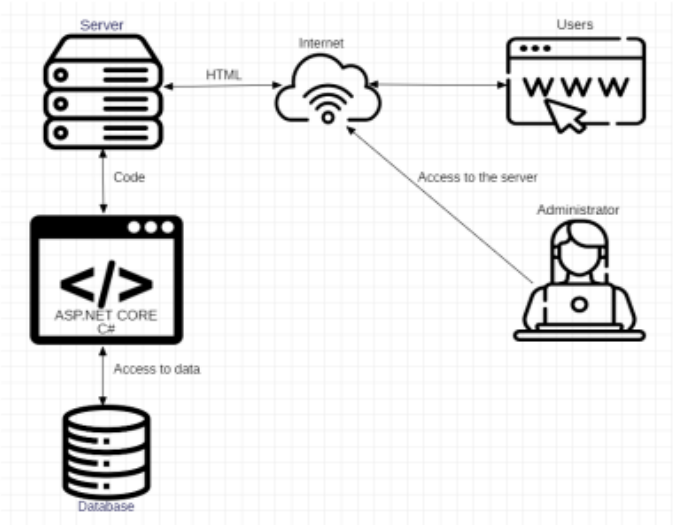

Figure 1. System Architecture

In our particular configuration, after HTML is generated, the user's browser receives the HTML content from the Apache web server. The web page is then rendered by the browser using a blend of CSS, Bootstrap, and JavaScript, which guarantees the best possible presentation and user experience. Figure 1 gives a clear visual representation of this system architecture and the content flow from server to client. [9]

To ensure strong connectivity and data integrity, the database schema keeps tables in a many-to-many relationship. Especially: [10]

- Every scientific journal in a faculty has a number of journal editors, years' worth of archived journals, and several journal indexes.
- A vast array of scientific publications can be found in archived periodicals, all of which add to the system's treasure of knowledge.
- Different scientific publications could be related to different research paths, and each research direction might contain more than one scientific paper.

The administrator of the institution is in charge of overseeing the thorough management of the entire system and is in charge of adding and editing journals, editors, indexes, and articles, among other things. The academic journal management system's efficient governance and coordination are ensured by this centralized oversight.[10] See Figure 2 for an illustration of the relationships and structure of the database. This diagram illustrates the connections between tables and the pre-existing relationships between them, providing insight into the complexities of the database schema. [10]

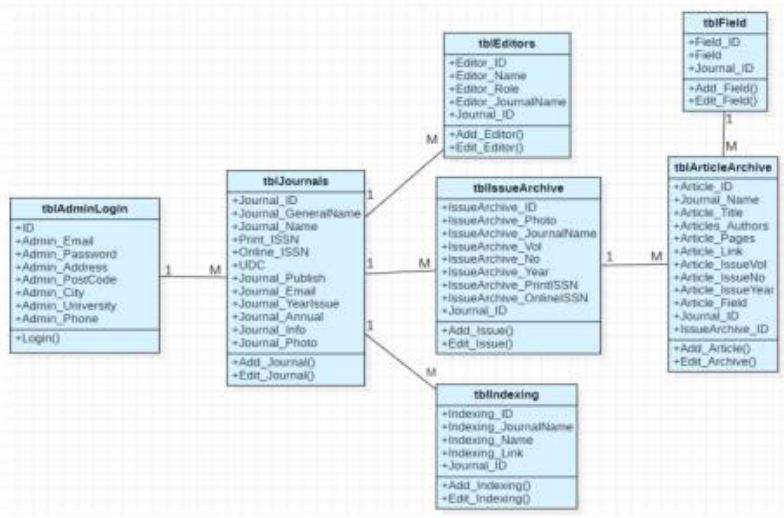

Figure 2. Class Model - Use Case

"JournalNet" is an electronic system for managing scholarly journals that consists of different functional modules for system creation, administration, and user interaction. [8]

- Administrator Management Module: This module helps with a number of administrative chores pertaining to academic journals. It is protected by the administrator's email address and password. Important characteristics consist of: [8]
  - Adding and updating academic journals: Journal titles, descriptions, and editor information are only a few of the crucial metadata that administrators can incorporate when adding new journals to the "JournalNet" system.
  - Managing papers: System administrators are in charge of adding and updating academic articles to the system's journals, along with managing author information and other pertinent details.
  - Editor management: Journal editors, including their additions and profile modifications, can be managed by administrators.

- Journal indexing: In order to improve searchability and organization inside the "JournalNet" system, administrators are in charge of indexing academic journals. They do this by allocating pertinent categories, tags, and keywords.

- System Developer Module: Provided to developers via database access, this backend module manages the system's coding and database. Important features include of: [8]
  - Managing entities associated to journals: Within the "JournalNet" system, developers have the ability to add, amend, and remove academic journals, editors, publications, and indexing data.
  - Administrator privileges: Within the "JournalNet" system, developers have the power to grant and oversee administrator access, allowing them to carry out their responsibilities.

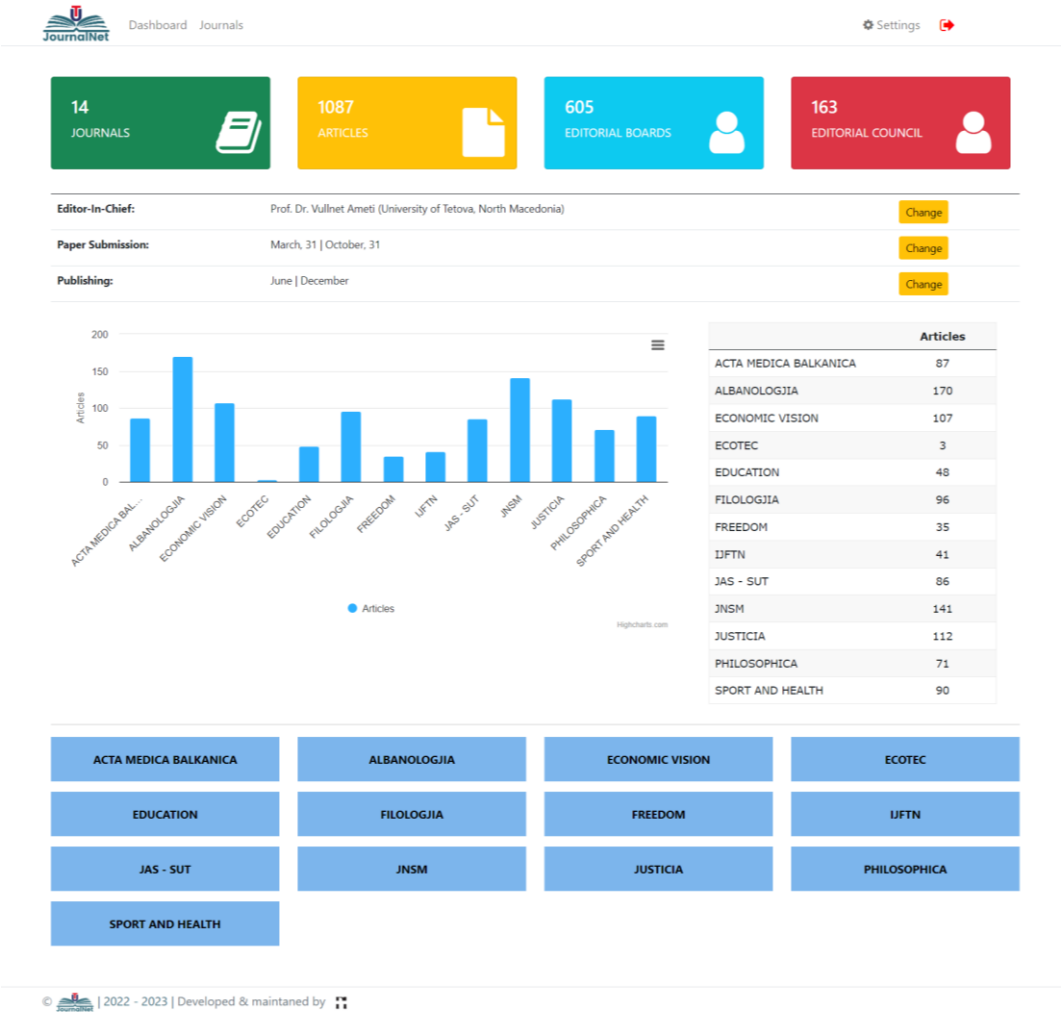

Figure 3. Administrator Dashboard

- The "Users" module: available to academic users who will work on scientific research, User capabilities [8]

- Academy Works: With the help of "JournalNet System" a lot of information can be collected on different academics journals from this site.
- Download Papers: many academic papers are available online in different formats (PDF, etc.) for your study and further understanding, which you can download from the journals.

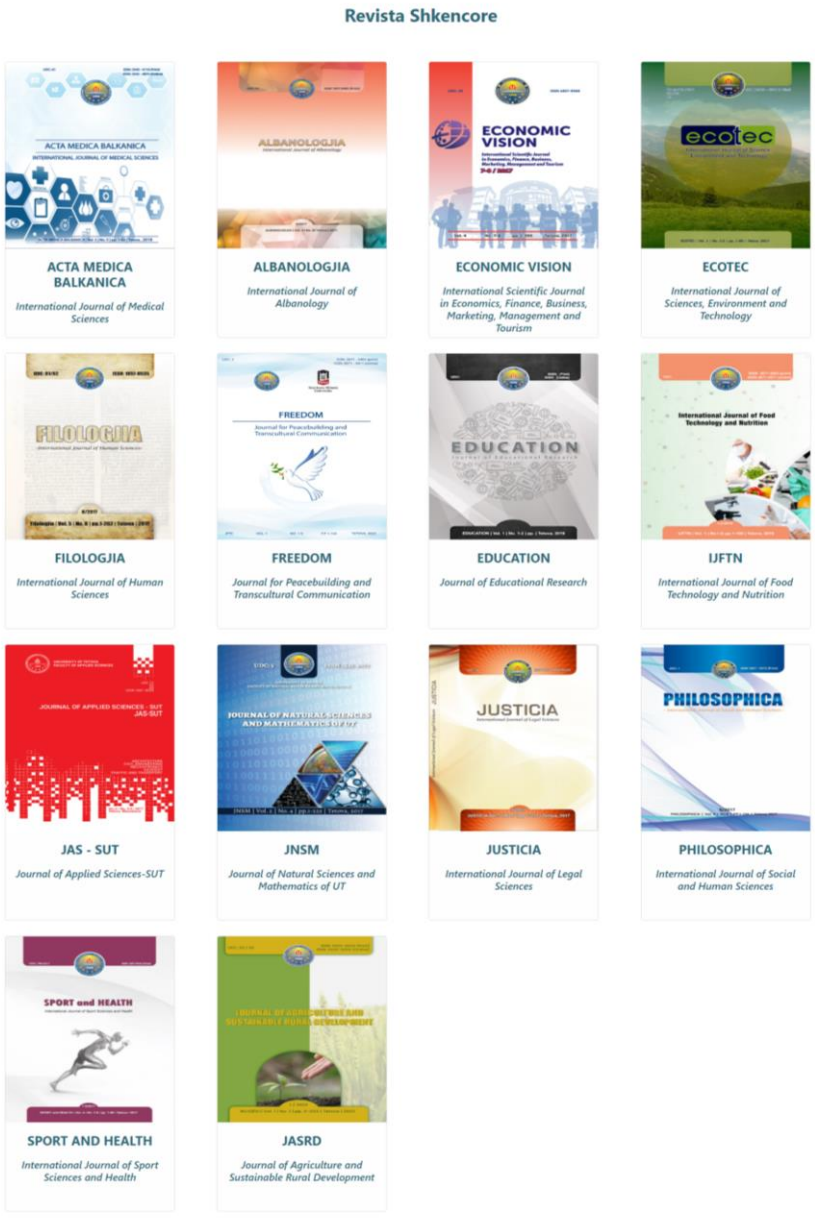

Figure 4. Journal Web Site (https://journals.unite.edu.mk/)

This modular approach to managing academic journals guarantees unique functionality and access for every type of user participating in the system's operation. Three main roles are involved in managing scholarly journals: system developers,

administrators, and users (writers, reviewers, readers, etc.). Using UML diagrams, such the use case diagram, makes it easier to understand the roles and how they interact with the system. [6]

Use cases describe the particular tasks that each position can execute, and actors (administration, author/reader, and system developer) are used to visually represent the relationships between roles and the functionality they utilize within the system. These linkages show how players interact with the system and make use of its features, as seen in Figure 4. By highlighting role-based actions and interactions in scholarly journal management, the use case diagram in this context aids in identifying user needs and guides detailed system development. It also gives a clear and structured overview of each actor's role and the functionalities they employ. [11]

7. CONCLUSION

All things considered, the "JournalNet" academic journal management system provides a complete solution that can be adjusted to meet the requirements of administrators, users, and system developers. "JournalNet"'s modular architecture and state-of-the-art technological base speed up administrative tasks, improve user interaction, and ease system development.

By utilizing web application technologies, the "JournalNet" deployment guarantees compatibility with a wide range of computing systems and gives users easy access to data. Furthermore, the system's dependability and correct operation are ensured by the thorough testing and verification procedures carried out during implementation. Because of this, "JournalNet" promises increased productivity and efficiency in this area and marks a significant development in the management of electronic scholarly journals.

In addition, upkeep is required to guarantee that the "JournalNet" system continues to function well and changes to accommodate changing needs of users and organizations. To guarantee "JournalNet"'s security, stability, and responsiveness, it is constantly developed, updated, and patched.

Overall, "JournalNet's" excellent implementation and careful maintenance show how relevant it is to the advancement of electronic journal management and the sharing of knowledge. Because of its user-centric design and dedication to continuous improvement, "JournalNet" has the potential to have a substantial impact on academic communication in the digital era.

REFERENCES

[1] C. Betancourt, ""An Information Systems Design Theory Proposal for Knowledge Management Systems"," 2009.

[2] H. Bogunović, P. Edgar, S. Lončarić and V. Mornar, ""An Electronic Journal Management System"," 25th International Conference on formation Technology Interfaces, 2003.

[3] I. Hebrang Grgic, ""Publishing Croatian scientific journals: to e- or not to e-?"," Libellarium Journal for the Research of Writing Books and Cultural Heritage Institutions, 2015.

[4] V. J. Janesick, "A Journal About Journal Writing as a Qualitative Research Technique: History, Issues and Reflections," Issues in Science and Technology Librarianship, vol. 5, no. 4, 2005.

[5] R. D. Llewellyn, L. J. Pellack and D. D. Shonrock, "The Use of Electronic - Only Journals in Scientific Research", 2002.

[6] M. Arkan and I. Taner Okumus, "Design and Implementation of an Electronic Document Management System," 2017.

[7] M. Albantani, A. and F. Arifin, "Management of Accredited Scientific Education Journals in State Islamic Universities," vol. 6, no. 2, 2020.

[8] P. Iseni, F. Imeri and F. Idrizi, "New Socio-Academic Platform Based on the Results Revealed from Comparative Analysis of the Existing Platforms," Journal of Natural Sciences and Mathematics of UT, vol. 7, no. 13-14, pp. 85-89, 2022.

[9] A. M. Elizarov, D. S. Zuev and E. K. Lipachev, "Electronic Scientific Journal - Management Systems", Scientific and Technical Information Processing, pp. 66-72, 2014.

[10] E. J. Naiburg and R. A. Maksimchuck, UML for Database Design, 2001.

[11] K. S. Hawkins, "A Model for Integrating the Publication and Preservation of Journal Articles", 15th All-Russian Conference "Digital Libraries: Advanced Methods and Technologies, Digital Collections", 2013.

ICENS 10TH INTERNATIONAL CONFERENCE ON ENGINEERING AND NATURAL SCIENCE
October 02-06 2024 Sarajevo (Hybrid Event)

ENHANCING CULINARY CREATIONS: A SERVICE-ORIENTED APPROACH TO RECIPE APP DEVELOPMENT

Suela Rushiti[1], Puhiza Iseni[2] Agon Memeti[3], Florinda Imeri[4] and Shkurte Luma-Osmani[5]

Abstract

This paper outlines the development of a recipe app rooted in Service-Oriented Architecture (SOA) principles, aiming to meet the rising demand for digital culinary solutions. Motivated by the absence of a dedicated culinary app in our local community, we embarked on this innovative journey to enable users to seamlessly explore, create, and share culinary creations within a digital space. By integrating advanced frontend and backend technologies, our app offers scalability, adaptability, and personalized user interactions. Our platform bridges the gap between culinary enthusiasts and diverse culinary experiences, to revolutionize the culinary landscape. We aim to foster creativity, community engagement, and culinary exploration on a global scale. Future endeavors involve continuous improvements based on user feedback and technological advancements, enhancing user experiences, and fostering culinary innovation..

Keywords: recipe app; Service-Oriented Architecture (SOA); culinary exploration; digital solutions; culinary innovation; user satisfaction

1. INTRODUCTION

The growing demand for digital solutions in the culinary realm necessitates the development of robust management systems.

Cooking is "one of the most interesting and worthwhile things we humans do". It connects the natural world and the social world. [1]

Cooking is not just personal, it also has a wider political implication - it "transforms us, too, from mere consumers into producers".[1]

However anecdotal evidence suggests that people lack nutritional and cooking knowledge and have problems following recipes.[1] A culinary recipe consists of a list of components (the ingredients) and a sequence of steps to be applied on these components to generate a dish.[10]

[1] *Corresponding author: Department of Computer Science, Faculty of Natural Sciences and Mathematics, University of Tetovo, North Macedonia, s.rushiti222501@unite.edu.mk*

[2] *Department of Computer Science, Faculty of Natural Sciences and Mathematics, University of Tetovo, North Macedonia, puhiza.iseni@unite.edu.mk*

[3] *Department of Computer Science, Faculty of Natural Sciences and Mathematics, University of Tetovo, North Macedonia, agon.memeti@unite.edu.mk*

[4] *Department of Computer Science, Faculty of Natural Sciences and Mathematics, University of Tetovo, North Macedonia, florinda.imeri@unite.edu.mk*

[5] *Department of Computer Science, Faculty of Natural Sciences and Mathematics, University of Tetovo, North Macedonia, shkurte.luma@unite.edu.mk*

Recipe apps have emerged as transformative tools, going beyond traditional cookbooks to offer dynamic platforms for culinary exploration. Due to the great competitiveness of the market, innovation is a necessity. And creativity is considered a factor of disruptive innovation.[10]

Grounded in Service-Oriented Architecture (SOA) principles, these apps have the potential to revolutionize culinary experiences by providing scalability, adaptability, and personalized interactions.

Our research focuses on creating an innovative recipe app rooted in SOA principles to meet the evolving needs of culinary enthusiasts. Recognizing a lack of dedicated culinary apps in our local context, we aim to fill this gap with our project.

By integrating SOA principles, our app aims to address challenges related to scalability, adaptability, and dynamic culinary preferences. We strive to empower users to seamlessly explore, create, and share culinary creations within a digital environment.

This paper outlines the methodology behind our app's development, highlighting the importance of SOA in creating loosely coupled, independent services to enhance user experience. We also discuss platform design, frontend and backend technology integration, and future project directions.

Our goal is to contribute to the culinary landscape by providing a dynamic, responsive, and tailored digital resource that enriches the culinary journey of users worldwide, catering to diverse tastes and preferences.

2. PROBLEM DEFINITON

Culinary enthusiasts in the Tetovo region face a persistent challenge: the lack of a tailored digital cookbook or culinary application. This absence not only limits access to diverse recipes and culinary inspiration but also stifles creativity in a community known for its culinary exploration. Existing digital cookbooks are rigid and fail to adapt to individual preferences, hindering user engagement and exploration.

Our recipe app, grounded in Service-Oriented Architecture (SOA) principles, aims to overcome these challenges. It provides a dynamic, responsive, and highly personalized culinary experience for Tetovo residents. Beyond offering recipes, our app empowers users to explore, create, and share culinary masterpieces seamlessly. By embracing SOA, we aim to foster a culture of culinary innovation and creativity within our community.

Our research not only fills the gap in digital culinary resources but also stimulates culinary exploration and creativity among residents. Through our app, we seek to enhance culinary journeys, promote creativity, and engage the community in the culinary arts.

To ensure the efficacy of our app, we thoroughly explore the existing landscape of culinary digital solutions. By examining technologies, frameworks, and methodologies used in similar projects, we gain valuable insights to inform our approach and improve our recipe app's success.

3. SERVICE-ORIENTED ARCHITECTURE MODEL

Our recipe app's architectural framework is built upon the principles of Service-Oriented Architecture (SOA), which prioritize modularity, scalability, and interoperability. By decomposing our application into loosely coupled and independently deployable services, we attain greater flexibility and resilience.

The provided descriptions outline various services and components of a culinary recipe application, each responsible for specific functionalities and interactions within the system. Let's further elaborate on how these services contribute to the overall architecture of the application:

User Interface (UI) Service:

- Responsible for presenting the user-friendly front-end of the application, including essential components like the home page, search functionality, and user profile management.
- Utilizes modern UI frameworks and design principles to ensure a visually appealing and intuitive user experience.

Recipe Service:

- Acts as the backbone for managing the storage and retrieval of diverse culinary recipes.
- Implements CRUD operations to allow users to create, read, update, and delete recipes seamlessly.
- Ensures efficient data storage and retrieval mechanisms to handle a large volume of recipe data.

User Profile Service:

- Manages user profiles and preferences, including user registration, login authentication, and profile updates.
- Implements robust security measures to safeguard user data and privacy.
- Allows users to customize their profiles and personalize their culinary experience.

Recommendation Engine:

- Analyzes user data and behaviors to generate personalized recipe recommendations.
- Utilizes machine learning algorithms and data analytics to improve the accuracy of recommendations over time.
- Enhances user engagement by suggesting relevant and appealing recipes based on individual preferences.

Search Service:

- Offers advanced search capabilities, allowing users to discover specific recipes based on various criteria such as ingredients, cuisine, and dietary restrictions.
- Implements efficient indexing and querying techniques to deliver fast and relevant search results.

User-Generated Content Service:

- Facilitates user interactions and contributions, enabling users to share their culinary creations, reviews, ratings, and recipe submissions.
- Implements moderation and content management features to ensure the quality and integrity of user-generated content.

Notification Service:

- Enhances user engagement by providing real-time notifications about recipe updates, user interactions, and app-related announcements.
- Utilizes push notifications and other communication channels to keep users informed and engaged.

Database Service:

- Serves as the central data repository for storing recipe data, user profiles, user-generated content, and application-related information.
- Utilizes MongoDB as the primary NoSQL database for its flexibility, scalability, and compatibility with the application's data model.

Authentication and Authorization Service:

- Ensures the security of user data through robust authentication and authorization mechanisms.
- Manages user access and privileges based on predefined roles and permissions, protecting sensitive data from unauthorized access.

Cloud Services:

- Leverages Amazon Web Services (AWS) for hosting, deployment, and scalability, ensuring high availability and reliable performance of the application.

- Utilizes cloud infrastructure services such as Amazon EC2, S3, and RDS to support the application's computing, storage, and database needs.

Communication between Services:

- Services communicate through standardized interfaces, typically using RESTful APIs for seamless data exchange.
- Adopts a microservices architecture approach, promoting loose coupling between services to enable individual scalability and facilitate changes without impacting the entire application.

By incorporating a modular and scalable design, leveraging various services and components, and utilizing cloud infrastructure and modern technologies, the culinary recipe application can deliver a robust, user-friendly, and engaging experience to its users. This approach enables the application to adapt to changing requirements, handle increasing user demands, and maintain a competitive edge in the market.

4. TOOLS AND TECHNOLOGY USED

Frontend Development

- React.js: React.js is chosen as the primary framework for frontend development due to its popularity, efficiency, and component-based architecture. This aligns well with our service-driven approach, allowing for the creation of interactive and responsive user interfaces.
- React Router: React Router is integrated to manage navigation and routing within the application. It enables seamless transitions between different sections of the app, ensuring a smooth and intuitive user experience.
- CSS and SCSS: Cascading Style Sheets (CSS) and SCSS (Sass) are utilized for styling the application. These technologies provide flexibility in designing visually appealing interfaces, which is crucial for enhancing user engagement and satisfaction.

Backend Development

- Node.js: Node.js is selected for backend development due to its ability to execute JavaScript on the server side. It offers a lightweight, efficient, and non-blocking architecture, which is well-suited for handling the dynamic nature of our recipe app. Node.js complements the flexibility of our service-oriented architecture (SOA) by supporting scalable and event-driven server-side development.
- Express.js: Express.js, a web application framework for Node.js, is used to develop the backend API services. It simplifies the process of defining routes, handling requests, and managing data, making backend development more streamlined and efficient. Express.js provides robust features and middleware support, enabling the creation of secure and scalable APIs for our recipe app.

By adopting React.js for frontend development and Node.js with Express.js for backend development, we ensure a cohesive and efficient development process that aligns with the requirements of our recipe app. These technologies enable us to deliver a user-centric and responsive application that meets the needs of culinary enthusiasts while maintaining scalability and performance.

5. PLATFORM DESIGN AND DEVELOPMENT

Our research focuses on developing a recipe app built upon the principles of Service-Oriented Architecture (SOA). This architectural approach serves as the cornerstone of our development process, with the aim of creating a robust platform that meets the diverse needs of culinary enthusiasts. In this section, we provide a comprehensive overview of our architectural framework and outline the detailed steps involved in crafting a platform designed to empower users in their culinary endeavors.

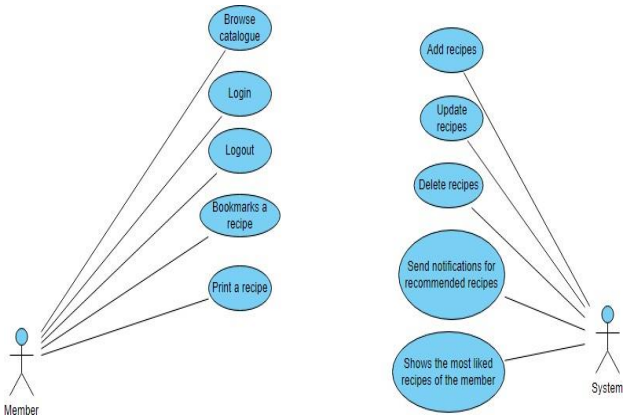

Figure 1. Use case diagram of the culinary app

Member Features:

- Browse Catalogue: Members can explore the extensive recipe catalogue, discovering diverse culinary recipes and various cuisines. This feature enriches their culinary knowledge and inspires creativity in their cooking endeavors.
- Login: Securely access personalized features like saved bookmarks, customized preferences, and tailored recipe recommendations.
- Logout: Ensure account and data security by securely logging out after completing interactions with the app.
- Bookmark a Recipe: Save preferred recipes for future reference, allowing easy access to favorite dishes at any time.
- Print a Recipe: Option to print selected recipes for a tangible cooking reference, reducing reliance on digital devices during culinary preparation.

System Actions:

- Add Recipes: Enrich the recipe catalogue by adding new culinary recipes to the app's database, ensuring its diversity and comprehensiveness.
- Update Recipes: Modify existing recipes to maintain accuracy and relevance, including ingredient adjustments, instructions, and other details.
- Delete Recipes: Remove irrelevant or flagged recipes to uphold the quality of the recipe catalogue, ensuring users have access to high-quality content.
- Send Notifications for Recommended Recipes: Proactively analyze member preferences and behaviors to send notifications recommending recipes aligned with their culinary interests, enhancing the user experience.
- Show the Most Liked Recipes of the Member: Present members with a curated list of the most-liked recipes based on user ratings and preferences, fostering a sense of culinary community, and encouraging exploration of highly regarded dishes.

These features and actions empower members to explore, save, and enjoy culinary delights while ensuring the app's recipe catalogue remains diverse, accurate, and relevant. Through personalized recommendations and curated content, the system enhances the culinary experience for members, fostering a vibrant culinary community. The app comprises several essential pages, each catering to a unique aspect of the culinary journey. These pages include the Home Page, Categories Page, Profile Page, Meal Details Page, and Menu Page.

The home page serves as the welcoming gateway for users, featuring a prominent search section for finding desired recipes quickly. Below the search bar, users discover a curated list of recipe categories, enticing them to explore culinary delights from various cuisines. With its intuitive and user-friendly interface, the home page sets the stage for an enjoyable culinary journey.

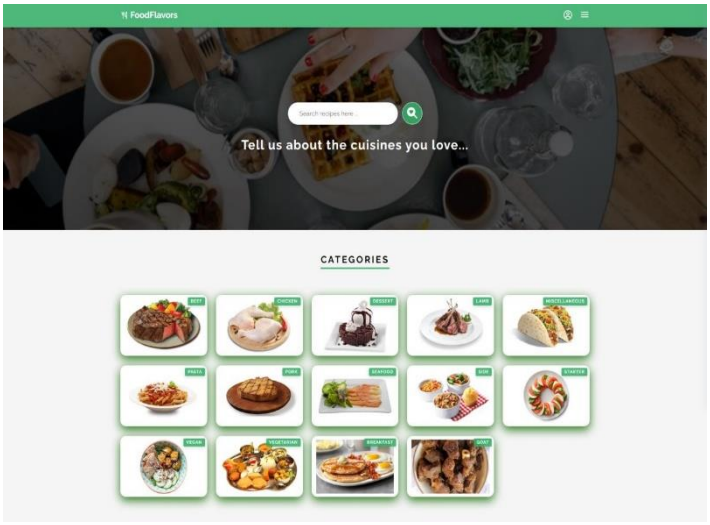

Figure 2. Home Page of the app

Upon initiating a search or browsing through categories, users are directed to the Categories Page. Here, they encounter a selection of culinary meals, providing a multitude of choices to explore. Alongside the initial category selection, users can navigate through different meals using convenient navigation buttons. These buttons offer users the flexibility to discover recipes from various cuisines and themes, ensuring an engaging culinary experience.

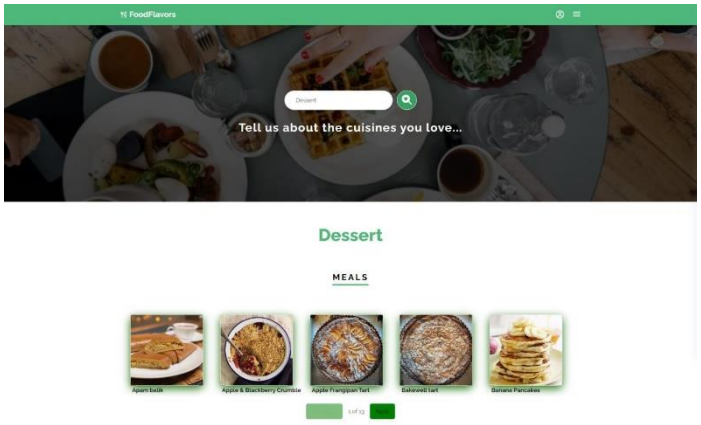

Figure 3. Search Page of the app

The Meal Details Page offers users a deep dive into the specifics of a particular recipe. Featuring an enticing image of the meal, it provides a visual preview of the culinary delight awaiting them. Alongside the image, users discover the meal's name, category, and associated tags, offering insights into its characteristics.

At the heart of this page lies a comprehensive breakdown of the recipe, including a list of ingredients and step-by-step instructions for preparing the dish. Users gain access to a wealth of culinary knowledge to craft the perfect meal. Additionally, the page offers convenient actions like "Bookmark" and "Print," empowering users to save their favorite recipes for future reference or print them for hands-on culinary experiences.

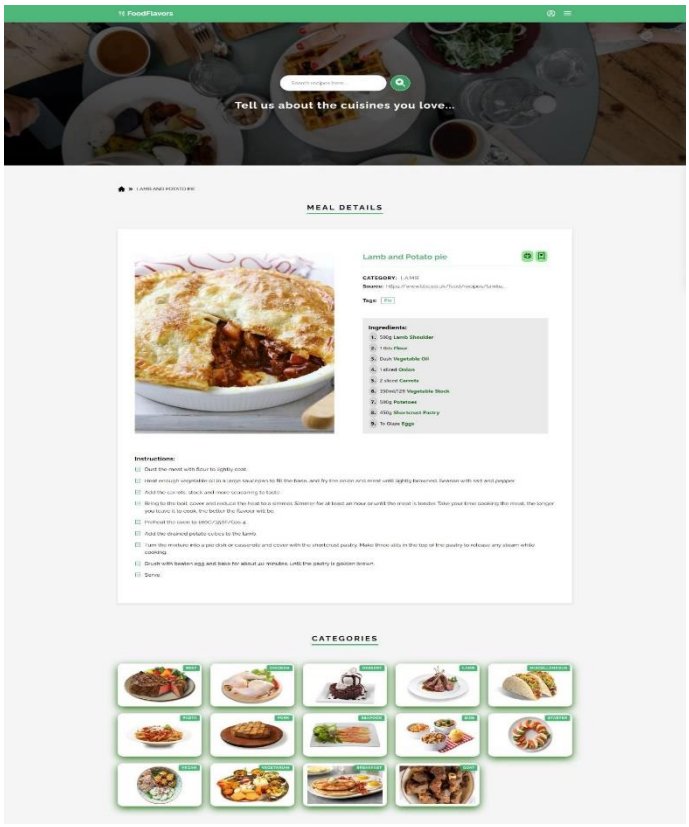

Figure 4. Meal Details Page

The Profile Page serves as the user's personalized hub within the app. Here, users can manage their culinary journey by accessing their activity history, saved recipes, and personalized recommendations. The page offers insights into their culinary preferences and showcases the most liked recipes.

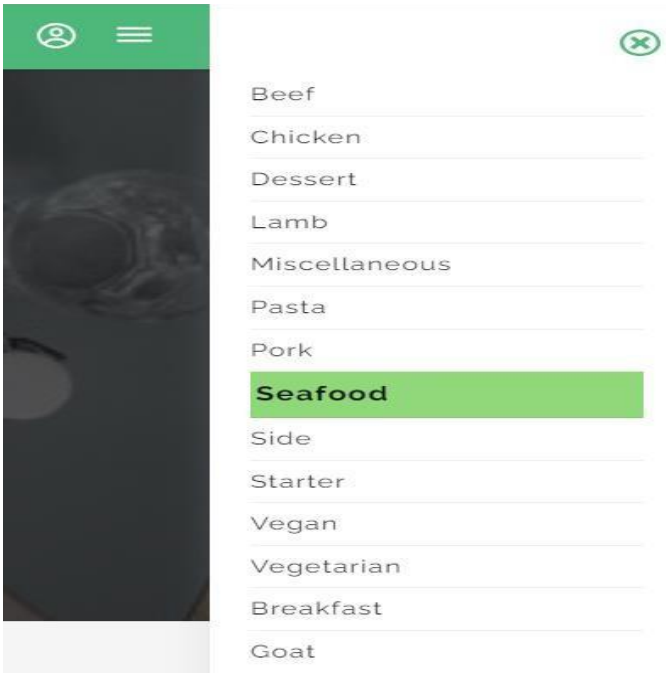

Figure 5. Menu Page of the app

As for the Menu Page, it acts as the central navigation hub within the app. Serving as the navigational compass, it guides users to various sections and categories. Users can seamlessly transition between categories and explore the wealth of culinary resources at their fingertips.

6. CONCLUSION

In conclusion, our research endeavors to meet the increasing demand for digital culinary solutions by developing a robust recipe app grounded in Service-Oriented Architecture (SOA) principles. Motivated by a fundamental gap in our local culinary landscape—the absence of a dedicated digital cookbook—our aim is to provide a diverse range of recipes, personalized recommendations, and user-centric features. Through the development of this recipe app, inspired by SOA principles, we ensure scalability, flexibility, and future enhancements.

By leveraging cutting-edge frontend and backend technologies, we have laid the groundwork for a seamless and immersive culinary experience. Our app's architecture, deeply rooted in SOA principles, ensures scalability, adaptability, and responsiveness to meet the evolving needs of users.

Moving forward, our focus will be on continuous enhancements based on user feedback and technological advancements. We envision further integration of features to enrich user experiences and promote culinary innovation.

In essence, our recipe app represents a step towards revolutionizing the culinary landscape, empowering users to explore, create, and share culinary masterpieces seamlessly within a digital environment. As we progress, our commitment to enhancing user engagement, culinary exploration, and user satisfaction remains unwavering. We are excited to continue our journey and provide culinary enthusiasts with a remarkable and ever-evolving digital culinary resource.

REFERENCES

[1]. Buykx, Lucy. "Interactive recipe instructions: supporting cooks with better designs." Thesis submitted for the degree of Doctor of Philosophy, University of York, Computer Science, September 2013.
[2]. Smith, John. "Introduction to Service-Oriented Architecture." Journal of Software Engineering 20.2 (2018): 45-58.
[3]. Patel, Ruchi, et al. "Modern Trends in Frontend Development: A Comprehensive Review." International Journal of Web Development 15.4 (2020): 112-125.
[4]. Brown, David. "Scalable Backend Development with Node.js." Proceedings of the International Conference on Web Technologies (ICWT) (2019): 78-89.
[5]. Kim, Susan. "User-Centric Design Principles for Web Applications." Human-Computer Interaction Review 25.3 (2021): 210-225.
[6]. Garcia, Maria, et al. "Global Cuisine at Your Fingertips: Exploring the Impact of Recipe Apps on Culinary Diversity." Journal of Food Culture 18.2 (2021): 78-89.
[7]. Patel, Rajesh, et al. "Exploring Culinary Creativity: A Study on Recipe Innovation in the Digital Era." International Journal of Food Innovation 22.3 (2019): 34-47.*FLEXChip Signal Processor (MC68175/D)*, Motorola, 1996.
[8]. Wang, Emily, et al. "Enhancing User Experience with Real-Time Notifications in Web Applications." Journal of Interaction Design 27.3 (2020): 88-101.Karnik, “Performance of TCP congestion control with rate feedback: TCP/ABR and rate adaptive TCP/IP,” M. Eng. thesis, Indian Institute of Science, Bangalore, India, Jan. 1999.
[9]. Brown, E., & Wilson, J. (2016). The Digital Kitchen: Culinary Apps and Their Impact on Home Cooking. Boston: Culinary Research Institute.
[10]. Antonio Dos Santos, Willian & Bezerra, Joao & Góes, Fabrício & Ferreira, Flávia. (2020). Creative Culinary Recipe Generation Based on Statistical Language Models. IEEE Access. 8. 1-1. 10.1109/ACCESS.2020.3013436.

ICENS 10TH INTERNATIONAL CONFERENCE ON ENGINEERING AND NATURAL SCIENCE
October 02-06 2024 Sarajevo (Hybrid Event)

Hydraulic Rebound Stopper Affect For Passenger Cars On Shock Absorber

Semih Çallı[1], Abdurrahim Arkan[2]

Abstract

The vehicles driving on the road, road-related impacts affect the chassis. These impacts should not be transmitted to the cabin. The That absorbs these impacts between the chassis and cabin is the shock absorber. The shock absorber does this damping by converting motion energy into heat energy. During this energy conversion, the hydraulic flow inside the shock absorber is limited by piston valve. The valve damping force is adjustable according to vehicle type for the passive Shock Absorbers and occurs reaction forces during driving. However, the damping force must be variable in order to meet driving dynamics and driver expectations that change over time. Active shock absorbers are used to provide this variability. However, active shock absorbers are more costly and more difficult to implement. For this reason, different technologies such as hydraulic rebound stopper and hydraulic compression stopper are used in passive shock absorbers to ensure the variability of force. In this study, comparative numerical data were obtained by applying the hydraulic rebound stopper system to the shock absorbers used in small family cars and lower middle-class cars. In road conditions where the reaction force of the valve against the hydraulic fluid is not sufficient, the hydraulic rebound stopper is activated by creating extra force. With this extra force, disturbing vibrations to the vehicle and the driver are dampened, increasing driving safety and comfort.

Keywords: Shock absorber, Hydraulic rebound stopper, Hydraulic flow, Piston Valve

1. INTRODUCTION

Shock absorbers used in passenger cars are hydro-mechanical parts that overcome road-related vibrations that occur during driving without breaking the wheel's contact with the road, with hydraulic reaction force, this increasing driving safety and comfort. Basically, it has an oil-filled cylinder group and a piston that can move vertically.

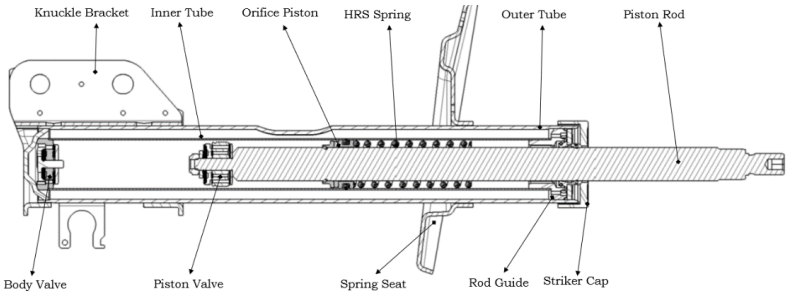

Figure 1. Shock absorber components

This piston rod moves up and down, compressing or releasing the oil in the shock absorber with the help of valves, providing damping. There are two types of valves working inside the shock absorber. These valves adjust the flow rates of the oil that will create the compression or rebound forces of the oil inside the shock absorber. Firstly, the piston starts its upward movement when the vehicle falls into a pothole. While this upward movement occurs, the washers in the piston valve make it difficult for the oil to passover. The oil is forced to pass through the washers, creating a rebound force. The rebound force may vary depending on the number of washers and the type of piston. The oil creates a rebound force as it is forced to pass through the valves for rebound. This makes the rebound force adjustable according to the weight of the vehicle and driving comfort. It dampens the force that will come to the vehicle with the rebound force before it reaches the driver. Driving safety and driver comfort increase with the damping of this force.

[1] *Maysan Mando A.Ş. Bursa, Türkiye, scalli@maysanmando.com*

[2] *Maysan Mando A.Ş. Bursa, Türkiye, aarkan@maysanmando.com*

When the vehicle hits the bump, the piston starts moving in the opposite direction. It tries to compress the oil in the shock absorber with the help of valves by moving downwards in a variable direction according to the height of the bump. When the movement starts, the oil starts to create a compression force by passing through the washers. This force can be adjusted with the help of washers or the variability of the valves. As the compression force is formed, the piston rod starts to move down further. The force continues to increase to the lowest point of the shock absorber. The force creates a damping force in the vehicle in proportion to the compression of the oil. With the damping, the force that will come to the vehicle while passing through the bump is eliminated. In addition, the driver's control of the vehicle remains constant and driving comfort is increased.

When we explain the working principle of the shock absorber, there are force graphs where we measure the performance of the shock absorber, where we match the verbal expressions with scientific data. The reaction forces that form the curves in these force graphs are the reaction forces given by the valves to the measuring device. Performance graphs vary according to speeds and incoming forces, and the shock absorber completes the force data in the curve by completing an up-down movement.

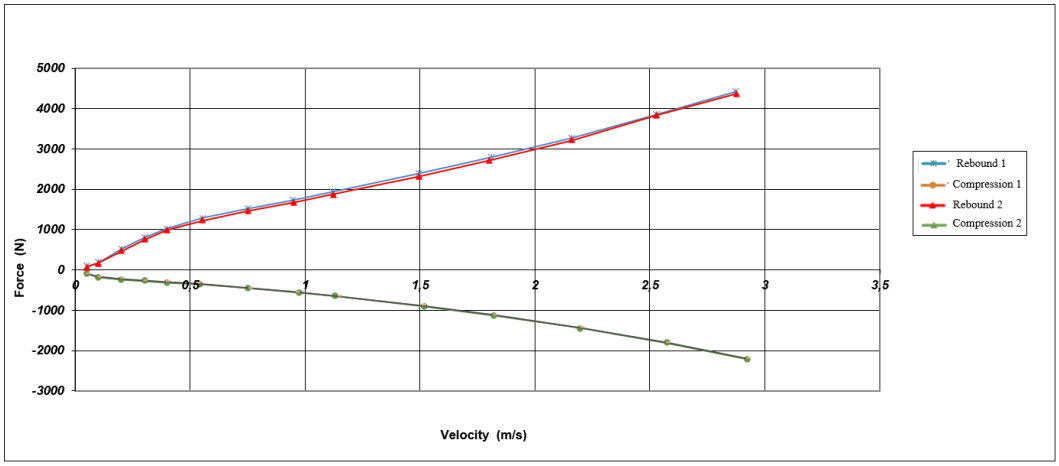

Figure 2. Shock absorber Damping Forces Chart

1.1 HYDRAULIC REBOUND STOPPER

Hydraulic Rebound Stopper is a hydraulic stop that dampens when the vehicle enters a pothole and is an add-on function for conventional shock absorbers. The hydraulic rebound stopper creates an additional damping force while working inside the shock absorber. It produces this additional force by compressing the oil with a different piston assembly and the compressive force of the spring used in the shock absorber. In this way, the high rebound stop forces that occur when the cars enter potholes are reduced in a controlled manner, this reducing the vibrations and noises coming to the driver. The graphic created by the hydraulic rebound stopper is defined as follows.

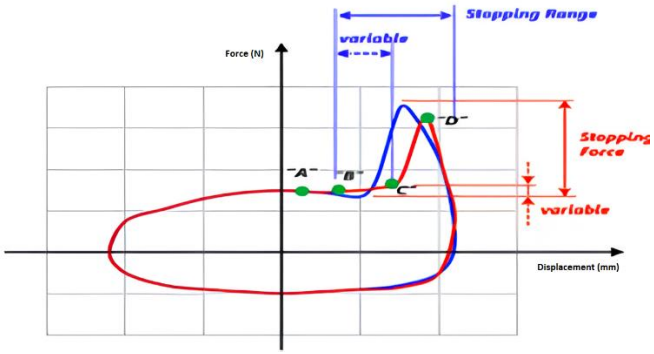

Figure 3. Hydraulic Rebound Stopper Diagram

2. DEVELOPMENT OF HRS

The most important titles for the HRS system are the amount of force and damping, HRS movement length, HRS starting point, adjustable force, sealing to create damping within the system and the fact that these features are easily adjustable or suitable for variability. A testing machine can obtain these parameters by measuring the shock absorber reaction force. Prototype production is important for this situation. Prototype production was produced with test springs and injection molded parts and tests and trials were carried out. After trying many designs, these trials were brought to dimensions suitable for placement in the shock absorber and tested. Adjustable shock absorbers made in the form of prototypes also provided fast testing opportunities.

2.1. HRS System Design of Parts

The most important factors affecting shock absorber designs are that the shock absorber performs its damping function as a suspension element well and provides durability and damping throughout the life of the vehicle. Other factors are its suitability for vehicle assembly, its adaptation to the flow and dynamism of the vehicle while working with the suspension in the vehicle, and its damping by providing the driver with road control without losing contact with the road during damping. While designing and developing this hydraulic rebound stopper system, a design was created to fit the inner tube inside the shock absorber. All parts in the system were designed in accordance with these limits and placed inside the shock absorber without hindering operation. The HRS system consists of a rebound spring, orifice piston, o-ring and hydraulic rebound bumper. Figure 4 shows the parts of the hydraulic rebound stopper system.

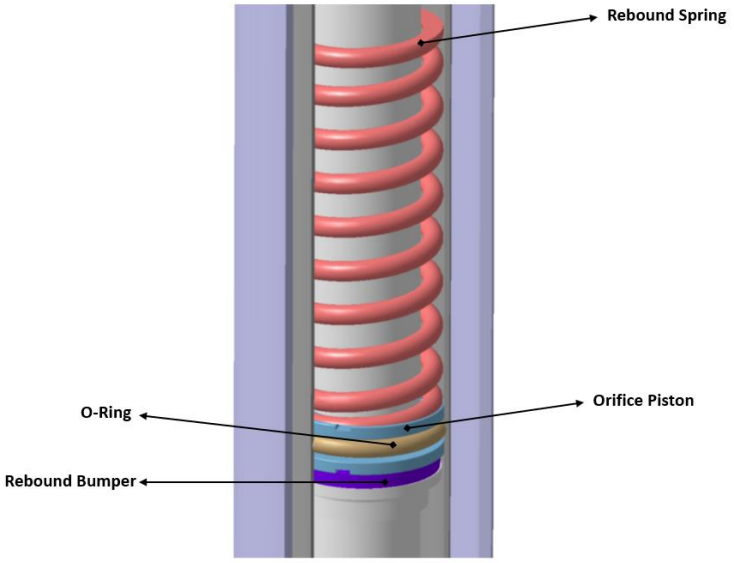

Figure 4. Parts Of Hydraulic Rebound Stopper

2.1.1 Rebound Spring

The most important factors in the design of the rebound stopper spring are the weight of the vehicle it is used in, the damping required while driving on the road, and the additional damping force it creates compared to a normal shock absorber. In addition, the height of the spring determines where the rebound stopper force will come into play. The number of spring coefficient determines how much force will increase or decrease in the vehicle. This number of spring coefficient and the height of the spring also determine the shock absorber damping force measurement graph. For this reason, the most optimum design was selected and an adjustable spring design was obtained according to the vehicle type.

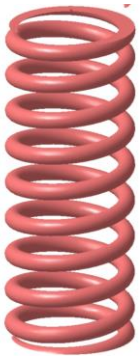

Figure 5. Rebound Stopper Spring

2.1.2 Orifice Piston

The first priority in orifice piston design is to provide suitable dimensions that can be mounted inside the inner tube. Then, it provides this extra force by compressing the oil by providing sealing in order to create an additional hydraulic force inside the shock absorber. It increases the damping force by not allowing the oil to pass with the o-ring mounted on it. This damping force can be adjusted with the variable grooves on it. The most suitable groove size is determined according to the vehicle and a universally usable design is created and applied to the shock absorber.

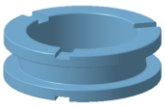

Figure 6. Orifice Piston

2.1.3 O-Ring

The o-ring must have dimensions that can be mounted on the orifice piston and that will seal inside the inner tube. Therefore, when selecting the material, rubber material was preferred instead of a hard plastic. Then, the dimensions were determined so that the oil in the shock absorber would not leak under the orifice piston and this dimension was adjusted so that it could be mounted on the orifice piston.

Figure 7. O-ring

2.1.4 Hydraulic Rebound Bumper

The most important criterion in the design of the hydraulic rebound buffer is to minimize the force coming from the hydraulic rebound stopper system while it is working and to minimize the sound that will reach the driver without breaking during operation by withstanding high heat in every operation. Therefore, the selected material is of great importance. Here, a material that can provide long-term durability, is heat-resistant and reduces noise according to the vehicle is selected. The part under the orifice piston is designed in accordance with the inner tube and piston rod dimensions and made operational within the system.

Figure 8. Hydraulic Rebound Bumper

3. DEVELOPMENT OF TEST METHOD

After the designs were made, the hydraulic rebound stopper system was mounted inside the adjustable shock absorber located in Maysan Mando R&D Center for testing. The shock absorber, which was mounted and connected to the test device, required certain speeds to be entered in the test device for measurement. These speeds are as in Figure 9.

0.52 m/s	0.39 m/s	0.26 m/s	0.13 m/s	0.05 m/s

Figure 9. Measurement Value Of HRS

The measurement to be made on the Test Device measures the damping that occurs according to the speed difference at the lower and upper points of the shock absorber. The soft or hard shock absorber is measured by the forces obtained from here. Since the hydraulic rebound stopper system is adjustable according to the vehicle, it can be adapted to every vehicle. The force measurement values of the shock absorber without hydraulic rebound stopper are in Figure 10.

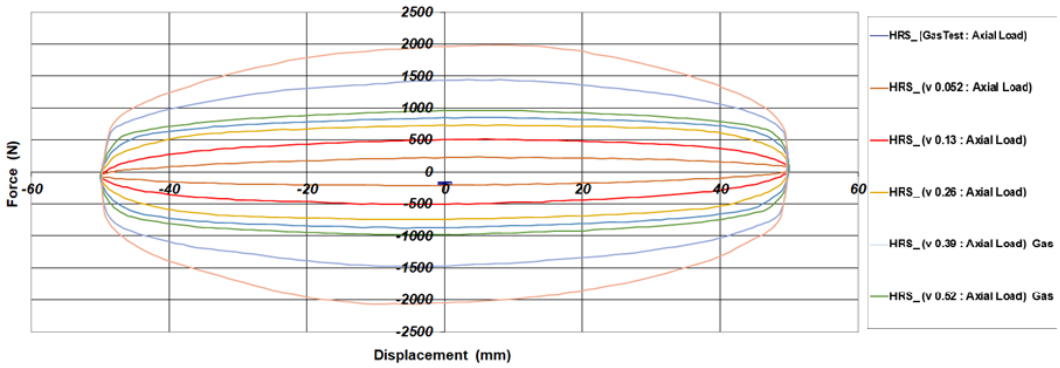

Figure 10. Damping Force Chart Without HRS

As seen in Figure 10, no additional damping force is obtained in the shock absorber without hrs. The graph of the measurement made with the test device also provides this. Shock absorbers in this form can transfer disturbing impacts to the chassis in very hard-entered holes.

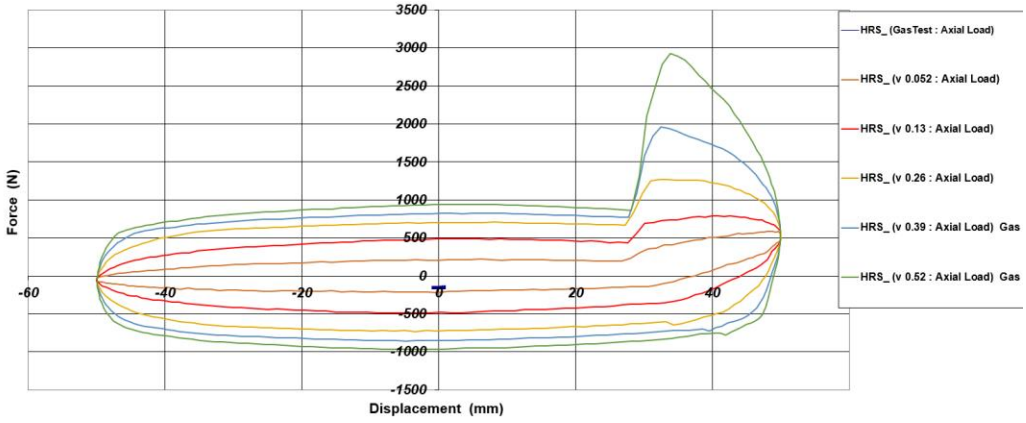

Figure 11. Damping Force Chart With HRS Setup 1

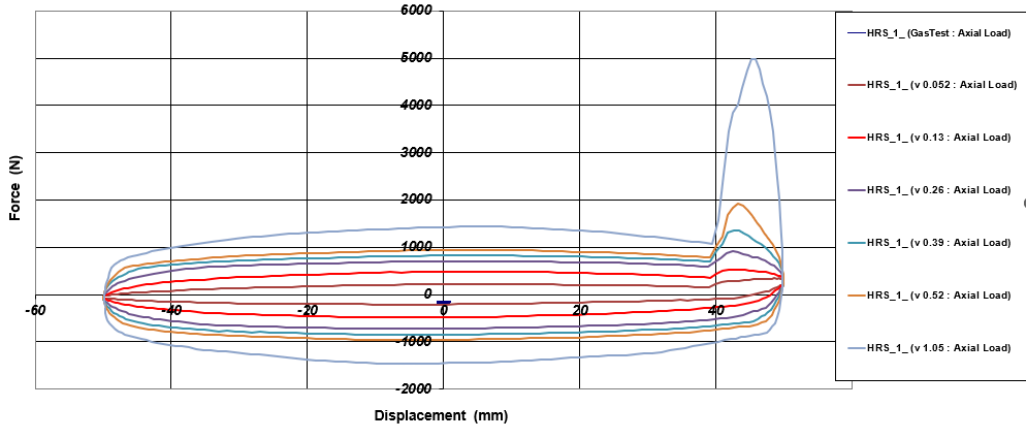

Figure 12. Damping Force Chart With HRS Setup 2

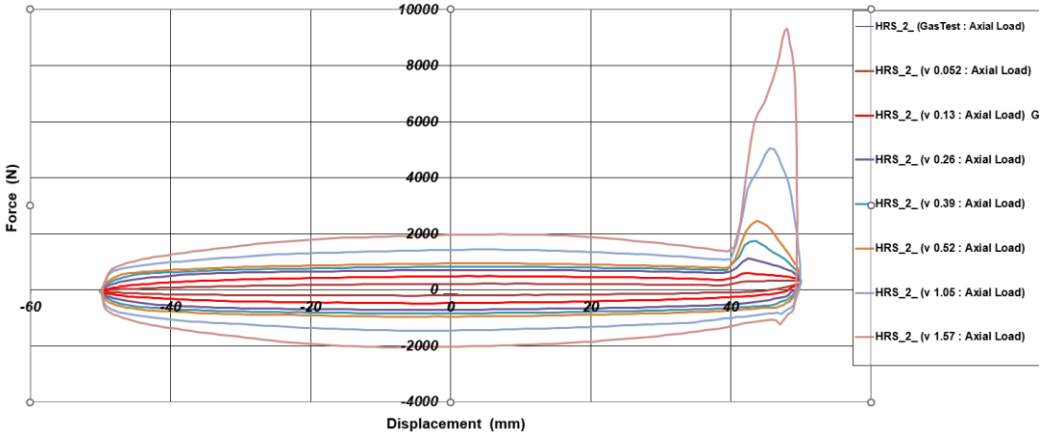

Figure 13. Damping Force Chart With HRS Setup 3

However, when we mount the hydraulic rebound stopper system we developed into the adjustable shock absorber, the effect of this technology on the shock absorber is revealed as a result of measurements. When we assembled the shock absorber with hydraulic rebound stopper to the test device, the force graph given by the test device is given in Figure 11. The additional damping force that appears in this graph occurs when the shock absorber starts to close. The graph, which normally does not create an additional force, creates an additional damping force at variable speeds when it starts to work with the addition of the hydraulic rebound stopper system. It works regardless of the operating speed of the shock absorber with this additional damping force. The height at which hydraulic rebound stopper is activated from the moment the vehicle starts to fall into the pithole. In addition, as seen in Figure-12-13, it has been observed that the adjustable hydraulic rebound stopper system can be obtained with variable forces in different tests.

4. CONCLUSIONS

In this study, the shock absorber can produce additional damping force during operation with the developed hydraulic rebound stopper. With these improvements, the newly developed system works and the benefits it provides to the vehicle have been determined in this study. According to the results obtained from the test device, the maximum rebound force that can be obtained without a hydraulic rebound stopper in the shock absorber is approximately 2500 N, while after the hydraulic rebound stopper is added, the maximum rebound force can be obtained from the same sample shock absorber up to approximately 10000 N. However, another advantage of the system is that this maximum force can be adjusted. The maximum force can be limited between 3000 N and 10000 N. In the 1st setup, the hrs channel height is 0.2mm and the maximum force received is 3000N. In the

2nd setup, the hrs channel height is 0.6mm and the maximum force received is 6000N. In the 3rd setup, the hrs channel height is 1mm and the maximum force received is 10000N.This allows the system to exhibit optimum performance in different vehicles. The newly designed hydraulic rebound stopper system was mounted on the vehicle with the results in the test device and this vehicle was tested dynamically on the roads. When the physical effects on the vehicle were examined after the test, a more comfortable and rigid ride was obtained. The shock absorber, which works together with the hydraulic rebound stopper system that is activated when the vehicle enters a pothole, reduces the vibrations coming from the potholes that the vehicle enters at high or low speeds, together with comfort, and creates a more dynamic ride. The parts used in the hydraulic recoil stopper have reduced the sounds transmitted from the shock absorber to the chassis.

The forces that emerge with the additional damping prove that this system can also be used in new types of electric vehicles. Since the secondary damping force will be sufficient for heavier vehicles, it has made it possible to integrate it into vehicles with increased weight together with the battery.

REFERENCES

[1]. Robert N., (2017), “Shock absorber and vehicle”, SAE International 2009-01-0223.

ICENS 10TH INTERNATIONAL CONFERENCE ON ENGINEERING AND NATURAL SCIENCE
October 02-06 2024 Sarajevo (Hybrid Event)

Effect Of Gas Pressure On Cavitation At Shock Absorber Used Passenger Car

Ramazan Ferik[1], Semih Çallı[2]

Abstract

Shock absorber is one of the main parts of suspension system. Road bumps or vehicle vibrations accumulate energy in the spring. The shock absorber absorbs this energy. It is an important part to guarantee comfort and safety. connects to the axon at the bottom and to the upper tower at the top. Roughness from the road moves the wheel in a vertical direction. the upper part, movement is undesirable. This is important for comfort. The difference in speed between the upper and lower connection generates energy. The kinetic energy here is absorbed by the shock absorber by converting it into heat energy. Valve system inside the shock absorber provides this transformation. The valves limit the oil flow, generating heat energy. The oil flows through small channels in the valves. Cavitation may occur in these channels during rapid velocity changes. Cavitation is an undesirable situation in the shock absorber and when it occurs, the shock absorber cannot produce reaction force and cannot perform its function. Gas is added into the shock absorber to prevent the low pressure that occurs here. The high pressure created by the gas prevents cavitation that may occur in the oil. It can be seen from the graphs during the force test if cavitation occurs. In this study, cavitation under different gas pressures was investigated. These values were determined as 0, 1, 2, 3 and 4 bar. At the end of the test, the effect of gas pressure on cavitation was analysed by comparing the graphs. As a result, the optimum gas pressure was determined as 3 bar.

Keywords: Shock Absorber, Hydraulic Fluid, Pressure, Cavitation

1. INTRODUCTION

In this study, the shock absorber, one of the important parts of the vehicle, and the vehicle shock absorber connection parts are examined. The working principle of the shock absorber and its position on the vehicle will be mentioned. In addition, structural improvements to the shock absorber fitting parts, and therefore improvements on the shock absorber, will be explained.

The suspension system has important functions on the vehicle. It is a system that must be included in the vehicle for handling and safety. It provides sporty or comfortable driving in the vehicle according to the driver's request. In vehicles designed for fast driving, the suspension provides a rigid and stiff ride. On the other hand, in vehicles designed for comfort, the suspension provides a soft and smooth ride. Bumps and potholes on the road move the wheel on the vertical axis. In this case, shaking and vibration occur. Task of the suspension is to reduce the transfer of these vibrations to the cabin. Another task of the suspension is to absorb vehicle oscillations caused by inertia forces. The oscillation movements occurring on the vehicle are given in the figure 1 below.

[1] *Maysan Mando A.Ş. Bursa, Türkiye, ramazanfrk16@gmail.com*

[1] *Maysan Mando A.Ş. Bursa, Türkiye, aarkan@maysanmando.com*

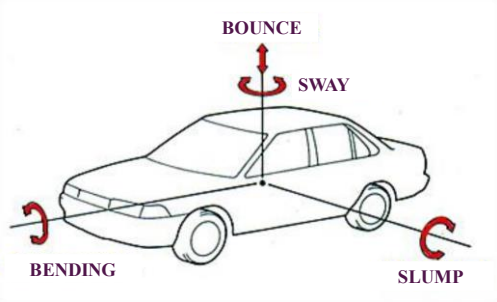

Figure 1. Oscillation movements on the vehicle [1]

In this figure;

Slump:

It is the movement of the front or rear of the vehicle in the vertical direction, relative to the centre of gravity of the vehicle. When passing over potholes or bumps, a wobble may occur. High acceleration occurs in case of rapid speeding or braking of the vehicle. This acceleration causes slump in the vehicle.

Bending:

When a vehicle turns or moves on a rough road, the spring on one side of the vehicle shortens while the other spring starts to lengthen. As a result, the body of the vehicle makes lateral movements from one side to the other.

Bounce:

It is the up and down movement of the vehicle as a complete vehicle. It occurs when driving at high speeds on rough roads. When the springs are softer, the bounce also increases.

Sway:

It is the movement of the vehicle to the right or left from the axial centre according to the centre of gravity. [1]

The tasks of the suspension system are to protect the stability and performance of the vehicle in these situations. To prevent the transfer of vibration and oscillation movements caused by road disturbances to the cabin. To provide comfort on long journeys. To provide vehicle stability and safety in fast and sports use.

The main parts of the suspension system can be taken as spring, shock absorber, balance bars and connection elements [2]. The more important of these elements are spring and shock absorber.

As the suspension dampens these movements, energy accumulates in the spring. The shock absorber absorbs this energy accumulated in the spring. It converts the movement energy into heat energy. The shock absorber creates a force in the opposite direction to the vertical movement of the spring. In this way the spring energy is completely damped. The connection of the shock absorber and spring assembly on the vehicle is given in figure 2.

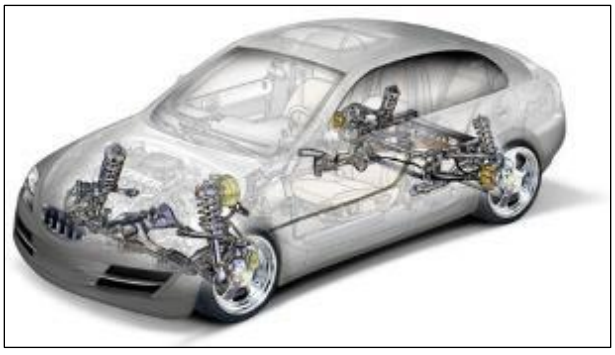

Figure 2. Overview of the vehicle suspension system [3]

The shock absorber is mounted to the vehicle body in the upper part. It is mounted to the vehicle chassis from the lower part. The weight of the vehicle in this case is carried by the shock absorber and the spring. The connection of the shock absorber and the spring on the vehicle is given in figure 3.

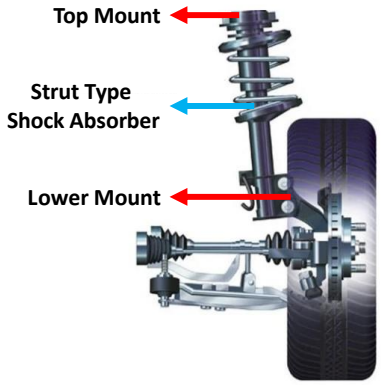

Figure 3. Shock Absorber Lower and Upper Fixation [4]

The vehicle body side is tried to be kept constant for comfort. The wheel side will move in a vertical direction due to road roughness.

In this case, there will be a speed difference between the lower and upper connection of the shock absorber. This difference in speed creates kinetic energy. The vertical movement is stopped by limiting the oil flow inside the shock absorber. In this way, the vertical movement of the wheel is not transmitted to the vehicle body and the driver. As a result, the movement is absorbed and provides comfort.

2. METHOD

There are valves inside the shock absorber to limit the oil flow. Oil flows through narrow channels in these valves. The valve construction and working scheme of twin tube shock absorber is shown in figure 4.

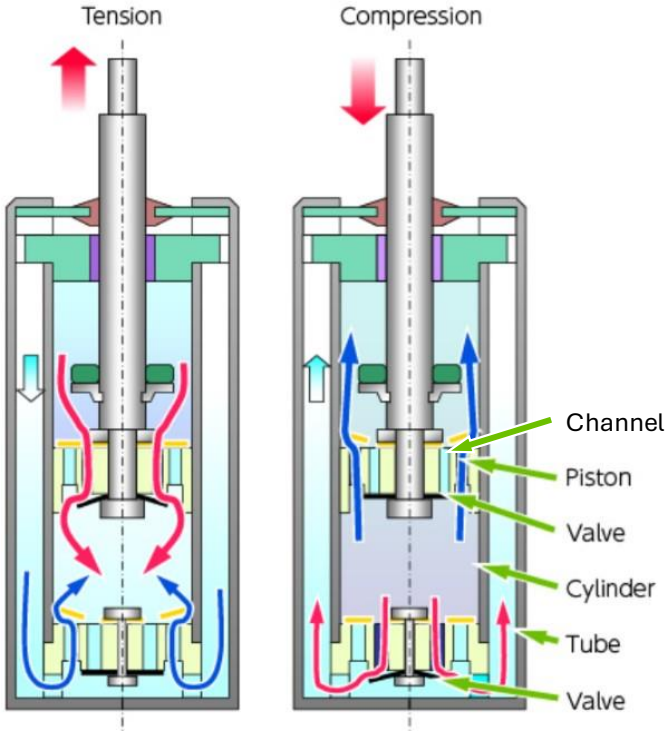

Figure 4: Shock Absorber Working Scheme [5]

Oil flow is limited inside the channels. As the shock absorber is a closed system, the oil is pushed to pass through the valve. During this flow, a resistance force is generated in the piston valve and thus in the piston rod. As long as the shock absorber provides this resistance force, it continues to absorb energy. For the resistance force to be correct, the oil flow must be continuous and smooth. Any interruptions in oil flow will prevent the resistance force.

Cross-sectional exchange may be high at the inlet and outlet of the channels. In this case, cavitation may occur. Cavitation can be called as bubbling in hydraulic flows. It is caused by rapid pressure drop at the inlet and outlet of narrow channels. In this case, air bubbles pass through the channels. In figure 5, cavitation is shown as a symbolic representation. There is no resistance force in the valves because the oil flow is disturbed. This is undesirable.

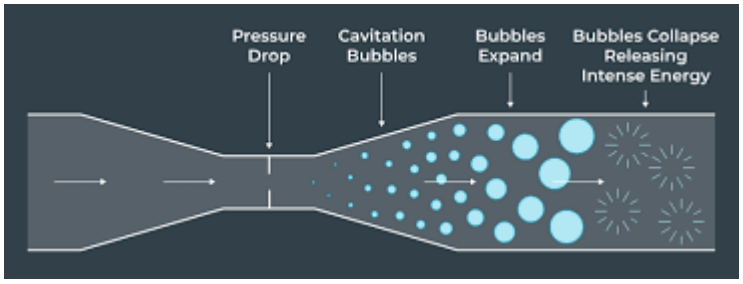

Figure 5: Cavitation in the flow due to the narrowed channel [6]

To eliminate this, gas is added into the shock absorber. The gas increases the pressure inside the shock absorber. This prevents rapid pressure drops.

2.1 Test Method

After the shock absorber has been tested for performance, a force-displacement graph is created. By analysing this graph, an idea about the shock absorber can be obtained. Cavitation can be recognised from the graph. If the graph obtained as a result of the test is distorted, cavitation has occurred. Figure 6 shows a sample graph resulting from the test.

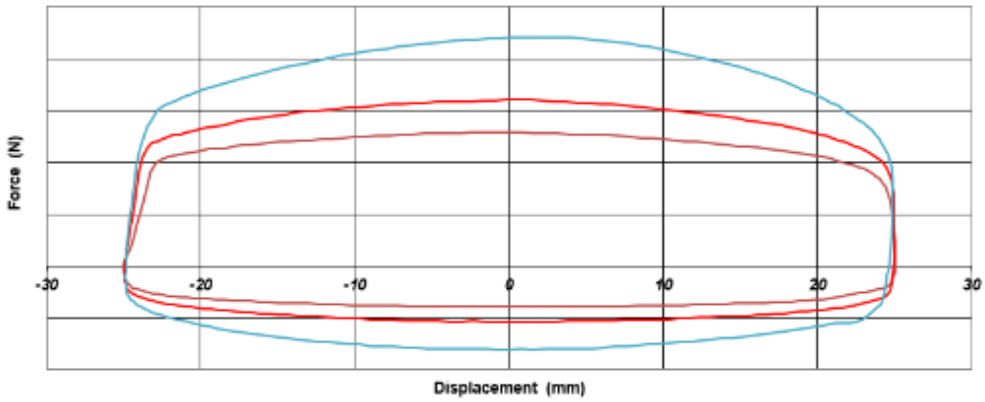

Figure 6: Shock Absorber Force-Displacement Graph

The given example graph occurs when the shock absorber works correctly. If cavitation occurs, distortions will be seen at the endpoints on the x-axis of the graph.

When the graph is analysed, for a complete cycle, the area inside the line shows the absorbed energy. When cavitation occurs, this area will decrease and the absorbed energy will reduce.

The devices used during the test are MTS brand and have a hydraulic load capacity of 50 kN. shock absorber test scheme is as in figure 7.

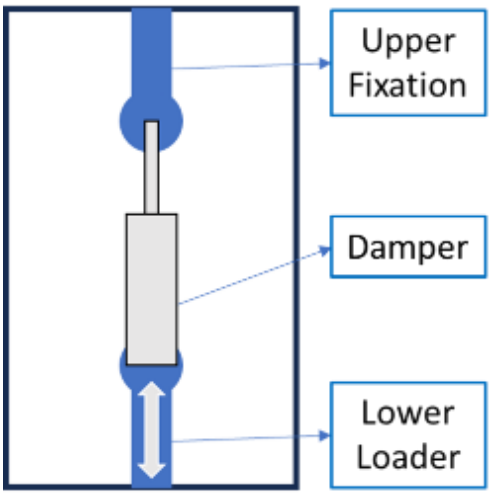

Figure 7: Test Scheme

The shock absorber is fixed at the upper connection point as shown in the test diagram. From the lower connection point, loading can be applied the vertical direction. This loading can be force controlled, velocity controlled or displacement controlled. The test method used in this study is velocity controlled test. The velocity values used as input in the test are as shown in table 1.

Table 1: Velocity inputs used in the test

	Vertical Velocity		
0,05 m/sn.	0,1 m/sn.	0,3 m/sn.	0,6 m/sn.

2.2 Design

The gas pressure in the sample shock absorber produced for test purposes must be adjustable. This is provided by a valve connected to the body. The valve is used to add gas into the shock absorber or to release gas from the shock absorber. The example shock absorber shown in figure 8. The test dampers can also be adjustable.

Figure 8: Test Damper

Gas pressure inside the shock absorber can be controlled by the valve added to the shock absorber. Cavitation can be prevented with gas added to the shock absorber. In this study, the effects of different gas pressures on cavitation were investigated. The gas pressures were 0, 1, 2, 3 and 4 bar. After these tests, the optimum gas pressure will be obtained.

3. TEST RESULTS

The test results at successively increasing pressures are given in the images below.

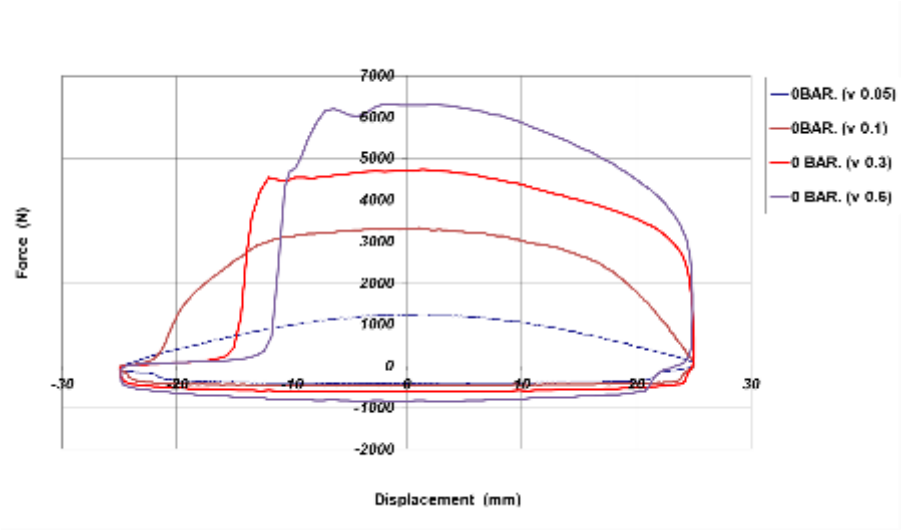

Figure 9: Test Results for 0 Bar Gas Pressure

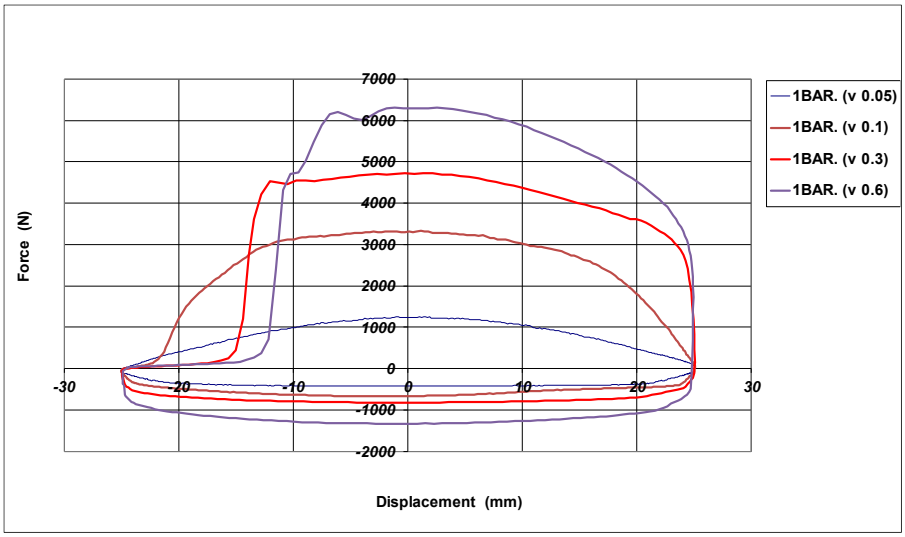

Figure 10: Test Results for 1 Bar Gas Pressure

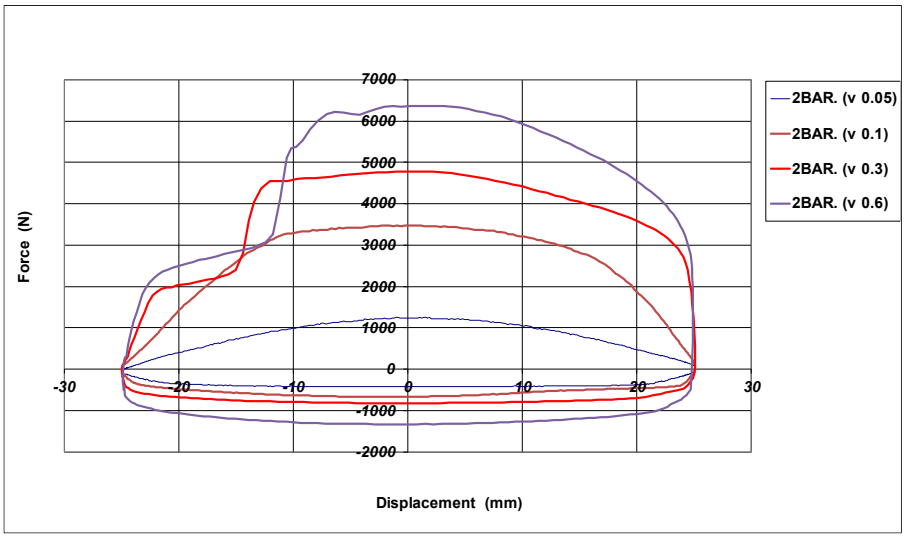

Figure 11: Test Results for 2 Bar Gas Pressure

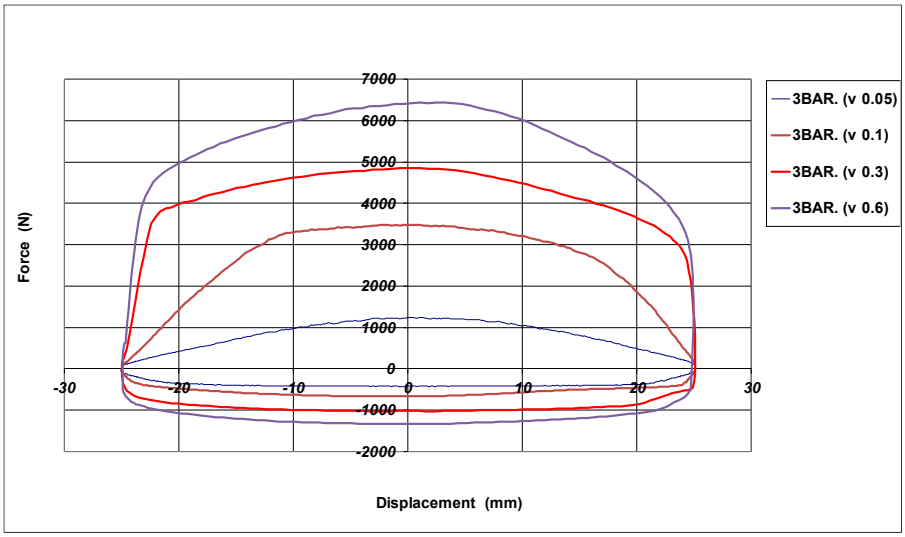

Figure 12: Test Results for 3 Bar Gas Pressure

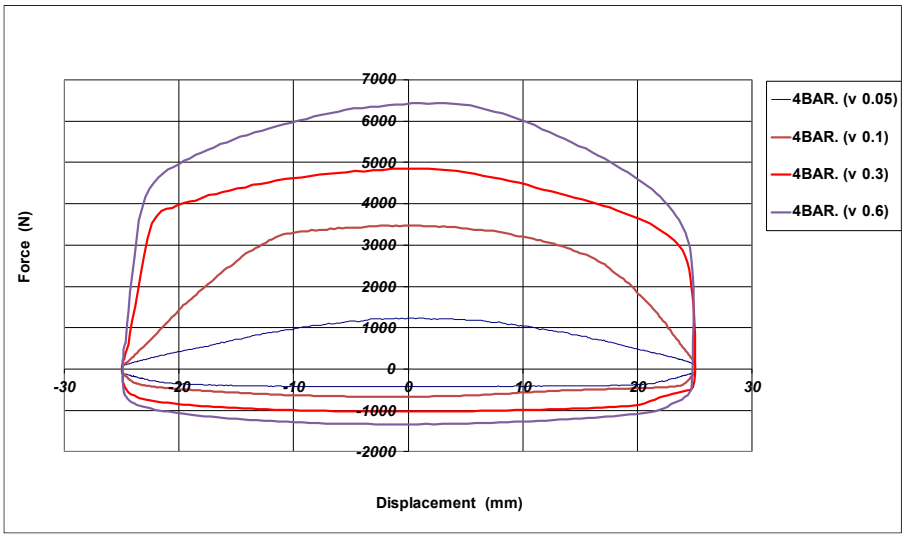

Figure 13: Test Results for 4 Bar Gas Pressure

4. CONCLUSION

Cavitation occurs in the compression and expansion phases in the non-gas shock absorber. When 1 bar pressurised gas was added, cavitation in the compression phase was eliminated. However, cavitation in the rebound phase continues. When increased to 2 bar pressure, cavitation in the rebound phase is eliminated at low speeds. However, cavitation continued to decrease at high speed. When 3 bar pressurised gas was added, cavitation was completely prevented. Cavitation was eliminated in compression and rebound phases. The shock absorber can work at full capacity. When we increase to 4 bar pressure, no advantage is provided except a very low increase in maximum damping force. As the process time and cost will increase as the pressure increases, 3 bar is determined as the optimum pressure.

3 bar gas was pressurised and cavitation was completely prevented. It is possible to perform this study with different types of shock absorbers. It is necessary to determine whether the gas pressure depends on the dimensions of the shock absorber. In the next study, gas will be added to shock absorbers of different sizes and different stiffness. As a result of that study, it is possible to have more information.

REFERENCES

[1]. Bakanlığı, T.M. E. (2013). Motorlu Araçlar Teknolojisi-Süspansiyon Sistemleri.
[2]. Putgül, Y., & Altıparmak, D. (2016). Taşıt süspansiyon sistemi çeşitleri ve ön düzen geometrisine etkileri. Gazi Üniversitesi Politeknik Dergisi, 19(2), 195-202.
[3]. Btg Maslak. (2017). Araçlarda Süspansiyon Nedir? Ne İşe Yarar? Nasıl Çalışır?.
Access Date: 14.10.2024
https://www.btgmaslak.com/araclarda-suspansiyon-nedir-ne-ise-yarar-nasil-calisir/
[4]. Makine Eğitimi. (2018) . Amortisör arızası nasıl anlaşılır. Amortisör arıza tespiti.
Access Date: 14.10.2024
https://www.makinaegitimi.com/amortisor-arizasi-nasil-anlasilir/
[5]. Motorcyclespecs. (2024). Shock Absorber
Access Date: 14.10.2024
https://www.motorcyclespecs.co.za/Techinicale/Shock_Absorber.html
[6]. Tribonet. (2023). Cavitation
Access Date: 14.10.2024
https://www.tribonet.org/wiki/cavitation/

ICENS 10TH INTERNATIONAL CONFERENCE ON ENGINEERING AND NATURAL SCIENCE
October 02-06 2024 Sarajevo (Hybrid Event)

Numerical Simulation of Mass Transfer Mechanism of Stratospheric Solar Powered Telecommunication Balloons

Öznur Kayhan[1]

Abstract

Stratospheric balloon systems, which have the ability to fly for longer periods of time such as months or even a year in 20 km or higher layers of the atmosphere, have been an elusive goal to achieve in recent years. It is critical issue to solve the energy problem of stratospheric balloon to operate at target altitudes for extended durations. As an ideal alternative, solar power units are supplied to the balloons by mounting them on the balloon's envelope and classified as solar powered balloons. This method can cause the buoyant gas inside the balloon to overheat and pressurize, leading to further gas leakage from the balloon's polymeric material. In this investigation, the mass transfer model of a solar-powered zero-pressure balloon has been built up and simulated in Fortran via iterative techniques for the first time in literature. The simulation has been run for solar powered balloon flight under one of the cities of Turkey's real atmospheric conditions including solar radiation flux and wind velocities. The temperature variation of interior helium and mass transfer coefficient and diffusion coefficient with thermal effect have been observed and compared with the unpowered balloon in summer atmospheric conditions. The maximum temperature, mass transfer coefficient and diffusivity of the interior helium for solar powered and unpowered balloon is obtained as 350.51 K, 1.74 x 10^{-2} m/s, $0.83x10^{-8}$ m/s^2 and 310.49 K, $1.48x10^{-2}$ m/s, $0.78x10^{-8}$ m/s^2 respectively. These results will be helpful to design the solar powered balloon systems to stay at higher altitudes for longer durations.

Keywords: Mass Transfer, Diffusion, Solar Energy, High Altitude, Zero Pressure Balloons

1. INTRODUCTION

Stratospheric balloons filled with helium or hydrogen as lift gases generally reach between 18.0 km and 36.5 km altitude or even higher providing a unique vantage point for civilian applications as a low cost alternative telecommunication platform to satellite, a continuous wide area coverage for key areas of interest for observation for the military, carrying equipments of several tons to desired altitude of the stratosphere for scientific experiments. Therefore, the ability to control balloons for long durations of years at high altitude has been attractive goal for many years. Renewable based power system is required to keep the balloon at high altitudes for extended duration. Solar energy is the ideal power choice for stratospheric platforms and this type of power system is a photovoltaic (PV) array coupled to an energy storage system. During daytime, the PV array converts solar energy into electrical energy by photoelectric and photochemical effects. During night, the energy storage system provides power to the balloon [1-3].

The PV can be positioned separately from the balloon as a load or mounted within the balloon envelope as seen in the Fig.1 [4]. When the photovoltaic panel is placed on the balloon's envelope, the heat transfer from the panel to the balloon envelope can cause the superheating and over-pressure of the balloon which affects the reliability, and duration of the balloon [5] and superheating effect on mass transfer mechanism should be investigated to predict the leakage amount of lifting gas through the balloon's polymeric material before launch. In recent years, the energy problem and thermal performance of high-altitude unmanned vehicles has been analyzed by some researchers but there is no research for mass transfer mechanism of the solar powered balloon in real field. Some researchers have neglected the variation of the inner pressure of helium as a lifting gas and regarded total volume as constant during the flight.

[1] *Corresponding author: Gebze Technical University, Department of Chemical Engineering, 41400, Gebze/Kocaeli, Turkey.* okayhan@gtu.edu.tr

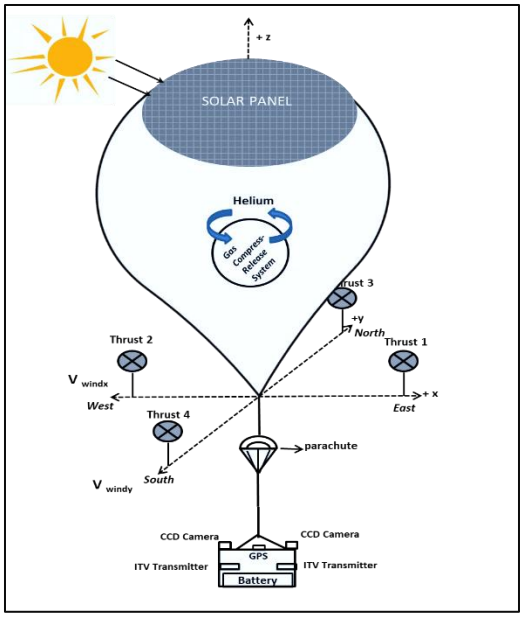

Figure 1. A sketch of the solar powered balloon system

In this research, solar-powered zero-pressure balloons based on a gas compress release system has been studied to analyze the effect of the thermal environment on the mass transfer mechanism in real regions. The mass transfer model of a solar-powered zero-pressure balloon has been built up and simulated in Fortran via iterative techniques with real time.

2. MASS TRANSFER MECHANISM

In stratospheric balloons, the inner gas leaks out through the balloon material over time. The mass and the number of moles of inner gas are obtained by calculating the escape of the gas. The mass transfer mechanism of gas can be shown schematically on a balloon film of Δx thickness, as in Fig.2.

Considering Fig. 2 for small wall thicknesses, the gas flux equation is given by the following equation:

$$N_A = k_{ci}\left(C_{ib} - C_1\right) = D_{ABre}\frac{\left(C_1 - C_2\right)}{\Delta x} = k_{co}\left(C_2 - C_{out}\right) \quad (1)$$

where "N_A" denotes the lifting gas flux (kmol/m^2. s), "k_{ci}" and "k_{co}" denotes the convective mass transfer coefficient at the inside and outside of the balloon surface, "D_{ABre}" denotes the real effective molecular diffusivity (m^2/s), "C_1" and "C_2" denotes lifting gas concentration (kmol/m^3) at the inside and outside of the balloon wall, "C_{ib}" and "C_o" denotes the inside and outside concentration of the lifting gas (kmol/m^3).

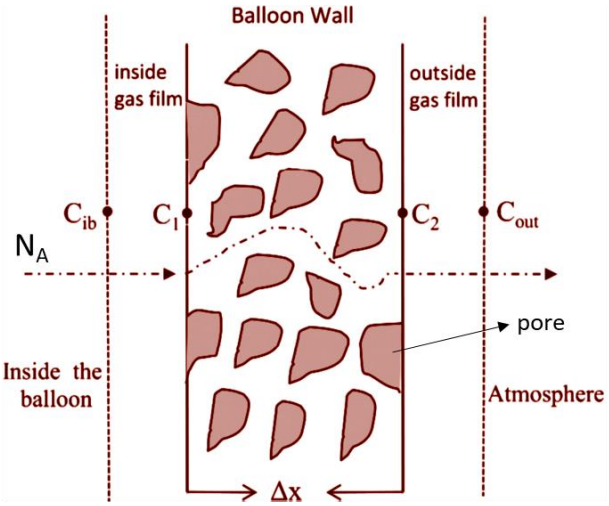

Figure 2. Mass transfer mechanism of gas through the balloon film.

From Eq. (1), differential leakage amount of the lift gas can be obtained as follows

$$dn_A = N_A A dt \tag{2}$$

where "A" is effective heat and mass transfer area, "dt" is time step. Real effective diffusion coefficient, (DAB_{re}) is a parameter that critically affects the transfer rate. Molecular diffusivity in a gas can be calculated from the Chapman–Enskog equation [6,7]

$$D_{AB} = \frac{1.8583\times10^{-7}T^{3/2}}{P\sigma^2\Omega}\left(\frac{1}{M_A}+\frac{1}{M_B}\right)^{1/2} \tag{3}$$

where "D_{AB}" is molecular diffusivity (m^2/s), "M_A" and "M_B" are molecular weight of lifting gas and air, (kg/kmol) , "P" is pressure (Pa), "T" is temperature (K). Balloon walls are made of porous material. Considering gas diffusion through the porous solid material, effective diffusivity (D_{ABe}) is calculated by [8]

$$D_{ABe} = (\mathcal{E}/\mathcal{T})\, D_{AB} \tag{4}$$

In porous structures, if the mean free path is larger than the pore size, the form of molecular transfer is Knudsen flow. In this case, molecules will collide with each other and the walls of the medium. Therefore, there will be a transition from molecular diffusion to Knudsen diffusion and Knudsen diffusion will be dominant and be calculated by Eq.(5) [9]

$$D_{KA} = \frac{2}{3} r_p \sqrt{\frac{8R_u T}{\pi M_A}} \tag{5}$$

where "D_{KA}" is knudsen diffusivity (m^2/s), "r_p" is pore radius (m). The effective diffusion coefficient is calculated by taking into account the effective Knudsen in Eq.6 and the real diffusion coefficient is calculated by Eq.7 [10]. Thus, the effect of Knudsen diffusion is reflected in the mass transfer mechanism.

$$D_{KAe} = (\varepsilon/\tau)\, D_{KA} \tag{6}$$

In the Eq.(6) "ε" represents porosity of balloon wall material and "τ" represents tortuosity.

$$\frac{1}{D_{ABre}} = \frac{1}{D_{ABe}} + \frac{1}{D_{KAe}} \tag{7}$$

Convective mass transfer coefficients "k_{ci}" and "k_{co}" are calculated by using dimensionless numbers from [11,12]

$$k_C = \frac{D_{AB}}{D}\left(2 + 0.6\, Re^{0.5}\, Sc^{0.33}\right) \qquad 1 \leqslant Re \leqslant 48{,}000 \;\; 0{,}6 \leqslant Sc \leqslant 2{,}7 \tag{8}$$

3. NUMERICAL METHOD

The solar-powered zero-pressure balloon-assisted gas compress release system is developed and coded by combining some subroutines such as transport phenomena (momentum, mass, and heat transfer) by using scientific software (FORTRAN). The iterative technique as a numerical method is used to solve the system. For the examination of the mass transfer performance of solar-powered zero-pressure balloons in real atmospheric conditions, Erzurum the city in Turkey has been determined as a flight station. As a summer day 14th day of August have been chosen for simulation. The balloon system has managed to reach the desired altitude of 16.785 km for the available wind data reason. To resist the wind drag acting on the solar-powered balloon system, thrust power is supplied to manipulate the wind force to establish station keeping.

In this research, the leading numerical program consists of subroutines to solve the mass transfer model of the solar-powered balloon is shown schematically in Fig.3, and design parameters are listed in Table 1. The differential equation of temperature changes in the program has been solved by an initial value method named the Euler method which calculates T at time step (t+1).

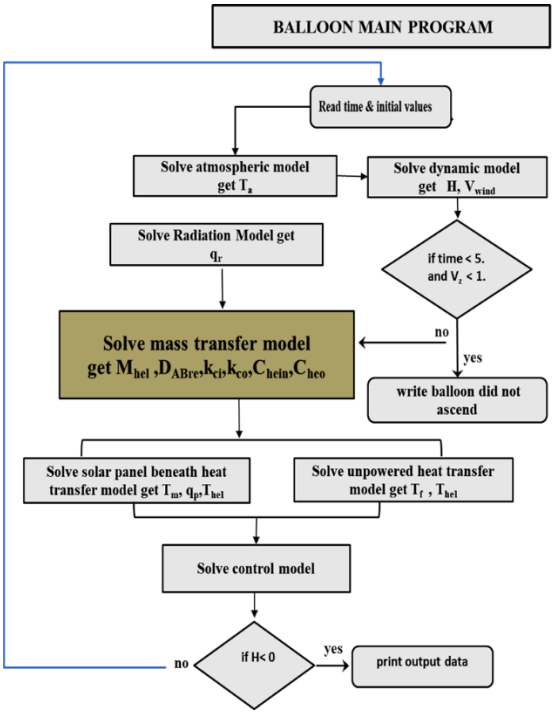

Figure 3. Balloon Main Program Flow Chart

Table 1. The design parameters of the solar powered balloon

Balloon		Solar Panel	
Volume, m^3 (max)	20,135	Absorptivity	0.9
Diameter, m (max)	33.754	Emissivity	0.9
Envelope area, m^2 (max)	3579.22	Type Flexible thin film amorphous silicon	
Absorptivity of envelope	0.33	Conversion efficiency	%7.5
Emissivity of envelope	0.8	Temperature coefficient, % 1/K	0.01
Thickness, mm	0.8	Thickness, mm	0.2
Helium Weight , kg 500 Stored Helium Weight, kg 500 Equipment Weight, kg 500			

4. RESULTS AND DISCUSSION

Fig.4 depicts the simulation of the mass transfer model results during day-night cycle of the solar powered baloon flight at the target altitude. It can be seen from the Fig. 4, when temperature of helium increases and reaches to the maximum value at noon time, molecular diffusivity of the helium through the balloon wall (DAB_{re}) and mass transfer coefficients of helium through the wall (k_{ci}) and mass transfer coefficient of helium (k_{co}) through the atmosphere increases and reaches maximum values of 16.75x 10^{-8} m^2/s, 1,09x10^{-2} m/s, 1.8 x 10^{-2} m/s,respectively as seen in the Table 2.

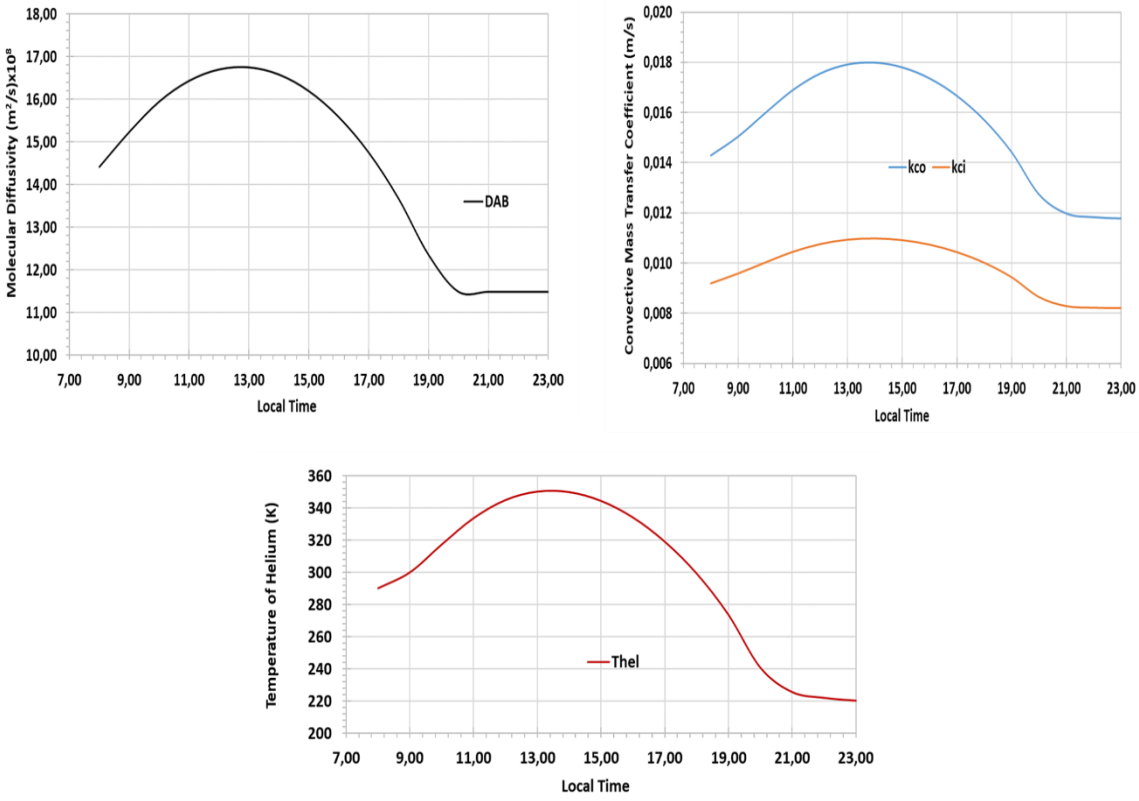

Fig.4. Mass Transfer output of 14th August flight at 16.785 km

To obtain longer flight duration, mass transfer coefficient and diffusivity of helium could be reduced by reducing the "ε/Ƭ". In real flight by the help of compress-release cycle of the helium, when the "ε/Ƭ" decreased from the 2.25x 10^{-4} to 1,125x10^{-4}, the flight time could be increased 95 hours as seen in the Figure 5 and Table 2 and for longer duration as 26 days, "ε/Ƭ" should be available as 4.9 x 10^{-5}.

Table 2 Mass Transfer output data of August flights at 16.785 km

		32 Hours Flight at 16.785 km altitude				
Launch Day :14 th August	Local Time	T_{hel} (K) (max)	K_{co} (m/s) x 10^2 (max)	K_{ci} (m/s) x 10^2 (max)	D_{ABre} (m^2/s) x 10^8 (max)	(ε/Ƭ)x 10^4
solarpowered balloon	*13:00*	*350,51*	*1,80*	*1,09*	*16,75*	*2,25*
unpowered balloon	*13:00*	*310,31*	*1,60*	*1,00*	*16,75*	*2,25*
		127 Hours Flight at 16.785 km altitude				
		T_{hel} (K) (max)	K_{co} (m/s) x 10^2 (max)	K_{ci} (m/s) x 10^2 (max)	D_{ABre} (m^2/s) x 10^8 (max)	(ε/Ƭ)x 10^4
solarpowered balloon	*13:00*	*350,53*	*1,75*	*1,07*	*4,19*	*1,125*
unpowered balloon	*13:00*	*310,46*	*1,55*	*0,98*	*4,19*	*1,125*
		26 Days Flight at 16.785 km altitude				
		T_{hel} (K) (max)	K_{co} (m/s) x 10^2 (max)	K_{ci} (m/s) x 10^2 (max)	D_{ABre} (m^2/s) x 10^8 (max)	(ε/Ƭ)x 10^5
solarpowered balloon	*13:00*	*350,46*	*1,74*	*1,06*	*0,83*	*4,9*
unpowered balloon	*13:00*	310,49	1,48	1,00	0,78	*4,9*

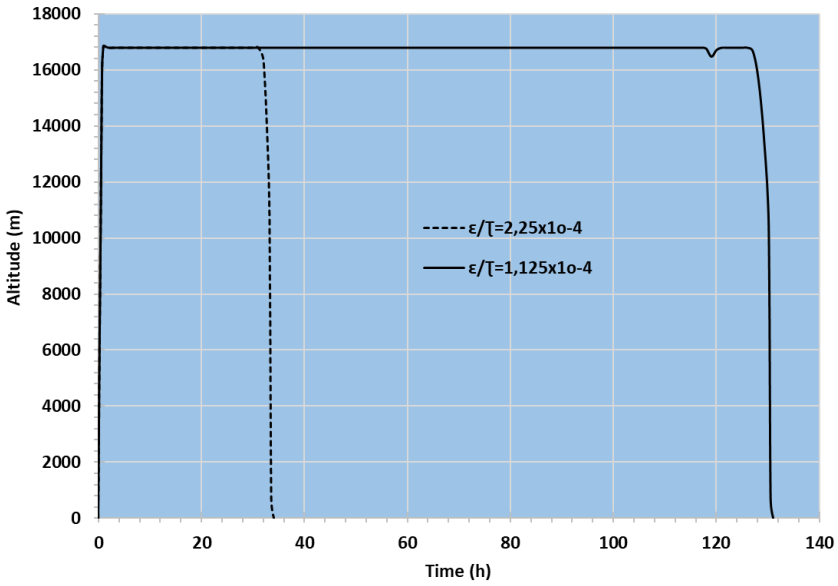

Figure 5. Trajectory of Balloon Flights

5. CONCLUSION

The flight time of solar powered balloon is a strong function of the real effective diffusion coefficient of lifting gas, "D_{ABre}" and porosity tortusity ratio, "ε / Ʈ" of balloon wall material. Compared with the unpowered balloon, the temperature variation of internal helium of the solar powered balloon is not notable for diffusivity of lifting gas during the day night cycle of the flight but it slightly effects the convective mass transfer coefficients, "k_{ci},k_{co}" of the lifting gas. Up to the present, there is no study of mass transfer performance of solar powered zero pressure balloon to observe and control the helium lekage through the balloon wall. In conclusion, the outcomes of this research would be beneficial to plan solar energy system to keep the balloon at target altitude for months, even years. Future work involves doing the mass transfer experimentally and validate the result with the proposed mathematical mass transfer model.

REFERENCES

[1] Ö. Kayhan and M.A. Hastaoğlu, Modeling of Stratospheric Balloon Based on Transport Phenomena and Gas Compress -Release System, Journal of Thermophysics and Heat Transfer, vol. 28, pp. 534-541, 2014.
[2] Ö. Kayhan, Ö. Yücel, M.A. Hastaoğlu , Simulation and Control of Serviceable Stratospheric Balloons Traversing a Region via Rransport Phenomena and PID, Aerospace Science and Technology, vol. 53, pp. 232-240, 2016.
[3] Ö. Kayhan, A thermal Model to Investigate the Power Output of Solar Array for Stratospheric Balloons in Real Environment. Applied Thermal Engineering, vol. 53, pp.113-120, 2018.
[4] Ö. Kayhan, Effect of Thermal Environment on Heat Transfer Mechanism of Solar Powered Balloon, Journal of Thermophysics and Heat Transfer (2024), accessed Oct 23, 2024: https://doi.org/10.2514/1.T6896
[5] Q. Liu,, Y. Yang,, Y. Cui,, J. Cai,, Thermal Performance Analyses of Stratospheric Airship with Photovoltaic Array, *Advances in Space Research*, Vol. 59, pp. 1486-1501, 2017.
[6] S. Chapman, and T. G. Cowling, "Mathematical Theory of NonUniform Gases," Cambridge Univ. Press, 1970, pp. 176–267.
[7] J. O Hirschfelder, C. F. Curtiss,, and R. B. Bird, Molecular Theory of Gases and Liquids, Wiley, New York, 1964, p. 539.
[8] M. A. Hastaoglu,, "Transient Modeling of a Packed Tower: Mass and Heat Transfer with Reaction," Fuel, Vol. 74, No. 11, pp. 1624– 1631, 1995.
[9] J. M. Thomas, and W. J. Thomas,, Principles and Practice of Heterogeneous Catalysis, VCH Publishers Inc., New York, 1997, pp. 294.
[10] W. E., Stewart, and M. F. L. Johnson,, "Pore Structure and Gaseous Diffusion in Solid Catalysts," Journal of Catalysis, Vol. 4, No. 2, 1965, pp. 248–252.
[11] W. E., Ranz, and W. R., Marshall, "Evaporation from Drops, Part I," Chemical Engineering Progress, Vol. 48, No. 3, 1952, pp. 141–146
[12] W. E., Ranz, and W. R., Marshall, "Evaporation from Drops, Part II," Chemical Engineering Progress, Vol. 48, No. 4, 1952, pp. 173–l80.

ICENS 10TH INTERNATIONAL CONFERENCE ON ENGINEERING AND NATURAL SCIENCE
October 02-06 2024 Sarajevo (Hybrid Event)

Is Plant-Based Milk a Functional Beverage?

***Rabia Serpil Günhan*[1]**

Abstract

Increasing demand for healthy food alternatives has a significant impact on the beverage market. The search for functionality in beverages makes plant-based milks gain importance in the food industry in the world and in our country. Cows' milk is highly valued for its high content of nutritional components such as protein, minerals, fat and sugar. However, plant-based milks are an alternative for person who are lactose intolerant, worried about calories, or allergic to animal milk. They come in varieties such as soybean, oat, almond, coconut, hemp seed. Plant milks are beverages obtained by dissolving cereals, semi-cereals, legumes, oil seeds, nuts in water and then homogenizing the liquids. The level of components such as carbohydrate, protein and fat content of plant-based milks varies according to the processing technique used. The nutritional properties of different plant-based milks also vary greatly. Plant-based milks are especially preferred for vegan diets, while they are beverages with lower protein quality and sweetened with added sugar compared to cow's milk. In order to obtain a product with a nutritional content close to cow's milk, plant-based milks need to be enriched (e.g. by the addition of proteins, enzymes...). It can be a functional beverage alternative, especially when cow's milk needs to be replaced in the diet due to health problems. Processing methods based on consumer preferences and functional properties are very important in the development of plant-based milk. In this review, the importance of plant-based milk, nutritional profiles, processing steps, its place in the functional beverage market and differences with cow's milk are explained.

Keywords: Cows' milk, Functional Beverage, Vegetable Milk,

1. INTRODUCTION

Plant-based milk-like beverages continue to rise rapidly in the functional food sector. Milk-like beverages derived from plants such as soy, oats, rice, hazelnuts and almonds are also called 'MILK'.Plant-based milk-like drinks often look like cow's milk, but their qualities are completely different functional beverages developed according to the changing lifestyle of the society have become the favorite subject of the last period. These drinks have functional properties such as boosting energy, fighting aging and relieving fatigue. Plant-based milks are an alternative for people with problems such as lactose intolerance and cow's milk allergy.

The estimated growth of the BSA market is reported to be 15% by 2018, reaching a value of $14 billion and will exceed $26 billion by 2023 [18]. However, according to the latest data, the increase was higher than expected. The plant-based milk market size is valued at USD 35.0 billion in 2021, USD 40.3 billion in 2022 and is expected to reach USD 123.1 billion by 2030[1].

2. WHAT IS PLANT-BASED MILK?

Plant-based milks are water-soluble extracts of legumes, oilseeds, cereals and nuts [2]. Plant-based milks are products that resemble milk in appearance that are obtained by grinding various plant sources such as cereals, legumes, oilseeds, etc. and mixing them with water, then filtering and homogenizing the part that passes into the water and determining its content, and are products that resemble milk in appearance. Plant-based milks contain functional properties, rich bioactive compounds, macronutrients, micronutrients and phytochemicals with health-promoting effects ([3]- [4]). The Food and Drug Administration (FDA) considers plant-based milks to be "imitation milk" or "imitation dairy products" that are similar to milk in flavor, aroma, texture, texture and appearance, but nutritionally inadequate.

[1] *Corresponding author: Konya Technical University,Vocational High School of Technical Sciences, Department of Food Technology, Konya, Turkey.* rsgunhan@ktun.edu.tr

Plant-based milk is classified according to the raw materials used. Although there is no standard category of plant-based milk in the literature, the widely accepted classification of plant-based milk is as shown in Table 1.

Table 1. Plant-based milk classification [5]

Origin	Plant-based Milk
Legumes	Soybean, Chickpea, Kidney Bean, Lupin, Pea, Cowpea, Peanut
Cereals	Corn, Rice, Spelt, Sorghum, Rye, Wheat
Nuts	Almond, Coconut, Pistachio, Walnut, Hazelnut
Seeds	Flax, Sunflower, Hemp, Sesame
Pseudocereals	Teff, Amaranth, Quinoa,

2.1. Plant-based milk production

The processing method of plant-based milk production is determined by the raw materials used and the desired target product. In general, several steps as shown in Figure 1such as soaking, grinding, separation, formulation of ingredients, homogenization, heat treatment and packaging ([5],[6]-[12]). Raw materials may require pretreatment to ensure or improve extraction, enhance nutritional quality, improve sensory properties and/or eliminate off-flavors [2]. Pre-treatments include shelling and soaking. This is done in water for 3-18 hours for cowpeas, cashews, soybeans, oats and sesame, and in alkaline solutions for soybeans, peanuts, beans and hazelnuts. It is also used as a pretreatment for blanching to remove the almond skin and remove the aroma of peanuts, and fermentation to improve the nutritional properties of soybeans, almonds, rice, oats and beans [2]. The first pre-treatment in plant-based milk production is soaking. This process helps the optimum extraction process by swelling and softening the outer layer shell of cereals, legumes and nuts. It increases extraction efficiency. Soaking is also useful for reducing the initial microbial load, inactivating enzymes, removing off-flavors, improving sensory properties and enhancing nutritional quality [5]. In plant-based milk production, extraction is very important on the composition of the products obtained. To increase efficiency, pH is increased using NaOH or bicarbonate, temperature is raised or enzymes are used [2]. In general, water, emulsifiers and additives are the most common ingredients used in plant-based milk formulation after the raw material. Water quality, in terms of water hardness and pH, is very important in plant-based milk production [7]. To improve the nutritional quality, bioavailability and shelf life of plant-based milk, food additives are added to its formulation. These additives include vitamins, minerals, stabilizers, colorants, emulsifiers, sweeteners, salts and preservatives [5].

Homogenization process reduces the size of particles, prevents the formation of lipid droplets and increases stability ([5]-[2]). Heat treatment is the most important processing step of plant-based milk. Heat treatments destroy pathogens and other spoilage-causing microorganisms and inactivate enzymes ([8]-[2]). The shelf life of plant-based milks mainly depends on the raw material, production process, emulsion stability, thermal and/or non-thermal treatments applied, packaging and storage temperature [2].

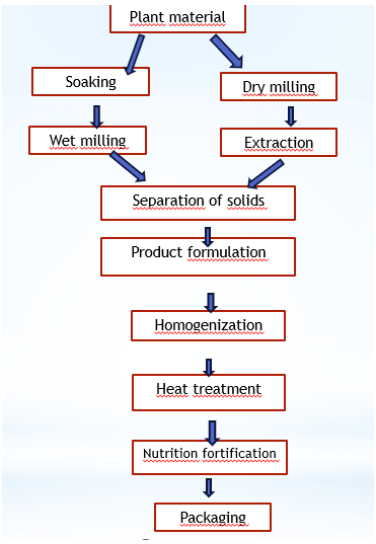

Figure 1. Production flow chart of Plant-based milk

2.2. Plant-based milk varieties

Rice milk can be made from white or brown rice. But it is possible to improve it in plant-based milks based on red rice. Black rice has high phenolic content and antioxidant capacity [19]. Rice is rich in carbohydrates and therefore has a sweet taste. Consumption of rice milk causes malnutrition as it is low in protein, lipids, vitamins and minerals. However, rice milk has a high selenium and magnesium content, which helps boost immunity [4].

Oat milk has gained importance due to its rich nutrient composition. Its soluble fiber content has beneficial health effects such as reducing weight, blood sugar, cholesterol and triglyceride levels. It is also recommended as a milk alternative for those with irritable bowel syndrome (IBS) and inflammatory bowel disease (IBD). The disadvantage of oat milk is the presence of phytic acid/ phytate- antinutritional factors in oats that prevent the absorption of some essential nutrients [4].

Soy milk has a similar nutritional composition to cow's milk. . It is a good source of macro and micronutrients. It should be noted that people with cow's milk protein allergy are also more likely to have a soy allergy. It contains some antinutritional components such as trypsin inhibitor, phytates, oxalates, which form an insoluble complex and inhibit mineral absorption [4].

Almond milk has 50% fewer calories than cow's milk and is becoming increasingly popular because of its low calorie content. Almond milk is reported to increase the flow of blood, oxygen and nutrients and maintain blood pressure [4].

Coconut milk is richer in calories and fat compared to cow's milk and other plant-based milks. It contains lauric acid, which strengthens the immune system. Coconut milk consumption can reduce the risk of cardiovascular diseases and stroke due to the presence of lauric acid. It also contains some phenolic compounds and has antioxidant properties (Vit E) [9]. As in this article [20], the milk developed based on chickpea and coconut, showed a good nutrient composition (such as protein, calcium and lipid content) compared to other plant-based milks. Therefore, chickpea and coconut-based plant milk could be a potential substitute for cow's milk considering the nutritional quality aspects, acceptability and low allergenicity.

Hemp seed milk is one of the important seed-based dairy products and is produced from industrial hemp. Hemp seed milk has been found to contain approximately 0.83-4% protein, 1.25-3% fat and 2.5-20% carbohydrates. There is potential in plant-based milk varieties such as quinoa milk. Quinoa protein is an interesting raw material to study further due to its balanced amino acid profile and high biological value [9].

Studies have suggested that blends of two or more plant-based milks improve nutritional or sensory properties. For example, an almond-soy milk blend improves sensory quality, a peanut-cowpea milk blend balances energy supply and improves flavor, and a soy-corn blend improves nutritional components [2].

2.3. The importance of processing method in plant-based milk

Pre-treatment of raw materials is an important processing step that affects the quality of plant-based milks. In this context, for example, soaking and autoclaving quinoa seeds in saline solution (0.03 mol/L NaCl acidified to pH 5) was reported to increase the protein content of quinoa milk by 36% compared to commercial alternatives [10]. Boiling is necessary to inactivate trypsin inhibitors and lipoxygenases that cause bad flavors in soy milk and peanut milk. Roasting some raw materials enhances the aroma and flavor of the final product (sesame) In the extraction of proteins and/or total solids, papain, β-glucanases, pectinases and cellulases have been shown to significantly increase the yield of peanut milk alternative and soy milk [11]..The time and temperature combinations of heat treatment (pasteurization and sterilization) must be correctly determined and applied. Excessive heating causes loss of nutrients and problems such as undesirable taste-odor and browning in the product.

In order to overcome these problems, the tendency towards non-thermal or innovative heat treatments is increasing [8]. These innovative technologies include ohmic heating, microwave heating, ultrasonic applications, high pressure applications, emphasized electric field applications and ultraviolet technologies [8, 12]. The use of microwave-assisted extraction was found to increase the extraction yield, protein content and protein solubility of soy milk by 24% and 44.44% when compared with the steam infusion extraction method [13].

In plant-based milk processing and formulation, it is important to apply the most efficient and feasible approaches to reduce the need for food additives. Future studies should focus on determining which processing methods are suitable for which plant-based milk types for optimal and effective incorporation into food production and design[14].

2.4. Differences between plant-based milk and cows' milk

Plant-based milks look like cow's milk but are not naturally high in nutrients. It is often enriched with calcium, vitamin D and vitamin B12 to capture the nutritional content of dairy products. Most fortified plant-based beverages are marketed as containing equal or greater amounts of calcium and vitamin D than cow's milk, but the bioavailability of such nutrients varies significantly. The low protein content in plant-based milks makes protein intake inadequate. In general, due to its low protein value and low amino acid content, plant-based milk is not recommended, especially for children in adolescence. The fat content in plant-based milks is also generally very low, with the exception of coconut milk (4.12 g per 100 mL) [5]. Cow's milk contains 3.27 g fat per 100 mL [5]. Sweetened plant-based milks, such as sweetened almond milk, contain added sugar that should be taken into account [1]. In terms of essential minerals Ca, K, Mg, Na and P, cow and goat milk are important sources of essential minerals, while soy and coconut milk are good sources of Mg. It has been stated that soy and coconut milk will contribute to the daily nutrition of consumers in terms of Fe and Cu, coconut milk in terms of Cr and Se, hemp milk in terms of Mo, and cow and goat milk in terms of Se and Zn [15]..Plant-based milks do not contain lactose and cholesterol but have low protein quality [5,4]. It is thought that if these products are used as a protein source instead of cow's milk in the diet, they may cause protein deficiency and serious diseases.

It is important to choose unsweetened to choose healthy plant-based milk. Another study on plant-based milks concluded that these products have an interesting nutritional composition and physico-chemical properties and could partially replace milk and dairy products [16]. Especially for young children, cow's milk remains important in terms of fat, protein and calcium. However, for children struggling with diabetes or obesity, skimmed cow's milk, unsweetened almond milk or oat milk are recommended instead of cow's milk. Children following a strict vegan or vegetarian diet and consuming plant-based milks other than soy milk should be checked to make sure they are consuming enough folate and B12 to prevent micronutrient deficiencies [17].

In general, plant-based milks have lower protein content, calcium availability, higher glycemic index values and the presence of anti-nutritional factors, making them nutritionally inferior to cow's milk. Furthermore, differences in beverage formulations between brands cause significant variability in nutrient composition even among the same plant-based milk.

3. CONCLUSION

*In conclusion, plant-based milks are not an alternative to cow's milk in terms of nutritional value. However, plant-based milks can be enriched with nutrients and can be considered in the functional beverage category as a result of the bioactive compounds, macronutrients, micronutrients and phytochemicals. Of course, the character of the raw material and the processing process should not be ignored the characteristics of the raw material and healthy processing methods.

*Changing lifestyles and increasing concerns about health, animal welfare and environmental impacts suggest that plant-based milks will further increase their market share in the coming years.

*In this context, it is very important for manufacturers to develop products with appropriate raw materials and novel processing technologies instead of adding low-cost supplements and additives.

*Consumers should also be better informed to choose plant-based milks based on their nutritional value and content.

REFERENCES

[1]. Satpal et al., (2023), Plant Based Milk - An Alternative to Nutritional Security, Available:https://agritechmagazine.com
[2]. Reyes-Jurado, F., et al. "Plant-based milk alternatives: Types, processes, benefits, and characteristics." Food Reviews International 39.4 (2023): 2320-2351.
[3]. Aydar, Elif Feyza, Sena Tutuncu, and Beraat Ozcelik. "Plant-based milk substitutes: Bioactive compounds, conventional and novel processes, bioavailability studies, and health effects." Journal of Functional Foods 70 (2020): 103975.
[4]. Velangi, Monal, and Mitali Savla. "Role of Plant Based Milk Alternatives as a Functional Beverage: A Review.", International Journal of Health Sciences and Research, vol.12, 273-281, 2022.
[5]. Romulo, Andreas. "Nutritional contents and processing of plant-based milk: a review." IOP Conference Series: Earth and Environmental Science. Vol. 998. No. 1. IOP Publishing, 2022.
[6]. Mäkinen, Outi E., et al. "Physicochemical and acid gelation properties of commercial UHT-treated plant-based milk substitutes and lactose free bovine milk." Food Chemistry 168 (2015): 630-638.
[7]. Maleš, Ivanka, et al. "The medicinal and aromatic plants as ingredients in functional beverage production." Journal of Functional Foods 96 (2022): 105210.
[8]. Baysan U., (2024), The Importance of Plant-Based Milks in the Food Industry and Ensuring Microbial Safety, Available:https://www.agrifoodscience.com/index.php/TURJAF/article/view/6464
[9]. Beşir, Ayşegül, Nour Awad, and Mustafa Mortaş. "A Plant-Based Milk Type: Hemp Seed Milk." Akademik Gıda 20.2 (2019): 170-181.
[10]. Pineli, Lívia de L. de O., et al. "Low glycemic index and increased protein content in a novel quinoa milk." LWT-Food Science and Technology 63.2 (2015): 1261-1267.
[11]. Mäkinen, Outi Elina, et al. "Foods for special dietary needs: Non-dairy plant-based milk substitutes and fermented dairy-type products." Critical reviews in food science and nutrition 56.3 (2016): 339-349.
[12]. Romulo, A. "Food processing technologies aspects on plant-based milk manufacturing." IOP Conference Series: Earth and Environmental Science. Vol. 1059. No. 1. IOP Publishing, 2022.
[13]. Varghese, Taruna, and Akash Pare. "Effect of microwave assisted extraction on yield and protein characteristics of soymilk." Journal of Food Engineering 262 (2019): 92-99.
[14]. Mehany, Taha, et al. "Recent innovations and emerging technological advances used to improve quality and process of plant-based milk analogs." Critical Reviews in Food Science and Nutrition 64.20 (2024): 7237-7267.
[15]. Astolfi, Maria Luisa, et al. "Comparative elemental analysis of dairy milk and plant-based milk alternatives." Food control 116 (2020): 107327.
[16]. Jemaa, Mariem Ben, et al. "Plant-based milk alternative: nutritional profiling, physical characterization and sensorial assessment." Current Perspectives on Medicinal and Aromatic Plants 4.2 (2021): 108-120.
[17]. Collard, Kalyn M., and David P. McCormick. "A nutritional comparison of cow's milk and alternative milk products." Academic pediatrics 21.6 (2021): 1067-1069.
[18]. Taşpınar, Tansu, Mehmet Güven, and Mehmer Sertaç Özer. "Bitkisel Esaslı Süt Alternatiflerine Genel Bir Bakış." Turkish Journal of Agriculture-Food Science and Technology 11.3 (2023): 587-602.
[19]. da Silva, Luan Ramos, José Ignacio Velasco, and Farayde Matta Fakhouri. "Use of rice on the development of plant-based milk with antioxidant properties: From raw material to residue." *Lwt* 173 (2023): 114271.
[20]. Rincon, Luana, Raquel Braz Assunção Botelho, and Ernandes Rodrigues de Alencar. "Development of novel plant-based milk based on chickpea and coconut." *Lwt* 128 (2020): 109479.

ICENS 10TH INTERNATIONAL CONFERENCE ON ENGINEERING AND NATURAL SCIENCE
October 02-06 2024 Sarajevo (Hybrid Event)

The Importance of Sumac Sour

Rabia Serpil Günhan

Abstract

In the course of healthy life, topics such as the type of foods we consume, their preparation, processing and how we should consume them has gained importance. One of the functional products with increasing importance and awareness is sumac sour. Sumac sour is obtained from sumac fruit containing phenolic compounds, flavonoids, organic acids, tannins, essential oil, anthocyanins and their derivatives. Sumac plant is used in food, pharmaceutical and dye industries due to its bioactive compounds and various phytochemical components such as phenolic compounds. It has high medicinal and nutritional value. It has bioactivities such as antifibrogenic, antifungal, anti-inflammatory, antimicrobial, antimutagenic, antioxidant, antitumorigenic, antiviral, cytotoxic and hypoglycemic. Sumac sour is produced in the traditional method by soaking the sumac (Rhus coriaria) fruit in water, straining the fruit and concentrated the extract in the sun. It is an aqueous extract of sumac fruits. Sumac sour is used to add a sweet/sour flavor to various dishes and salads. Beyond flavoring, it has a strong antioxidant and antimicrobial effect, which allows it to be used as a natural preservative to extend the shelf life of foods. The use of natural preservatives against synthetic preservatives ensures healthy production and consumption. The aim of this review is to emphasize the importance of sumac syrup and to provide awareness to our nutrition and the innovative change and development of the food industry.

Keyword: Functional Food, Sumac, Sumac sour

1. INTRODUCTION

Sumac is cultivated in the Mediterranean and Southeastern Anatolia regions of Turkey. It is widely used as a spice and sauce added to kebabs, grilled meats, salads and soups. Sumac sauce has a sour and fruity flavor. Sumac (Rhus coriaria L.) is a shrub or small tree, 1-3 m high, in clusters with reddish or dark brown, round drupe fruits. Sumac is a plant that grows spontaneously in the natural flora and is widespread in temperate and tropical regions, especially along the Mediterranean, Middle East and West Asian coasts. Sumac is often called "acetic tree because of the sour taste of its fruits and leaves ([1]-[2]). Sumac (Rhus coriaria L), a member of the Anacardiaceae family, is one of the most popular spices in the Mediterranean and Arab countries, obtained by crushing its dried fruits [3]. Sumac has been used in the past as a traditional medicine to treat many diseases (liver disease, ulcers, hemeroid, pain, ophthalmia, stomach tonic, conjunctivitis...) [1].

The sumac plant contains more than 200 biomolecules. The most important of these are hydrolyzable tannins, phenolic acids, anthocyanins and flavonol glycosides [2]. Sumac fruits and leaves collected in autumn are used separately [4]. One of the uses of sumac fruit, which has a highly functional feature, is sumac sour. Although sumac is widely used as a spice, sumac sour is more preferred in the regions where it grows.

This review provides information on what sumac sour is, its production and studies on its importance.

[1] *Corresponding author:Konya Technical University, Vocational High School of Technical Sciences, Department of Food Technology, Konya, Turkey.* rsgunhan@ktun.edu.tr

2. PRODUCTION OF SUMAC SOUR

Various methods are used to obtain extracts from plant raw materials, such as maceration, percolation and other methods. Like other plant extracts, the importance of the extraction process when obtaining sumac extract is indisputable. Extraction efficiency depends on technological factors such as extraction temperature and time, degree of grinding of raw materials, type of solvent, hydromodule (ratio between raw material and solvent) [5].

According to Ref.[6], according to their research, the use of rotary pulse extractors will strengthen the extraction process of extractive substances of vegetable raw materials compared to traditional methods, increase the energy efficiency of the process and create minimal losses of active substances.

The ripening fruits of the sumac plant are used in sumac sour production. In traditional sumac production, 2±250 kg of sumac sour is obtained from 10 kg of fresh sumac. The color of sumac sour is brown or dark pink rose depending on the raw material. The type of sumac, environmental factors, soil characteristics and climate differences may cause differences in the chemical content of sumac [7].

The sumac fruit, which ripens in August and September, is harvested by plucking it from the branch of the plant. Water is added to the sumac fruits separated from the stems and stir until the sourness passes into the water. The sour water is separated from the sumac fruit pulp using a strainer or cheesecloth. The second and third process is repeated four times to minimize the amount of sour remaining in the pulp. The resulting sour water is left to clarify for 7- 8 hours to allow the sediment to settle to the bottom. After the clarification process, the sour water is separated from the sedimented part and left in the sun for 3 to 6 days. Its color is dark burgundy. The sour juice, whose sourness becomes quite sharp, is placed in suitable containers and stored in a cool environment [9]. The production of sumac sour is shown in Figure 1.

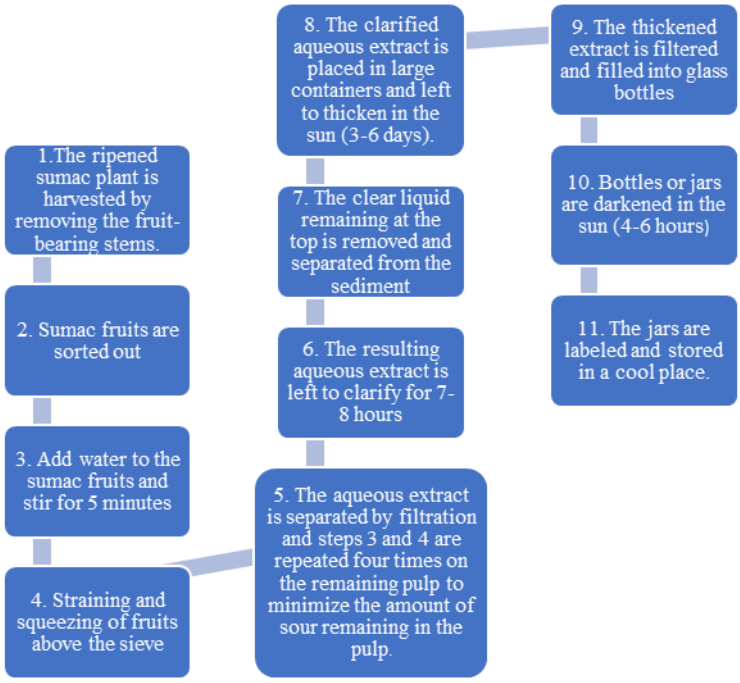

Figure 1. Production flow chart of Sumac Sour [9]

Understanding the rheological properties of liquid foods is essential for quality control, sensory evaluation and design of industrial plants. Ref. [10] investigated the effect of concentration and temperature on viscosity to characterize the rheological properties of sumac extract. It was stated that the viscosity of sumac extracts decreased with increasing temperature, while the activation energy increased with increasing concentration. It was also concluded that viscosity increases nonlinearly with concentration.

Ref. [11] examined some quality parameters of pomegranate sour, sumac sour and grape concentrate samples sold in Kilis market. They reported that they found the highest total phenolics, total flavonoids, ascorbic acid and antioxidant activity values in homemade sumac sour.

Ref. [12] investigated the effect of infrared drying on the qualitative characteristics (total color changes, total phenolic content, organic acids and vitamin C) of sumac fruit. As a result, it was observed that the drying time of sumac fruit was reduced compared to traditional drying methods (shade and sun drying). It was also reported that infrared drying is a suitable method to preserve the phytochemical properties and color changes of sumac fruits.

2.1. The Use of Sumac Extracts

Sumac fruits can be used to make tea or, more commonly, dried and ground into a reddish purple powder that is used as a spice in many countries. Sumac sauce is used in kitchens instead of pomegranate syrup and fruit juice. Sumac extract is dark burgundy in color. In Turkey, sumac sour is used in juicy dishes, especially in salads, bulgur meatballs and dolmas [13].

In North Africa and the Middle East, Sumac is used as a spice or sauce to add a sour and lemony flavor to meat, chicken or fish. It is also added to marinades and added to dishes and salads to enhance their taste and flavor ([14], [15]). Studies show that sumac fruit can be used as a new source of natural antimicrobial and antioxidant substances for the food and pharmaceutical industries [16]. Sumac is reported to have the greatest activity against the food pathogen Staphylococcus aureus. One study reported that among five plants, sumac extracts showed the best antibacterial activity against all microorganisms and was also used as a natural preservative to extend the shelf life of tomato paste [17].

Ref. [18] added sumac powder to fresh carrot juice and investigated its shelf life. It was observed that enrichment of freshly squeezed carrot juice with sumac in an amount not exceeding 3% prevented the growth of microorganisms in the juice during storage and improved the shelf life.

In a study on commercial barley soup, the antimicrobial effect of different concentrations of water extract of sumac (0%, 0.1%, 0.3%, 0.5%, 1% and 2.5%) on Bacillus cereus was evaluated. The results showed that this extract was effective against Bacillus cereus in soup and could be considered as a natural preservative [19].

Ref. [20] investigated the antimicrobial effects of fruit (sumac, pomegranate, plum and Seville orange) sauces on some pathogenic bacteria. Sumac fruits were not subjected to heat treatment during the preparation of sumac sour and kept at room temperature until the residues were visible to the naked eye. The filtrate was then sun-dried until it reached a dark color, then filtered and bottled. Sumac sauce was found to have the highest antimicrobial activity on chilled chicken breast.

Ref. [21] investigated the effect of sumac juice extract, thyme oil and lactic acid on the microbial quality and shelf life of chilled rabbit meat. Sumac and lactic acid were found to extend the shelf life of rabbit meat by 3-6 days in the refrigerator at 2 ± 1 °C. The sumac juice was reported the highest extract group about sensory acceptability by the panelists.

In another study, the effect of sumac juice extract on the quality and safety of chilled minced meat was investigated. It was reported that microbial contamination was minimized during storage and shelf life was prolonged [22].

In a study, application of sumac extract to peanut oil was found to prevent oxidation and prolong shelf life. In addition, tannin-rich sumac extracts are observed to increase the oxidative stability of animal-derived food products such as milk and meat. [17]

Ref. [23] added ground sumac flour to enrich wheat flour with bioactive compounds and reduce salt content for functional bread production. The quality parameters and acceptability of the resulting bread were examined. As a result, it was reported that the phenolic and fiber content of the enriched bread increased and the salt content decreased by providing a salty taste of sumac.

Addition of sumac extracts to meat can extend shelf life by reducing total microbial count. It is stated that the bioactive component that plays an important role in reducing pathogenic bacteria in meat and consuming meat in a safer way is the high tannin content.

Ref. [18] sumac fruit powder to fruit and vegetable smoothies and evaluated its quality characteristics. On the first day of the storage period of the smoothies, it was observed that the level of polyphenolic compounds increased by 54% in the product containing 30 g/L sumac compared to the control sample. During the three-day storage period, the total number of aerobic mesophilic bacteria increased in control samples, while the growth of these microorganisms was prevented in sumac-added smoothies.

Sumac is considered a promising natural additive that can be used instead of salt in older adults, especially to improve the taste and flavor of foods [24].

2.2. Bioactive compounds of sumac

Sumac fruits are rich in flavonols, phenolic acids, hydrolyzable tannins, biflavonoids, anthocyanins and organic acids. Vitamins, minerals, oleic and linoleic acids are also the main components of sumac fruits ([15]- [25]). Flavonoids and flavonoid derivatives are found in large amounts in sumac fruits as aglycone or glycoside derivatives such as isorhamnetin, myricitrin, apigenin, quercetin, chrysoeriol, eriodictyol and kaempferol [25]. Cyanidin and delphinidin derivatives are the most abundant anthocyanins in sumac and give the rich red color to the pericarp of sumac fruits [25]. It can be seen even with the naked eye that sumac fruits are rich in pigments. Anthocyanins are bioactive compounds that have high antioxidant activity, are effective in the prevention of esophageal and colon cancer, and give purple, blue, brown, red and orange colors. It is used as a water-soluble natural food coloring. Sumac contains nearly 20 vitamins and minerals such as vitamin K, vitamin E, vitamin C, calcium and folate. Sumac also contains phytosterols and carotenoids such as lutein and zeaxanthin [3].

2.3. Bioactivities and health of sumac

It has been reported that sumac reduces oxidative stress and thus protects DNA and liver from oxidative stress damage. It has been emphasized that the antioxidant properties of sumac are due to its flavonoids, especially Gallic acid content [26]. Sumac has been reported to be very powerful in preventing atherosclerotic cardiovascular diseases due to its flavonoid content [17].

Ref. [27] concluded in their study that sumac sour obtained from different regions of Turkey has antimicrobial properties and hypoglycemic effect.Sumac is highly beneficial against risks associated with oxidative stress and inflammation [15]. The powder of sumac fruits is widely used as an herbal medicine to its anti-fibrogenic, antimicrobial and anti-inflammatory activities [28].

Sumac has a hypoglycemic role due to its flavonoid content and improves glucose tolerance in diabetic patients [17].Sumac is reported to have potential antioxidant, anti-inflammatory, hypoglycemic, hypolipidemic and neuroprotective activities [23].The health-promoting properties of sumac extracts are reported to be due to phenolic acids, flavonoids and mainly hydrolyzable tannins([28], [25]- [17]).

The effect of antioxidant and physicochemical properties of sumac fruits collected from different regions in Turkey on antimicrobial activity was investigated. As a result, it was revealed that antimicrobial effect was directly proportional to antioxidative values [46].

3. CONCLUSION

In conclusion, Sumac is considered to be a potential source for functional food production due to its high amount of phenolic compounds and high antioxidant capacity. In this context, sumac sour, which is a kind of sumac extract, should be supported by scientific studies to take its place in the functional food market as a value-added product.

In order to better understand the full potential of sumac sour, the value-added product of the sumac plant, production process development and optimization issues should be given importance. In addition, scientific studies are needed to include this superfood more in our diet and food industry.

REFERENCES

[1]. Mazzara, Eugenia, et al. "Phytochemical investigation of sumac (Rhus coriaria L.) fruits from different sicilian accessions." *Foods* 12.23 (2023): 4359.
[2]. Hafizov, Gharib, Ilham Qurbanov, and Samir Hafizov. "RHUS CORIARIA (SUMAC): FROM OF UNDERSTANDING THE BIOTECH POTENTIAL TO İTS INDUSTRIAL USES." *Актуальная биотехнология* 3 (2020): 63-71.
[3]. OI, El-Nahas, and Samah A. Elsemelawy. "Effect of Sumac (Rhus Coriaria L.) Herbal on Induced Osteoporosis in Female Rats." *Egyptian Journal of Nutrition* 33.1 (2018): 1-28.
[4]. Yegin, Sevim Çiftçi. "Farklı yörelere ait sumak (Rhus Coriaria L.) ekşisinin antioksidan kapasitesinin belirlenmesi." *Cumhuriyet Üniversitesi Sağlık Bilimleri Enstitüsü Dergisi* 2.2 (2017): 35-39.
[5]. Hafizov, Gharib. "Research and Development of Technology for Obtaining Red Food Coloring from Sumac Fruits." (2023).
[6]. Polishchuk, Galyna, Oksana Bass, and Artur Mykhalevych. "Reasoning of the selection of technological parameters for the extraction of sumac." *in proc.of university of Ruse*, (2020), vol 59, book 10.2., p 43-47.
[7]. Tiryaki G.Y., Kahramanmaraş İlinde Üretilen Simgesel Geleneksel Bir ürün: SUMAK EKŞİSİ, Gıda Mühendisliği Dergisi, Sayı 31, s 54-60.
[8]. Türk Patent ve Marka Kurumu , 'Maraş Sumak Ekşisi Akıtı', sayı 27, Nisan,16, 2018.
[9]. Aldıoglu, Ali. "Sumak ekşi akıtı ve Kahramanmaraş mutfağında kullanımı." *Aydın Gastronomy* 6.1 (2022): 39-49.
[10]. Bozdogan, Adnan, et al. "Rheological behavior of sumac (Rhus coriaria L.) extract as affected by temperature and concentration and investigation of flow behavior with CFD." *Biointerface Research in Applied Chemistry* 10.6 (2020): 7120-7134.
[11]. Turkmen, F. Ucan, et al. "Investigation of some quality parameters of pomegranate, sumac and unripe grape sour products from Kilis markets." *Quality Assurance and Safety of Crops & Foods* 11.1 (2019): 61-71.
[12]. Hasani, A., M. H. Khosh Taghaza, and Mohammadtaghi Ebadi. "Effect of infrared drying on qualitative characteristics of sumac fruit (Rhus coriaria L.)." *Journal of Horticultural Science* 34.3 (2020): 493-504.
[13]. Çekiç, İbrahim. "An indispensable spice in multicultural Hatay cuisine: Sumac." *Journal of Mediterranean Tourism Research* 2.2 (2023): 141-152.
[14]. Alhadi Shawar, "Biological Activities and Nutritional Composition of *Rhus coriaria* L. (Sumac)," M.Sc. Thesis, Hebron University, Palestine, 2024.
[15]. AlJuhaimi, Fahad, et al. "Effects of maturation on bioactive properties, phenolic compounds, fatty acid compositions and nutrients of unripe and ripe sumac (Rhus coriaria L.) fruits." *Food and Humanity* 2 (2024): 100281.
[16]. Mahdavi, Saman, B. Hesami, and Y. Sharafi. "Antimicrobial and antioxidant activities of Iranian sumac (Rhus coriaria L.) fruit ethanolic extract." *J. Appl. Microbiol. Biochem* 2.5 (2018): 2576-1412.
[17]. El Ghizzawi, Fatima, et al. "A focused insight into sumac: biological, chemical, health benefits and its applications in food industry." *Food Science and Engineering* (2023): 191-203.
[18]. Osmólska, Emilia, et al. "Effect of Supplementation of Freshly Pressed Carrot Juice with Rhus coriaria L. on Changes in Juice Quality." *Sustainability* 15.1 (2022): 719.
[19]. Ahmadi, Reza, Majid Alipour Eskandani, and Dariush Saadati. "Evaluation of antimicrobial effect of Iranian sumac on Bacillus cereus in a commercial barley soup." *Slovenian Veterinary Research* 54.2 (2017).
[20]. Var, Işıl, Sinan Uzunlu, and I. Değirmenci. "Antimicrobial effects of fruit sauces on some pathogenic bacteria in vitro and on chicken breast meat." *Journal of the Hellenic Veterinary Medical Society* 72.1 (2021): 2703-2712.
[21]. Ali, Fatma HM, A. R. H. Hassan, and Ahmed EM Bahgat. "Study of sumac extract (Rhus coriaria L.), lactic acid and thyme oil as decontaminants for shelf life extension of refrigerated rabbit meat." *Food Sci. Qual. Manag* 38 (2015): 71-78.
[22]. Abd Elaal, Reham, et al. "Enhancing the shelf life of minced beef with sumac extract." *Journal of Advanced Veterinary Research* 14.5 (2024): 904-908.
[23]. El Khatib, Sami, and Abir Salame. "Sumac (Rhus coriaria) extracts to enhance the microbiological safety of the red meat." *Food Science and Technology* 7.4 (2019): 41-52.
[24]. Soleymani Majd, Nasim, et al. "The effect of high-polyphenol sumac (Rhus coriaria) on food intake using sensory and appetite analysis in younger and older adults: A randomized controlled trial." *Food Science & Nutrition* 11.7 (2023): 3833-3843.
[25]. Khalil, Mohamad, et al. "Role of Sumac (Rhus coriaria L.) in the management of metabolic syndrome and related disorders: Focus on NAFLD-atherosclerosis interplay." *Journal of Functional Foods* 87 (2021): 104811.
[26]. Mosayyeb Zadeh, Amir, et al. "Effects of sumac fruit powder (Rhus coriaria L.) supplementation on productive performance, egg quality traits and serum biochemical parameters in old laying hens." *Italian Journal of Animal Science* 20.1 (2021): 1348-1356.
[27]. Yegin, Sevim Çiftçi, and Duygu Odabaş Alver. "Investigation of Antimicrobial Activities and Antidiabetic Effect of Sumac Shrups (Rhus Coriaria L.) in Different Region." *Bitlis Eren Üniversitesi Fen Bilimleri Dergisi* 9.1 (2020): 85-90.
[28]. Grassia, Melania, et al. "Chemical composition and microencapsulation suitability of sumac (Rhus coriaria L.) fruit extract." *European Food Research and Technology* 247 (2021): 1133-1148.
[29]. Özaydın, Fatma, and Hasan Vardin. "Effects of antioxidant and physicochemical properties on antimicrobial activity of sumac (Rhus coriaria L.) plant spices which are collected from the southeastern anatolia region of Turkey." *Harran Tarım ve Gıda Bilimleri Dergisi* 26.3 (2022): 327-335.

ICENS 10TH INTERNATIONAL CONFERENCE ON ENGINEERING AND NATURAL SCIENCE
October 02-06 2024 Sarajevo (Hybrid Event)

Wire Selection for Dissimilar Welding Between G24Mn6+QT3 and S355j2+N Steels by GMAW

Ali Akay[1], Fatih Güven[2]

Abstract

In this study, the performance of two types of filler wires for the dissimilar welding of G24Mn6+QT3 cast steel and S355J2+N structural steel was investigated. The plates were joined with ER70S-6 and ER110S-G fillers by GMAW, which is widely used in the industry. The tensile strength of the welded joint, the impact toughness of the weld zone and the hardness values were investigated. In terms of tensile strength, both wires were successful and the welded joint was fractured from the base metal on the S355J2+N side. The yield strengths of were more than 400 MPa and the tensile strengths were more than 550 MPa for both filler types. When the toughness values of the heat-affected-zones (HAZs) were compared, no difference was observed. However, the weld seam toughness values were 33J and 108J on average for ER110S-G and ER70S-6 wires, respectively. ER70S-6 wire gave better results for toughness. Considering that they have sufficient tensile strength, ER70S-6 wire would be more suitable for joining these two metals.

Keywords: MAG; ER110S-G; ER70S-6; Tensile strength

1. INTRODUCTION

Using steels with different mechanical and chemical properties together in construction is required cost reduction, functionality, and safety. When employing different metals together, a method preference emerges to join them. Welding is widely preferred in industry due to the flexibility it offers. Gas metal arc welding (GMAW) is usually the first choice due to its speed in manufacturing and versatility. It is possible to weld different steels with GMAW, but it requires expertise and meticulous work. In addition to the need to skillfully adjust parameters such as current, voltage, wire feeding speed and travelling speed, the filler selection that takes into account the properties of the materials to be welded requires utmost care. The S355J2+N steel examined in this study is widely used in steel construction, pressure vessels, moulds, mining and the construction machinery applications. G24Mn6+QT3 cast steel is preferred in the same industries due its wear resistance, strength, and hardenability. This metal can be welded in special conditions. However, there are no sufficient studies on the dissimilar welding of these materials in the literature.

Wu et.al [1] studied the mechanical and fatigue behavior of the welded G20Mn5 cast steel. They employed ER50-6 filler composing of 0.08% C, 0.90% Si, and 1.46% Mn. They observed an overmatching welding since the GMAW affected microstructure and mechanical properties prominently. Lu et.al [2] conducted experiments on the corrosion and corrosion fatigue behavior of G20Mn5QT cast steel and Q355D steel. They used ER50-6 type welding wire and mixed gas (80% Ar and 20% CO2). Han et.al [3] investigated the fatigue behavior of welded joint of G20Mn5QT Cast Steel and Q345B Steel. They adopted ER50-6 solid wire and was preheated the materials to a temperature of 150 °C for the welding.

In this study, the dissimilar welding between G24Mn6+QT3 cast steel and S355J2+N steel was studied. The use of ER70S-6 and ER110S-G filler wires was compared in terms of tensile strength, toughness, and hardness. Before the welding process, a preheating was done and the plates were joined by gas metal arc welding (GMAW) under a mixed gas atmosphere.

[1]*Birikim Engineering Co. Başkent OSB, Ankara, Türkiye, a.akay@birikimmuhendislik.com.tr*

[2] *Corresponding author: Hacettepe University, Department of Machinery and Metal Technologies, Başkent OSB Vocational School of Technical Sciences, Ankara, Türkiye, fatihguven@hacettepe.edu.tr*

2. MATERIALS AND METHODS

2.1. Material identification and welding process

The performance of two types of wires for welding S355J2+N structural steel and G24Mn6+QT3 cast steel using GMAW method was investigated. AWS A5.18/ER70S-6 (EN ISO 14341-A/G 42 5 M21 3Si1) and AWS A5.28/ER110S-G (EN ISO 12534/G Mn3Ni1CrMo) were used in the experiments [4]. The chemical composition and mechanical properties of the materials and filler wires were given in Table 1 and Table 2. The chemical compositions obtained by spectral analysis performed at ambient temperature according to the ASTM E415 standard. The certified chemical composition of the filler gathered from the manufacturer data.

Table 1. Chemical composition (by mass) of materials and filler material

%	Fe	C	Si	Mn	P	S	Ni	Cr	V	Mo	Al	Cu
S355J2+N	Base	0.070	0.019	1.39	0.021	0.024	0.14	0.12	0.042	0.021	0.020	0.46
G24Mn6+QT3	Base	0.209	0.451	1.566	0.014	0.011	0.191	0.216	0.004	0.055	0.014	
ER70S-6	Base	0.08	0.90	1.45								
ER110S-G	Base	0.09	0.60	1.65			1.50	0.30	0.10			<0.25

Table 2. Mechanical properties of filler material (manufacturer data) and base plates

	S355J2+N	G24Mn6+QT3	ER70S-6	ER110S-G
Yield Strength, MPa	403	582	440	770
Tensile Strength, MPa	479	700	560	880
Toughness, J	60 (20°C)	27 (-30°C)	160 (20°C)	180 (20°C)
Elongation, %	25	22	28	21

200x350 mm plates with a thickness of 20 mm were prepared for a bevel welding with 60° by grinding. GMAW was applied manually in 13 runs in the PA position with reverse polarity (DC+). The first pass was applied after preheating to a temperature of 120°C and the interpass temperature was 300°C. Weld pool shielded by a gas consisting of 18% CO_2 and 82% Ar with a gas flow rate of 12 dm^3/min. Both filler wires had a diameter of 1.2 mm. Arc stability was good during the welding process and no discontinuity was observed in weld seams. The welding parameters for each welding pass were shown in Table 3.

Table 3. Welding parameters for each welding pass

	ER110S-G			ER70S-6		
Run	Current (A)	Voltage (V)	WS (mm/min)	Current (A)	Voltage (V)	WS (mm/min)
1	90-100	16.8	154.1	100-110	17.2	157.7
2	225-235	28.5	410.0	210-220	28	512.5
3	250-260	29.8	286.7	245-255	29.6	315.4
4	250-260	29.8	512.5	250-260	29.6	585.7
5	255-265	29.8	450.5	250-260	29.6	315.4
6	250-260	29.8	353.4	250-260	29.6	410.0
7	260-270	29.8	512.5	245-255	29.6	431.6
8	260-270	29.8	410.0	250-260	29.6	525.6
9	250-260	29.5	338.8	245-255	29.4	450.5
10	260-270	29.5	450.5	250-260	29.4	465.9
11	260-270	29.5	427.1	250-260	29.4	427.1
12	250-260	29.5	273.3	245-255	29.4	410.0
13	240-250	29.5	410.0	240-250	29.4	379.6

WS: Welding speed

2.2. Mechanical tests

Tensile tests, Charpy notched impact tests, and Vickers hardness tests were performed on the samples taken from the welded plates. The dimensions of the samples and hardness measurement points (SPs) are shown in Fig. 1. Three tensile test samples were taken from each welded plate and tests were performed according to ISO 4136 standard [5]. A total of nine Charpy notch impact samples, three each from the weld metal, S355J2+N-HAZ and G24Mn6+QT3-HAZ, were prepared and tested according to ISO 9016 standard [6]. Vickers hardness tests (HV10) were carried out according to ISO 9015 standard [7] by taking three repeated measurements from the base of S355J2+N, the HAZ of S355J2+N, weld zone (WZ), the HAZ of G24Mn6+QT3, and the base of G24Mn6+QT3 as shown in Fig. 1a.

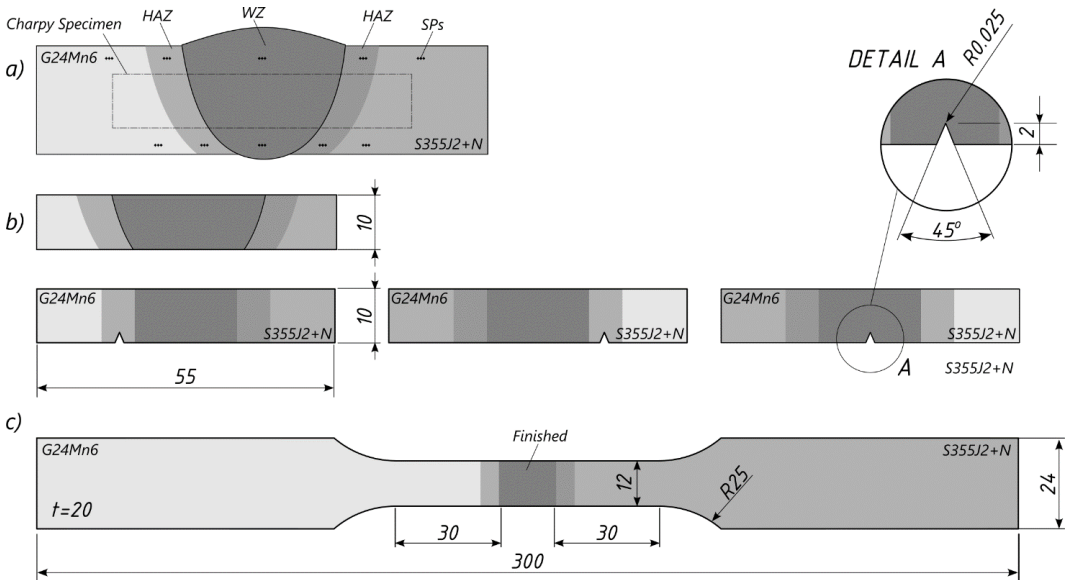

Fig. 1. Test specimens and hardness measurement (HAZ: Heat affected zone, WZ: weld zone, SPs: Sampling points). (a) hardness specimen; (b) Charpy test specimens with different notch zones; (c) tensile test specimen

3. RESULTS AND DISCUSSION

Fig. 2 shows macrographs taken from the cross-section of welded parts. The applied welding passes, the weld zone (WZ), and the heat affected zones (HAZs) are seen in the macrographs. No discontinuity was observed in the welding. The notched impact test results of the specimens with ER110S-G and ER70S-6 filler wires were shown in Fig. 3. The bar length shows the average toughness and the caps show the standard deviation. As a result of the impact test, no difference is observed in terms of impact toughness in the HAZ regions for both welding wires. The toughness of the HAZ on the G24Mn6+QT3 side of the sample welded using ER110S-G was about 190J on average while the toughness for the sample welded using ER70S-6 wire was about 183J on average. On the other hand, the HAZ toughness on the S335J2+N side was 60J on average for both samples. However, the toughness of ER70S-6 samples notched in weld seam in was higher than of ER110S-G. The weld seam toughness values are 33J and 108J on average for ER110S-G and ER70S-6 filler wires, respectively. Since the weld seam toughness was higher than the HAZ (S335J2+N) for ER70S-6, it was acceptable levels. ER70S-6 wire can be preferred in cases where toughness is required since the HAZ toughness was higher than the toughness of weld seam for ER110S-G.

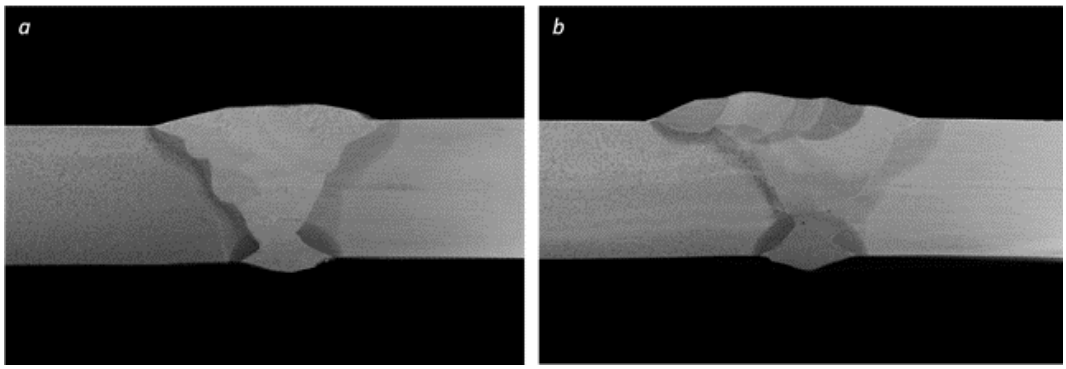

Fig. 2.Macrographs of welded specimens. (a) ER70S-6 filler; (b) ER110S-G filler

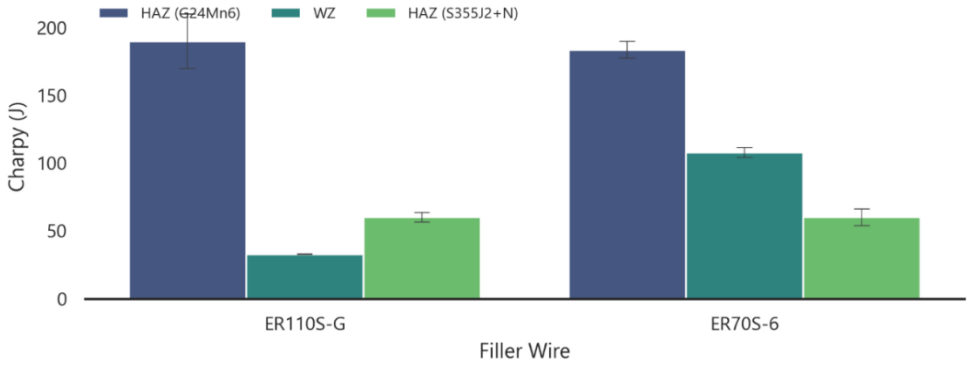

Fig. 3. Toughness of welded specimens.

The hardness of the parts joined with ER110S-G and ER70S-6 wires were shown in Fig. 4. The diamond marker with continuous lines in the graph belongs to the samples joined with ER110S-G and the round marker with dashed lines belongs to the samples joined with ER70S-6 wires. No significant difference was observed in the BM and HAZ hardness values for both samples. Although it was slightly lower in the bottom side in the sample welded with ER110S-G wire, the hardness of the weld seam reached an average of 300 HV. There was a significant difference between the hardness values of the bottom side and the front side in ER70S-6 wire. While the hardness of front side of ER70S-6 wire was 172 HV on average, it was 238 HV in the bottom side. Moore [8] showed that there is a linear relationship between abrasive wear resistance and bulk hardness for ferritic materials. Białobrzeska and Jasiński [9] showed that the abrasive wear resistance was most strongly correlated with hardness and yield point for low alloy cast steels. From this point of view, ER110S-G wire can be considered more promising in terms of wear. However, special work needs to be done according to the type of wear mechanism for wear resistance.

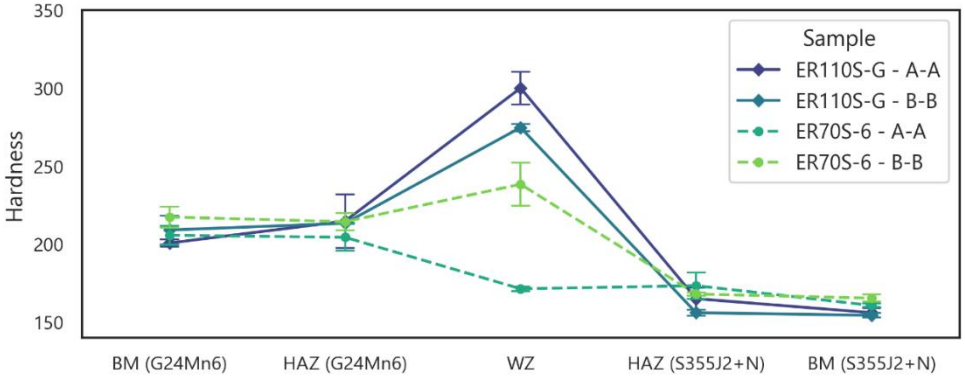

Fig. 4. Hardness of welded specimens (A-A: Front side, B-B: Bottom side)

Table 4 shows the results of the tensile tests. All samples fractured from the base metal on the S355J2+N side. No discontinuity was observed in the test samples that would affect the breaking point. The yield strengths of the samples were more than 400 MPa and the tensile strengths were more than 550 MPa for both filler wires. Since the fracturing occurred from the base metal, no difference can be mentioned between the wires in terms of tensile strength. Nevertheless, it can be said that both wires are possible in dissimilar welding of G24Mn6+QT3 and S355J2+N materials when considering the tensile strength.

Table 4. Tensile test results of welded specimens

Filler Wire	Sample	Rp0.2 (MPa)	Rm (MPa)	Elongation (%)	LoF
ER70S-6	T1	405.1	559.0	21.6	Base (S355J2+N)
	T2	404.7	556.2	19.2	Base (S355J2+N)
	T3	404.9	554.8	19.2	Base (S355J2+N)
ER110S-G	T1	403.6	561.2	16.8	Base (S355J2+N)
	T2	404.9	554.8	16.8	Base (S355J2+N)
	T3	409.6	560.8	16.8	Base (S355J2+N)

Rm: Tensile strength, LoF: Location of fraction

4. CONCLUSION

In this study, the dissimilar welding of G24Mn6+QT3 and S355J2+N was successfully applied using ER70S-6 and ER110S-G filler wire by GMAW method. The main outcomes could be drawn as follows:

- The yield strengths of the samples were more than 400 MPa and the tensile strengths were more than 550 MPa for both filler wires. Considering the tensile strength, it can be said that the use of both wires is possible, assuming that the post-welding strength of the base metal is sufficient.
- The weld seam toughness values are 33J and 108J on average for ER110S-G and ER70S-6 filler wires, respectively. ER70S-6 wire can be preferred in case where toughness is required.
- There was a clear difference between the hardness of the filler wires after welding. If a preference is made based on hardness in terms of wear resistance, it can be said that ER110S-G wire is superior. However, special work needs to be done according to the type of wear mechanism for wear resistance.

REFERENCES

[1] Wu SC, Qin QB, Hu YN, et al. The microstructure, mechanical, and fatigue behaviours of MAG welded G20Mn5 cast steel. *Fatigue Fract Eng Mater Struct* 2020; 43: 1051–1063.

[2] Lu Y, Wang R, Han Q, et al. Experimental investigation on the corrosion and corrosion fatigue behavior of butt weld with G20Mn5QT cast steel and Q355D steel under dry–wet cycle. *Eng Fail Anal* 2022; 134: 105977.

[3] Han Q, Guo Q, Yin Y, et al. Fatigue behaviour of G20Mn5QT cast steel and butt welds with Q345B steel. *Int J Steel Struct* 2016; 16: 139–149.

[4] AWS A. 18/A5. 18M: 2005: Specification for carbon steel electrodes and rods for gas shielded arc welding. *Am Weld*

Soc (Miami, 2005).
[5] ISO. ISO 4136:2022 Destructive tests on welds in metallic materials — Transverse tensile test.
[6] ISO. ISO 9016:2022 Destructive tests on welds in metallic materials — Impact tests — Test specimen location, notch orientation and examination.
[7] ISO. ISO 9015-1:2001 Destructive tests on welds in metallic materials — Hardness testing Part 1: Hardness test on arc welded joints.
[8] Moore MA. The relationship between the abrasive wear resistance, hardness and microstructure of ferritic materials. *Wear* 1974; 28: 59–68.
[9] Białobrzeska B, Jasiński R. Resistance to abrasive wear with regards to mechanical properties using low-alloy cast steels examined with the use of a dry sand/rubber wheel tester. *Materials (Basel)* 2023; 16: 3052.

ICENS 10TH INTERNATIONAL CONFERENCE ON ENGINEERING AND NATURAL SCIENCE October 02-06 2024 Sarajevo (Hybrid Event)

Fertilization zones generation using satellite imagery

Štefan Horvat[1], Damjan Strnad[2], Matej Brumen[2], Domen Mongus[2]

Abstract

One of the main goals of precision agriculture is to maximize crop yields, which requires efficient utilization of fertilizers. We present an automated procedure for generating a vector layer of zones that require different intensity of fertilization based on the value of vegetation index obtained from Sentinel-2 imagery. After obtaining the images we create a histogram, where the number of bins determines the number of fertilization zone classes we wish to obtain. Using the marching squares algorithm, we produce a final vector layer, which is exported to the GeoPackage format, making it compatible with modern agricultural equipment. We observe that fertilization zone generation depends on the field size, as large fields can generate more compact zones. Smaller fields tend to result in fragmented zones, due to bigger influence of neighboring regions pixels intensities. This approach thus offers a scalable solution for generation of fertilization zones, that can be used in fertilization map generation, but adjustments would be needed to reduce the effect of fragmentation.

Keywords: fertilization, precision agriculture, prescription maps, remote sensing

1. INTRODUCTION

The development of earth observation and processing technologies, such as Sentinel-2 satellites network and remote sensing, lead to widespread integration of precision agriculture in modern agricultural practices. Precision agriculture enables for site specific interventions without physical presence [1, 2]. With growing demand for food and the goal of sustainability while being respectful to the environment, generation of fertilization maps has recently been proposed to enable a more efficient planning of fertilizer disposal in the fields [1, 2, 3]. Application rates of fertilizer are important, as overfertilization can have negative consequences on the environment and be economically inefficient, while underfertilization does not utilize full crop potential and can lead to lower yield expectation [2].

Existing approaches to generation of fertilization maps usually involve satellite or UAV captured images [4] in combination with on-site soil sampling for wheat and barley [1, 2, 4, 5], rice [3, 6] and other types of crops. Soil sampling can be very costly and time consuming, since it requires a technician to take samples from fields and analyze them in the laboratory. After the analysis the agricultural experts prescribe the rate of fertilizer on corresponding locations [2, 7]. In this paper, an automated procedure is proposed, which omits onsite sampling and generates a vector layer of zones that require different intensity of fertilization based on the values of a vegetation index. The procedure does not generate fertilization maps directly, but instead generates the zones that are prescribed with fertilization rates by agricultural experts.

The study area can be seen on Figure 1, located in northwestern Slovenia and is dominated by small and medium sized fields. Only fields that were planted with wheat or barley are considered in this study.

[1] *Corresponding author: University of Maribor, Faculty of Electrical Engineering and Computer Science, Maribor, Slovenia*

[2] *University of Maribor, Faculty of Electrical Engineering and Computer Science, Maribor, Slovenia*

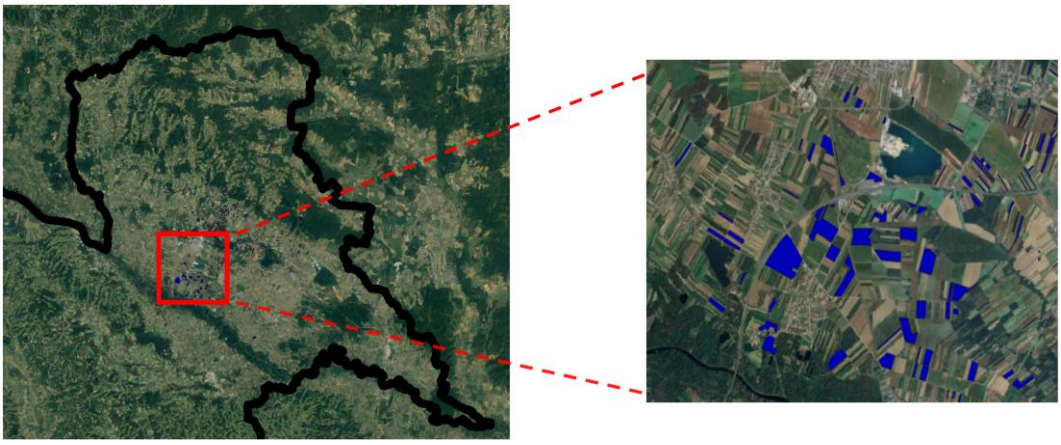

Figure 6: The study area located in NW Slovenia. Fields with blue color are included in the study and range from small to medium size fields (0.2 ha to 40 ha).

2. MATERIALS AND METHODS

The whole process of zone map generation consists of four steps. The most important step is the user defined number of fertilization zones, followed by execution of marching squares algorithm. In the last step all segmented zones are merged into a single vector layer. An example of the process is depicted in Figure 2.

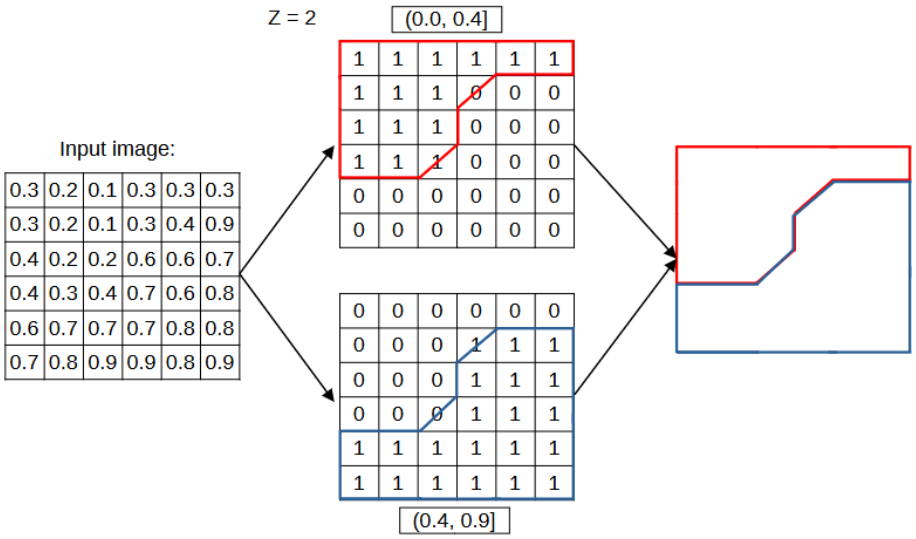

Figure 7: Histogram with 2 bins is created from an input image, followed by a segmentation with the marching squares algorithm and final merging into a single vector layer.

First we obtain the satellite imagery of the study area for a specified date and location from the Sentinel-2 satellite network. To estimate the crop health, the normalized difference vegetation index (NDVI) is used:

$$NDVI = \frac{NIR-R}{NIR+R} \quad (1)$$

Healthy crops have a greener response, which is effectively reflected by the index. The index values are from the interval [-1, 1], where 1 indicates excellent crop health [8].

In the second step, the number of classification zone classes are defined by the user. Based on the number of classification zones, a corresponding number of nonoverlapping bins in the histogram are created. The pixels are divided into bins based on their intensities.

In the third step, the segmentation of satellite images into fertilization zones is performed by the marching squares algorithm that generates a closed shape from isoline contours. The image of NDVI values is thresholded according to histogram bin limits and converted to a binary image for every bin. The value of 1 represents the pixels between the minimum and maximum thresholding value, other pixels are set to 0. A 2x2 window is slid over the binary image and a contour is assigned to it. There are 16 possible contours, which can be seen in Figure 3 and are stored in a lookup table. The contour is decided based on the values of neighboring pixels in 2x2 block [9].

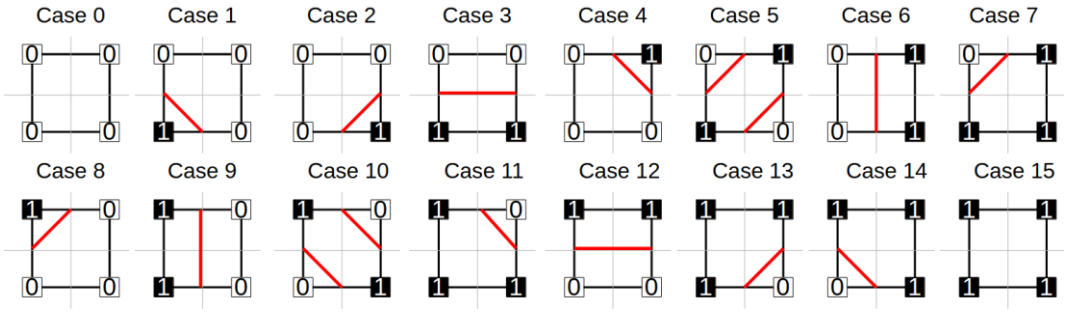

Figure 8: All 16 possible contour combinations that are stored in the lookup table in marching squares algorithm.

After the sliding, closed shapes that represent segments for each bin are saved to a vector layer. Finally, vector layers are merged into a final vector layer and exported to GPKG (GeoPackage) format. Attributes are assigned to classified fertilization zones. Attributes are used to set the amount of fertilizer to be disposed in the detected fertilization zones.

3. RESULTS AND DISCUSSION

The aim of this methodology was to segment fertilization zone classes from satellite images based on vegetation health, which we obtain from NDVI. The first batch of tests is visible on Figure 4a and was run in the early March 2024 with the number of fertilization classes set to 4. The greener areas in fertilization zone maps represent areas with excellent crop health, red color indicates poor crop health. The number of fertilization classes was chosen with the help of agricultural expert's advisory. The second batch of tests, visible on Figure 4b, was run in early May of 2024 with the same number of fertilization classes. Both time windows were chosen in coordination with agricultural experts just before the application of fertilization.

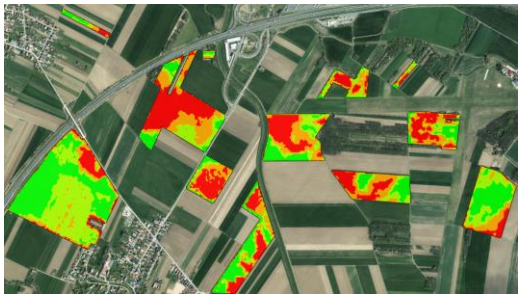

Figure 4. (a) An example of segmentation with 4 fertilization classes on an image from early March 2024.

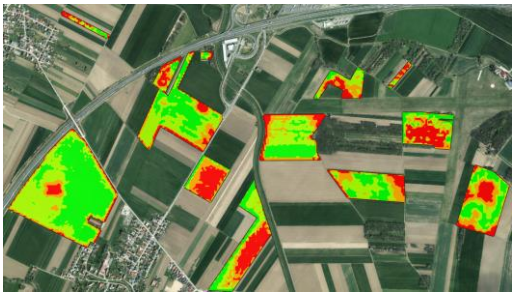

(b) An example of segmentation with 4 fertilization classes on an image from early May 2024.

In Figure 4a the zones appear to be more compact. Figure 4b displays a different scenario, as zones appear to be smaller and much more fragmented. We observed that pixel intensities before segmentation were more homogenous in Figure 4a and less so in Figure 4b. We also observed considerable fragmentation of edges in Figure 4b, which is caused by an overlap of pixels from neighboring regions.

We ran another experiment on a single field for early May of 2024 with 2, 3 and 4 classification zones (Figures 5a, 5b and 5c). We can clearly see, that with higher number of classification zone classes the fragmentation becomes more apparent.

Figures 4 and 5 highlight the problem of fertilization layers appearing blocky, which is one of the problems of the marching squares algorithm. As per advice by farmers and agricultural experts, a better shaped border in practice would be with rounder or oval edges.

Figure 5. (a) Fertilization segmentation using 2 classification classes.

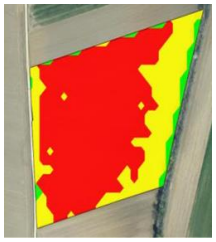

(b) Fertilization segmentation using 3 classification classes. The effect of fragmentation is noticeable here.

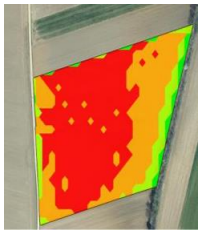

(c) Fertilization segmentation using 3 classification classes. The effect of fragmentation is evident here.

Results were also tested in practice by agricultural experts and farmers. The attributes of classified zones were manually set by agricultural experts in form of needed application of fertilizer and tested by farmers in the fields. The GPKG can easily be transferred to modern agricultural equipment and the experiment performed without problems.

4. CONCLUSION

The described method provides a scalable solution for generation of fertilization zones. Adequate fertilization zones can be generated, but one must be careful to avoid fragmentation when choosing the number of fertilization zone classes. In the future, we intend to tackle the problem with fragmentation by utilizing morphological operators. The application should reduce the number of small, isolated segmented shapes.

Another goal is to integrate fertilizer mapping to classification zone attributes automatically, without manual interventions. Currently, the agricultural experts must review the fertilization zones and manually assign fertilization rates, which takes a lot of time and effort. Avoiding this step would increase the efficiency and usability of the methodology in practice.

ACKNOWLEDGMENT

This research has received funding from the European Union through project Green.DAT.AI under grant agreement no. 101070416.

REFERENCES

[1] L. R. Amaral and D. D. D. Justina, "Spatial Dependence Degree and Sampling Neighbourhood Influence on Interpolation Process for Fertilizer Prescription Maps" Engenharia Agrícola, 2019.

[2] D. Radočaj, M. Jurišić and . M. Gašparović, "The Role of Remote Sensing Data and Methods in a Modern Approach to Fertilization in Precision Agriculture" Remote Sensing, 2022.

[3] F. Yu, J. Bai, Z. Jin, H. Zhang, Z. Guo and C. Chen, "Research on Precise Fertilization Method of Rice Tillering Stage Based on UAV Hyperspectral Remote Sensing Prescription Map" Agronomy, 2022.

[4] A. Uribeetxebarria, A. Castellón and A. Aizpurua, "A First Approach to Determine If It Is Possible to Delineate In-Season N Fertilization Maps for Wheat Using NDVI Derived from Sentinel-2" Remote Sensing, 2022.

[5] D. Bonfil, Y. Michael, S. Shiff and I. Lensky, "Optimizing Top Dressing Nitrogen Fertilization Using VENμS and Sentinel-2 L1 Data" Remote Sensing.

[6] M. Yang, X. Xu, Z. Li, Y. Meng, X. Yang, X. Song, G. Yang, S. Xu, Q. Zhu and H. Xue, "Remote Sensing Prescription for Rice Nitrogen Fertilizer Recommendation Based on Improved NFOA Model" Agronomy, 2022.

[7] R. Mihelič, J. Čop, M. Jakše, F. Štampar, D. Majer, S. Tojnko and S. Vršič, "Smernice za strokovno in utemeljeno gnojenje" 2011.

[8] S. Huang, L. Tang, J. P. Hupy, Y. Wang and G. Shao, "A commentary review on the use of normalized difference vegetation index (NDVI) in the era of popular remote sensing" Journal of Forestry Research, 2021.

[9] C. Maple, "Geometric design and space planning using the marching squares and marching cube algorithms" 2003 International Conference on Geometric Modeling and Graphics, 2003. Proceedings, 2003.

[10] C. Fiorentino, A. R. Donvito, P. D'Antonio and S. Lopinto, "Experimental Methodology for Prescription Maps of Variable Rate Nitrogenous Fertilizers on Cereal Crops" Innovative Biosystems Engineering for Sustainable Agriculture, Forestry and Food Production, 2020.

ICENS 10TH INTERNATIONAL CONFERENCE ON ENGINEERING AND NATURAL SCIENCE
October 02-06 2024 Sarajevo (Hybrid Event)

Optimization of a 33-Bus Power Distribution System Using Artificial Hummingbird Algorithm for Power Loss and Voltage Stability Enhancement

Nisa Nacar Çıkan[1]

Abstract

This paper presents an optimization study on the 33-bus power distribution system using a reconfiguration technique to enhance system performance. The optimization process employs two objective functions: minimizing active power losses and improving voltage stability through the reduction of the voltage stability index. The Artificial Hummingbird Algorithm (AHA), a novel metaheuristic approach, is adopted due to its efficiency in handling complex optimization problems. The proposed methodology is applied to both single-objective and multi-objective scenarios to comprehensively evaluate the system's performance. Results demonstrate significant improvements in power loss reduction and voltage stability enhancement, underscoring the effectiveness of the AHA in optimizing reconfigured power distribution networks.

Keywords: Reconfiguration, Power Distribution Networks, Metaheuristic Algorithm, Power Loss Minimization

1. INTRODUCTION

Power distribution systems are typically designed in either grid or radial configurations, with specific switching points set throughout. Reconfiguring radial power systems plays a key role in enhancing the distribution grid's performance. Adjusting switching points appropriately can boost the distribution system's power quality, reduce energy losses, and maintain the stability of distribution lines. The power network employs two types of switches: sectionalizing switches (S.S.'s), which are generally closed, and tie switches (T.S.'s), which are typically open [1]. During reconfiguration, certain switches alter their status based on optimization outcomes. The task of determining the best switching positions is complex due to the vast number of potential configurations [2]. Both classical (deterministic) and meta-heuristic (stochastic) approaches are frequently used to solve the reconfiguration problem in power distribution network (RPPDN) [3],[4]. Because deterministic methods might become stuck in local optima and are difficult to distinguish, they frequently fail to identify a global optimal solution for highly nonlinear or nonconvex situations. Consequently, meta-heuristic techniques have been devised for this investigation.

The two main configurations of power distribution networks that are examined in the literature are balanced and unbalanced. Assuming that the loads and phases are spread equally, balanced networks make analysis easier and are frequently employed for idealized modeling. However, the presence of single-phase and multi-phase connections, fluctuations in phase loading, and uneven load distributions often result in imbalanced distribution networks in the real world. Since unbalanced systems more closely reflect the operational difficulties and asymmetries present in real-world power distribution networks, more sophisticated modeling and analysis techniques are needed to evaluate their performance [5],[6]. A comprehensive study and literature review focused on balanced power distribution networks (PDNs) is presented in [2], offering detailed insights and findings specific to this network type. In contrast, [5],[6] provides an in-depth literature review and extensive analysis dedicated to unbalanced PDNs, covering the complexities and unique characteristics associated with these systems. Together, these sources serve as valuable references for understanding the distinct challenges and methodologies applied to both balanced and unbalanced PDNs in the field.

In this study, a reconfiguration analysis was performed on a 33-bus power distribution network (PDN) using the Artificial Hummingbird Algorithm (AHA). The fitness function was designed to minimize active power loss and enhance the voltage stability index (VSI). The remainder of the paper is structured as follows: Section 2 presents the 33-bus PDN system along with the constraints; Section 3 discusses the AHA algorithm; Section 4 provides the results and discussion; and finally, the conclusion is given.

[1] *Corresponding author: Cukurova University, Electrical and Electronics Engineering Department, 01330, Balcali,Sarıcam/Adana, Turkiye.* ncikan@cu.edu.tr

2. 33- BUS TEST SYSTEM

A popular standard test system in the literature, the 33-bus power distribution system is especially preferred for research on distribution network optimization and reconfiguration. Power is delivered to designated load centers by 33 buses that make up this medium-voltage distribution network, which normally operates at 12.66 kV. This system consists of distribution lines connecting load sites and a single power source, usually a main transformer station. There is just one power source and one power flow line, as it is typically portrayed in a radial layout or tree structure. This topology restricts the alternatives for redundant power flow even though it helps in fault current control. The system has 33 nodes and 32 lines, with power flowing through lines connecting each bus. Loads are distributed across various nodes; these loads vary depending on whether the distribution system is balanced or unbalanced. Figure 1 shows the 33-bus test system, commonly used as a standard model for analyzing distribution network reconfiguration, optimization, and performance under various operating conditions.

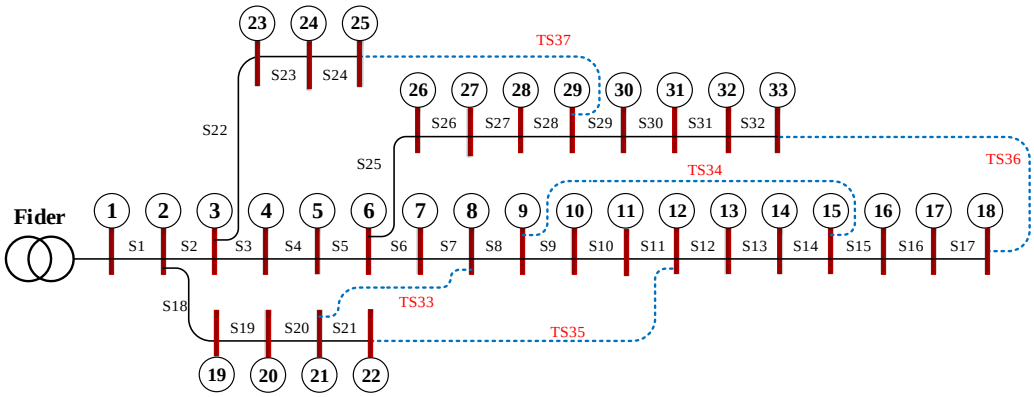

Figure 1. 33-bus test system [2].

2.1. Problem Formalization

The aim of this study is to minimize active power loss while enhancing the voltage stability index. Equation 1 presents the formula for minimizing power loss [2].

$$\mathbf{P_{Loss}^{min}} = \left(\sum_{\mathbf{i,k=1,}}^{\mathbf{N_{br}}} \mathbf{r_{(i,k)}} \cdot \left(\frac{\mathbf{P_k}^2+\mathbf{Q_k}^2}{\mathbf{V_k}^2}\right) . \mathbf{Sw_{(i,k)}}\right) \quad \textbf{(1)}$$

Equation 1 presents the formula for improvement of voltage stability index [2].

$$\mathbf{VSI} = \frac{\mathbf{4|V_i|^2|C||D||S_k|\cos(\varphi_k+\delta_S).\sin(\delta_i)}}{\mathbf{|S_i|^2.\cos^2(\varphi_i+\delta_k)}} \leq \mathbf{1} \quad \textbf{(2)}$$

More thorough investigation is required into the voltage stability of systems functioning near the limit values. The literature contains a wide variety of voltage stability indices. But the majority of them are predicated on a variety of ignorance or presumptions. This study makes use of a newly proposed index that takes into account several line properties and is based on line loading [4]. It has been noted that the recommended index consistently produces results under all situations and loading scenarios.

Voltage fluctuations must remain within specified limits in power systems as shown in Equation 3 [2].

$$V_{i,\phi}^{min} \leq V_{i,\phi} \leq V_{i,\phi}^{max} \qquad \forall\phi \in \{a,b,c\}, \quad \forall i \in \text{Buses} \quad (3)$$

The cable in the system should not carry more current than the limit outlined in Equation 4 [2].

$$I_{i,\phi} \leq I_{i,\phi}^{max} \quad \forall\phi \in \{a,b,c\}, \quad \forall i \in \text{Branches} \quad (4)$$

Equation 5 ensures that the total generated power equals the total load and losses in the system [2].

$$\sum_{i=1}^{N_{Gen}} P_{i,Gen}^{\emptyset} = \sum_{i=1}^{N_{Load}} P_{i,Load}^{\emptyset} + \sum_{i=1}^{N_{Branch}} P_{i,Loss}^{\emptyset} + \sum P_{i,Loss}^{equipment} \qquad \forall \phi \in \{a, b, c\} \tag{5}$$

The transformers need to function within the designated voltage and current boundaries for each phase to guarantee their optimal performance and prevent any harm, as indicated in Equation 6 [2].

$$X_{i,\emptyset}^{trfmin} \leq X_{i,\emptyset,trf} \leq X_{i,\emptyset}^{trfmax} \quad \forall \phi \in \{a, b, c\} \tag{6}$$

Equation 7 demonstrates that the amount of power flowing on a line cannot exceed a certain limit in order to maintain line security [2].

$$S_{i,\emptyset,line} \leq S_{i,\emptyset,line}^{max} \qquad \forall \phi \in \{a, b, c\}, \quad \forall i \in Lines \tag{7}$$

3. ARTIFICIAL HUMMINGBIRD ALGORITHM

The Artificial Hummingbird Algorithm (AHA) imitates the distinctive foraging and flight actions of hummingbirds for optimizing purposes. Hummingbirds are famous for their remarkable ability to quickly find food sources by using precise and agile movements to hover, change directions, and efficiently use energy while searching for nectar [7]. The AHA replicates these actions through different search patterns, such as exploration (wide search for possible solutions) and exploitation (targeted search around promising solutions), to maintain a equilibrium between uncovering new areas in the solution space and improving existing high-quality areas [7]. The AHA's flexibility allows it to excel in tackling intricate, nonlinear optimization issues across a variety of fields like power distribution networks, engineering design, and machine learning, with a focus on enhancing system performance and identifying global optima [7].

4. RESULTS AND DISCUSSION

The comparison of active power loss and power flow at each branch before/after optimization is shown in Figure 2. Upon examining Figure 2, it can be observed that voltage improvements have occurred across all buses, with the exception of buses 20, 21, and 22. Specifically, the voltage levels have increased from 0.92 p.u. to approximately 0.94 p.u., reflecting an overall enhancement in voltage stability throughout most of the network.

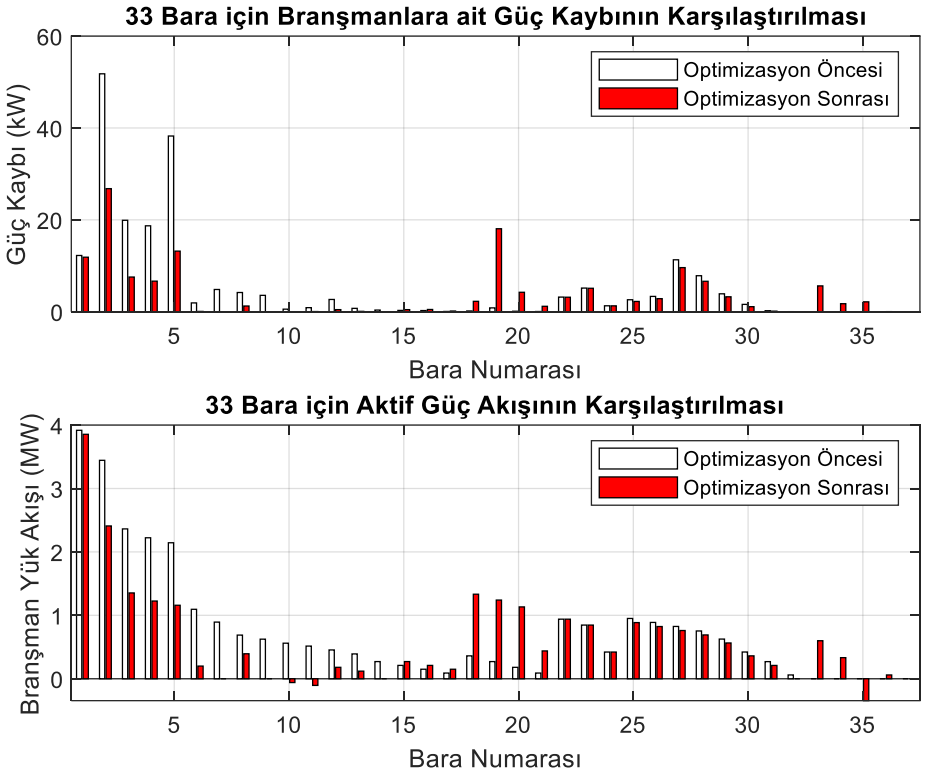

Figure 2. 33-bus power distribution network power loss and power flow results before and after reconfiguration.

Figure 3 illustrates the bus voltages before and after the optimization process, which is influenced by the reconfiguration performed using the Artificial Hummingbird Algorithm. The comparison clearly highlights the effects of the optimization on the voltage levels across the buses, demonstrating the improvements achieved through this algorithmic approach.

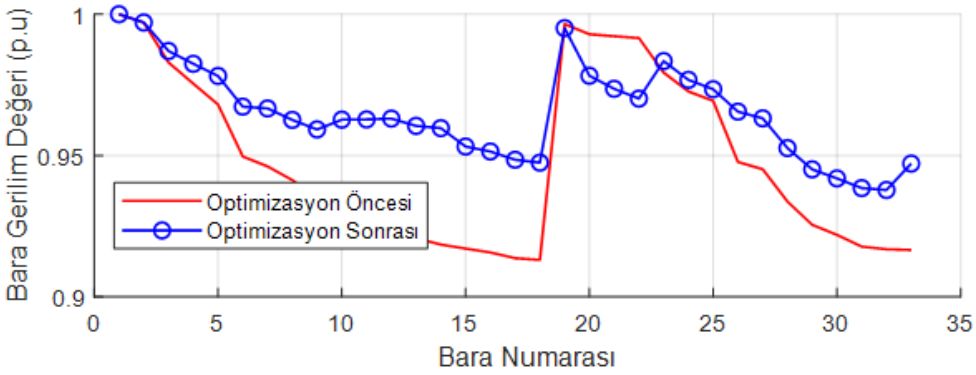

Figure 3. Bus voltages before and after reconfiguration.

Upon examining Figure 3, it is evident that there are improvements in the voltage levels across all buses, with the exception of buses 20, 21, and 22. Notably, the voltage has increased from 0.92 p.u. to 0.94 p.u., indicating a positive enhancement in the overall voltage stability of the network, with most buses benefiting from the optimization.

Figure 4 presents the results of an optimization study conducted on a 33-bus PDN) focusing on the relationship between active power loss and the VSI. The graph features a Pareto front that illustrates the trade-off between these two objective functions, where each point on the front represents an optimal solution. Notably, four significant points are highlighted: the minimum VSI of 0.0024 associated with an active power loss of 235.154 kW, the minimum active power loss of 0.1548 kW with a VSI of 139, and two intermediate points at (0.0774027, 139.895) and (0.15481, 139.457).

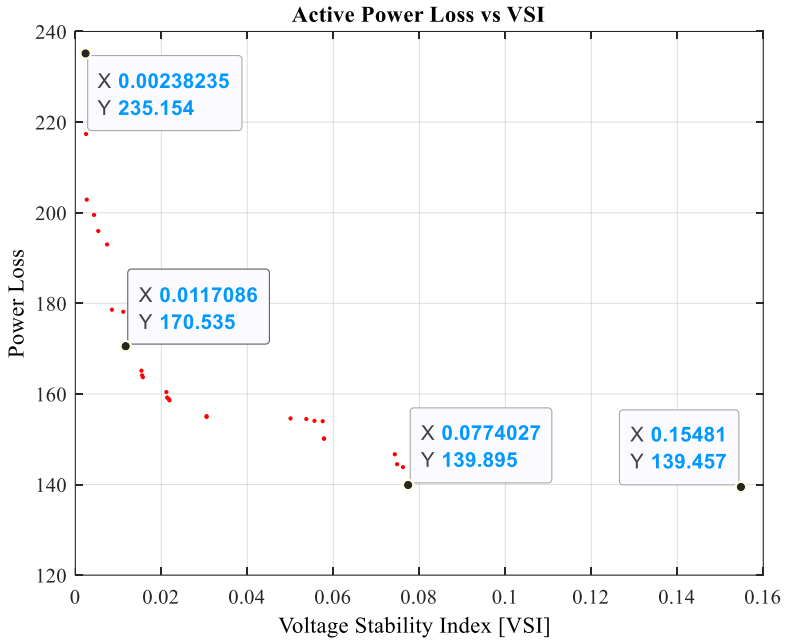

Figure 4. Pareto front analysis of active power loss vs. voltage stability index in a 33-bus test system

A trade-off analysis reveals that the lowest VSI value (0.00238235) corresponds to the highest power loss (235.154 kW), while the minimum power loss (170.535 kW) is achieved with a relatively higher VSI value (0.0117086). The intermediate points provide balanced solutions that reconcile the competing objectives of minimizing power loss while maintaining acceptable voltage stability. Overall, the VSI values range from 0 to 0.16, indicating that the system is generally in good condition regarding voltage stability. Meanwhile, the power losses fluctuate between approximately 139 kW and 235 kW, showcasing a significant optimization range within the study.

The Table 1 presents 30 distinct configurations, each characterized by various tie-switch combinations, enhancing the clarity and readability of the data. Among these configurations, one notable observation is that the lowest Voltage Stability Index (VSI) value of 0.0024 corresponds to the highest power loss of 235.2043 kW, indicating a less favorable balance between these metrics. Conversely, configuration 5 achieves the lowest power loss at 139.8948 kW; however, it does not represent an optimal solution regarding VSI, which stands at 0.0774.

Table 1. Dominated / Non-dominated pareto front results

No	Tie-Switches					VSI	Active Power Losses [Kw]	
1	3	7	11	14	34	0.0024	235.2043	
2	3	7	10	14	34	0.0024	235.1539	**Minimum VSI**
3	7	10	14	16	28	0.0578	150.1566	**Configuration**
4	**7**	**9**	**14**	**32**	**37**	**0.1548**	**139.4572**	**Minimum Active Power**
5	7	9	14	28	32	0.0774	139.8948	**Loss Configuration**
6	10	16	28	33	34	0.0537	154.4588	
7	7	10	14	15	28	0.0305	154.9194	
8	7	9	14	16	28	0.0578	150.1112	
9	10	28	32	33	34	0.0762	143.8421	
10	7	11	14	15	28	0.0305	155.1004	
11	9	14	25	33	34	0.0111	178.1375	
12	9	14	28	32	33	0.0748	144.4929	
13	9	15	28	33	34	0.0217	158.8707	
14	3	8	9	14	25	0.0053	195.9564	
15	3	8	10	14	25	0.0027	202.8829	
16	3	6	8	9	14	0.0025	217.3672	
17	10	14	28	32	33	0.0743	146.6760	
18	3	8	9	14	26	0.0074	192.9956	
19	10	14	15	28	33	0.0212	160.4115	
20	8	9	14	28	33	0.0117	170.5351	
21	9	14	28	33	34	0.0155	164.1114	
22	9	16	28	33	34	0.0556	154.0579	
23	9	14	16	28	33	0.0500	154.5985	
24	8	14	16	28	33	0.0575	153.9846	
25	10	14	28	33	34	0.0154	165.1299	
26	8	10	14	28	33	0.0085	178.5942	
27	3	8	10	14	26	0.0044	199.5078	
28	9	14	15	28	33	0.0214	159.2061	
29	8	14	15	28	33	0.0219	158.5957	
30	8	14	28	33	34	0.0157	163.6877	

This variability in configurations underscores the practical applications for system operators, who can strategically select configurations based on their operational needs. For instance, during periods of high load, configurations that minimize power loss may be favored, while during low load periods, those with higher VSI values can be selected to enhance voltage stability. This flexibility allows operators to effectively manage the trade-off between power losses and voltage stability in the distribution network.

5. CONCLUSION

In summary, this research highlights the efficacy of the Artificial Hummingbird Algorithm in optimizing a 33-bus Power Distribution Network, focusing on the dual objectives of minimizing active power loss and improving the Voltage Stability Index. The findings indicate notable enhancements in the system's performance through network reconfiguration, showcasing the advantages of optimized network topologies in power systems. The Pareto front generated from the multi-objective optimization

effectively demonstrates the balance between reducing power loss and improving voltage stability, thereby serving as a crucial decision-making tool for system operators.

The variety of solutions provided by this approach enables the selection of optimal configurations tailored to specific operational needs. These results advance the field of power system optimization and suggest that implementing strategic reconfiguration methods in power distribution networks can yield significant operational advantages, such as reduced costs and enhanced reliability. Future studies could investigate the application of this methodology in larger networks and its potential integration with other optimization challenges in power systems, thereby further improving the efficiency of power distribution networks.

REFERENCES

[1]. M. Çıkan and N. Nacar Çıkan, "Elektrikli araç şarj istasyonlarının enerji dağıtim hatlarına optimum şekilde konumlandırılması," Kahramanmaraş Sütçü İmam Üniversitesi Mühendislik Bilimleri Dergisi, vol.27, pp.340-363, Jun. 2024.
[2]. M. Çıkan and B. Kekezoglu, "Comparison of metaheuristic optimization techniques including Equilibrium optimizer algorithm in power distribution network reconfiguration," Alexandria Engineering Journal., vol.61, pp.991-1031.
[3]. M. Çıkan, "Çita optimizasyon algoritması kullanarak kısmi gölgelenme altındaki fotovoltaik sistemlerde maksimum güç noktası izleyicisinin tasarlanması," Gazi Üniversitesi Mühendislik Mimarlık Fakültesi Dergisi, vol.40, pp.555-572.
[4]. M. Çıkan and K. Dogansahin, "A Comprehensive Evaluation of Up-to-Date Optimization Algorithms on MPPT Application for Photovoltaic Systems," Energy Sources, Part A: Recovery, Utilization, and Environmental Effects, vol. 45, pp.10381-10407.
[5]. M. Çıkan and N. Nacar Çıkan, "Optimum allocation of multiple type and number of DG units based on IEEE 123-bus unbalanced multi-phase power distribution system," *International Journal of Electrical Power & Energy Systems*, vol.144, pp.108564.
[6]. N. Nacar Çıkan and M. Çıkan, "Reconfiguration of 123-bus unbalanced power distribution network analysis by considering minimization of current & voltage unbalanced indexes and power loss," *International Journal of Electrical Power & Energy System*s, vol.157, pp.109796.
[7]. W. Zhao, L.Wang, and S. Mirjalili, " Artificial hummingbird algorithm: A new bio-inspired optimizer with its engineering applications, " *Computer Methods in Applied Mechanics and Engineering*, vol.388, pp.114194.

ICENS 10TH INTERNATIONAL CONFERENCE ON ENGINEERING AND NATURAL SCIENCE
October 02-06 2024 Sarajevo (Hybrid Event)

Simultaneous Allocation, Sizing, and Power Factor Optimization of Wind Turbines and EV Charging Stations in Power Distribution Networks

Murat ÇIKAN

Abstract

This study explores the application of the Runge-Kutta Algorithm (RKO), a cutting-edge metaheuristic search technique, for the simultaneous allocation, sizing, and power factor optimization of wind turbines in power distribution systems. The research also involves the concurrent allocation of three 2 MW electric vehicle (EV) charging stations, integrated alongside the wind turbine installations. The objective is to minimize power loss while ensuring the efficient integration of renewable energy sources and EV charging infrastructure. The proposed RKO-based approach is evaluated for its effectiveness in optimizing component placement and enhancing overall system performance under dynamic load conditions. Simulation results indicate that the RKO algorithm offers a robust and efficient method for reducing power loss, making it a promising tool for future energy distribution system optimization.

Keywords: Dg Allocation, Meta-heuristic Search Algorithm, Electric Vehicle (EV) Charging Stations, Runge-Kutta Algorithm

1. INTRODUCTION

The integration of renewable energy sources and electric vehicle (EV) charging infrastructure [1], [2], [3] into existing power distribution networks is increasingly critical in the transition toward sustainable energy systems. Wind turbines and EV charging stations, as prominent distributed generation (DG) assets, provide opportunities for improving energy efficiency, reducing carbon emissions, and enhancing the reliability of power systems. However, the effective placement and sizing of these DG units within a distribution network are complex tasks, requiring careful consideration of power loss minimization [4], voltage stability, and operational constraints. Recent advances in optimization techniques have enabled more sophisticated approaches to DG allocation in distribution networks. Among these, population-based algorithms have shown promise due to their adaptability and efficiency in handling non-linear, multi-objective problems typical of power systems [5], [6]. In this context, the 136-Bus Test System is used as a model to evaluate the impact of DG [4]integration on a large-scale power distribution network, offering a realistic representation of the challenges faced in modern grid systems [7].

This study employs the Runge-Kutta Algorithm (RKA) to determine the optimal locations and sizes of wind turbines and EV charging stations in the 136-Bus Test System. The objective functions focus on minimizing power losses and optimizing the Voltage Stability Index (VSI) to ensure network stability under varying load conditions. Additionally, operational constraints related to current limits, voltage levels, and power capacities are incorporated to maintain reliable network performance [8]. The results highlight the potential of RKA to enhance system efficiency by achieving substantial reductions in power losses and improvements in voltage stability.

This paper is structured as follows: Section 2 presents the mathematical formulation of the power system, including objective functions and constraints. Section 3 describes the methodology and implementation of the RKA for DG optimization. Section 4 discusses the placement and sizing results of wind turbines and EV charging stations and their effects on system performance. Finally, conclusions and recommendations for future research are provided in Section 5.

2. MATHEMATICAL EXPRESSION OF POWER SYSTEM

The mathematical modelling of the power system is fundamental for analysing and optimizing network performance. This section presents the mathematical expressions governing the power flow, voltage stability, and loss minimization in the system. The power system model incorporates key parameters such as bus voltages, line impedances, power injections, and load demands, which collectively determine the system's operational state.

2.1 Constraint

This study defines several constraints related to current, power, and system capacity to ensure that the optimization process adheres to operational and safety limits. The current constraints prevent network branch overloading by maintaining current flow within each branch's permissible maximum. Power constraints are applied to regulate the distribution of active and reactive power throughout the network, ensuring that each bus and branch operates within designated bounds. These constraints, as shown in Equations (1) to (3), are essential for maintaining system stability, reliability, and efficiency. Each constraint is implemented as an inequality, effectively limiting the solution space to configurations that meet these technical and safety requirements.

- Voltage Constraints

$$V_{min}^{\varphi} \leq V_i^{\varphi} \leq V_{max}^{\varphi} \qquad \forall i \in n, \varphi \in \{A, B, C\} \tag{1}$$

- Current constraints

$$I_{ij}^{\varphi} \leq I_{ij,max}^{\varphi} \qquad \forall (i,j) \in m, \varphi \in \{A, B, C\} \tag{2}$$

- Power balance constraint

$$\sum_{i \in N} P_i = \sum_{j \in N} \left(P_j + P_{L,j}\right) \tag{3}$$

2.2. Objective Function

The primary objectives of this research are centred around two key objective functions. The first objective is the minimization of power losses [9] within the network, expressed by the formula in Equation (4). The second objective involves the optimization of the Voltage Stability Index (VSI) [8], as defined in Equation (5). These dual objectives are designed to enhance both the efficiency and reliability of the power distribution system.

$$P_{Loss}^{min} = \sum_{i,k=1,}^{N_{br}} r_{(i,k)} \cdot \left(\frac{{P_k}^2 + {Q_k}^2}{{V_k}^2}\right) . Sw_{(i,k)} \tag{4}$$

$$VSI = \frac{4\,|V_S|^2\,|C||D||S_R|\cos(\phi_R + \delta_S)\sin(\delta_S)}{|S_S|^2 . \cos^2(\varphi_S + \delta_R)} \leq 1 \tag{5}$$

2.3. 136-Bus Test System

The 136-Bus Test System [10], [11], representing a complex power distribution network, was employed to evaluate the effectiveness of the optimization algorithms. This system presents a network structure reflective of real-world scenarios, enabling a rigorous assessment of algorithmic performance. The 136-bus system includes 156 branches, with 21 left de-energized to maintain a radial configuration suitable for distribution network operations, as shown in the circuit diagram. The network comprises 107 spot loads, all modelled as PQ loads, distributed across the buses. The total active and reactive loads for the distribution line are 18.3 MW and 7.9 MVAR, respectively. Additionally, the system experiences total active and reactive power losses of 0.32037 MW and 0.70295 MVAR, respectively, across the distribution line. This test setup provides a robust framework for examining optimization solutions in power distribution contexts.

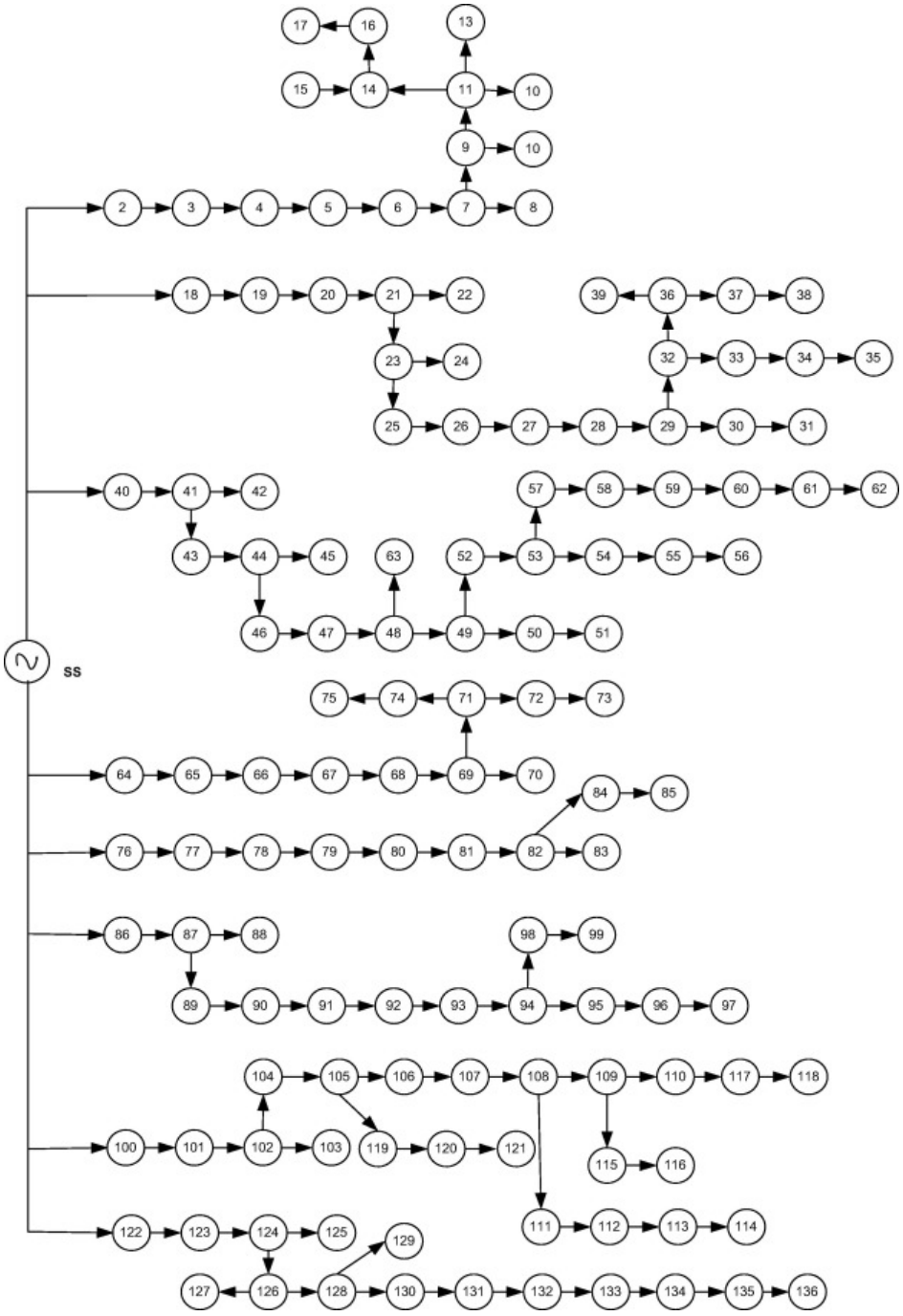

Figure 9 *13-Bus Power distribution network [10], [11]*

3. RUNGE-KUTTA OPTIMIZATION ALGORITHM

The Runge-Kutta Optimizer (RUN) is a population-based optimization model developed based on the slope calculation principles of the fourth-order Runge-Kutta (RK4) method [12]. RUN systematically leverages RK4 to explore and exploit promising

regions within the solution space, providing a robust framework for global optimization. The algorithm begins with the random initialization of population members, iteratively updating their positions based on a slope-driven mechanism derived from RK4. This approach strategically balances exploration and exploitation phases, maximizing solution quality and achieving rapid convergence. To further enhance robustness and prevent premature convergence to local optima, an Enhanced Solution Quality (ESQ) mechanism is integrated into RUN. Testing revealed that RUN achieved superior performance across a diverse range of mathematical benchmark functions and engineering design problems, consistently outperforming several state-of-the-art metaheuristic algorithms in both convergence speed and accuracy. RUN's high exploration capability originates from its elevated randomness, which facilitates a comprehensive search of the solution space. Meanwhile, its exploitation phase refines solutions around the best candidates, ensuring that high-quality solutions are consistently obtained. The mathematical expressions underpinning RUN's design are systematically defined from Equation (6) to Equation (12).

$$k_1 = \frac{1}{2\Delta_x}\left(rand_{no}.\left(x_{worst} - u.x_{best}\right)\right) \tag{6}$$

$$u = round(rand_{no} + 1).(1 - rand_{no}) \tag{7}$$

$$k_2 = \frac{1}{2\Delta_x}\left(rand_{no}.\left(x_{worst} - k_1.\Delta_x.rand_{no,1}\right) - \left(u.x_{best} + k_1.\Delta_x.rand_{no,2}\right)\right) \tag{8}$$

$$k_3 = \frac{1}{2\Delta_x}\left(rand_{no}.\left(x_{worst} - \frac{k_2}{2}.\Delta_x.rand_{no,1}\right) - \left(u.x_{best} + \frac{k_2}{2}.\Delta_x.rand_{no,2}\right)\right) \tag{9}$$

$$k_4 = \frac{1}{2\Delta_x}\left(rand_{no}.\left(x_{worst} - k_3.\Delta_x.rand_{no,1}\right) - \left(u.x_{best} + k_3.\Delta_x.rand_{no,2}\right)\right) \tag{10}$$

$$\begin{aligned} &rand_{no} < \frac{1}{2}, \quad x_{n+1} = SM.SF + \mu.x_s + x_c \quad exploration\ phase \\ &otherwise\ , \quad x_{n+1} = SM.SF + \mu.\acute{x_s} + x_m \quad exploitation\ phase \end{aligned} \tag{11}$$

$$SF = \left(1 - \frac{rand_{no}}{2}\right).\left(a.e^{-b.rand_{no}.\left(\frac{i}{Max_i}\right)}\right) \tag{12}$$

4. WIND TURBINE AND EV CHARGING STATIONS ALLOCATION AND SIZE

The allocation and sizing of wind turbines (WT) and electric vehicle (EV) charging stations in the 136-Bus Test System were optimized using the Runge-Kutta Algorithm (RKA). This approach aimed to enhance the system's efficiency by reducing power losses and improving voltage stability. The optimization process considered both active and reactive power limits for the wind turbines and the demand capacity for EV charging stations. The constraints for each parameter were set based on network load capacity, Voltage Stability Index (VSI) limits, and spatial constraints associated with EV charging infrastructure. Lower (lb) and upper (ub) bounds were defined to guide the optimization (in Table 1), setting minimum and maximum values for active and reactive power output, as well as EV charging power requirements.

Table 2 *Lower and Upper boundary of Variables*

Variab.	WT	Active Power Size	Reactive Power Size	EV Location	Demand Power
Lb	Min	0	-10	Min	0
Ub	Max	20	10	Max	2

where minimum and maximum are first (1) and last (136) busbar no. The Table 2 and Table 3 illustrates various scenarios tested during this study, showing the impact of DG additions on power loss and voltage stability. In the initial case, without DG, the system experiences an active power loss of 320.36 kW and a reactive power loss of 702.95 kVAR, with the minimum voltage recorded at 0.971 p.u. at bus 85. These baseline values serve as a reference for evaluating the effectiveness of DG integration.

Case 1: This scenario introduces a single wind turbine at bus 106, sized at 2828.4 kW and 1210.0 kVAR, along with an EV charging station at bus 1 with a demand of 2000 kW. These additions result in a significant reduction in system losses, with active power loss decreasing by 33.5% to 213.03 kW, and reactive power loss decreasing by 35.14% to 455.92 kVAR.

Case 2: In this configuration, two wind turbines and two EV charging stations are incorporated. The first wind turbine remains at bus 106 (2828.4 kW, 1209.8 kVAR), and a second turbine is added at bus 11 with a capacity of 2326.7 kW and 930.57 kVAR. Both EV charging stations are set at bus 1 with a demand of 2000 kW each. This setup further reduces active and reactive power losses by 45.87% (173.42 kW) and 47.74% (367.36 kVAR), respectively, compared to the initial case.

Table 3 *Allocation and Size of DGs*

Panel No	DG Type	Location	Size of DG / EV	Size of DG / EV	P_{Loss}^{Active}	Q_{Loss}^{Active}
		(Bus No)	(kW)	(kVAR)	(kW)	(kVar)
Initial	w/o DG	-	-	-	320.3642	702.9472
Case 1	1st WT	106	2828.4	1210.0	213.0293	455.9170
	1st EV	1	2000	0		
Case 2	1st WT	106	2828.4	1209.8	173.4170	367.3586
	1st EV	1	2000	0		
	2nd WT	11	2326.7	930.57		
	2nd EV	1	2000	0		
Case 3	1st WT	11	2326.7	930.57	142.1032	297.5572
	1st EV	1	2000	0		
	2nd WT	29	2061.5	1012.6		
	2nd EV	1	2000	0		
	3rd WT	106	2828.4	1209.8		
	3rd EV	1	2000	0		

Case 3: The most extensive configuration includes three wind turbines and three EV charging stations. The turbines are located at buses 11 (2326.7 kW, 930.57 kVAR), 29 (2061.5 kW, 1012.6 kVAR), and 106 (2828.4 kW, 1209.8 kVAR). The EV charging stations remain at bus 1 with a demand of 2000 kW each. In this scenario, the system achieves the highest reduction in losses, with active power loss minimized by 55.64% to 142.10 kW, and reactive power loss decreased by 57.67% to 297.56 kVAR. The voltage stability is also improved, maintaining a minimum voltage of 0.971 p.u. at bus 85 across all cases.

The table provides a detailed breakdown of each scenario, including DG type, location (bus number), size of DG in kW and kVAR, active and reactive power losses, Voltage Stability Index (VSI), minimum voltage, and the bus location of the minimum voltage. Additionally, the percentage reductions in active and reactive power losses are shown, illustrating the incremental benefits of each DG configuration. These results emphasize the role of optimized DG placement and sizing in enhancing system performance, particularly through reduced losses and improved voltage stability.

Table 4 *Power system network active and reactive power loss*

Panel No	DG Type	VSI	Minimum Voltage	Bus No	P_{Loss}^{Active} Reduction	Q_{Loss}^{Active} Reduction
			(p.u.)	V_{min}	(%)	(%)
Initial	w/o DG	-3.182e-1	0.971 p.u.	bus 85	---	---
Case 1	1st WT	-2.1156e-2	0.971 p.u.	bus 85	33.50	35.14
	1st EV					
Case 2	1st WT	8.6273e-01	0.971 p.u.	bus 85	45.87	47.74
	1st EV					
	2nd WT					
	2nd EV					
Case 3	1st WT	8.6273e-01	0.971 p.u.	bus 85	55.64	57.67
	1st EV					
	2nd WT					
	2nd EV					
	3rd WT					
	3rd EV					

5. CONCLUSIONS

This study presented an optimization framework for the placement and sizing of wind turbines and EV charging stations in a complex power distribution network, utilizing the 136-Bus Test System as a representative model. The Runge-Kutta Algorithm (RKA) was employed to optimize system performance by minimizing power losses and enhancing voltage stability. Through multiple scenarios, the impact of distributed generation (DG) on system efficiency and reliability was evaluated, demonstrating significant reductions in active and reactive power losses and improvements in voltage stability. The results indicate that strategic allocation and sizing of DG sources, specifically wind turbines and EV charging stations, can substantially enhance network performance. The optimized configurations led to reductions in power losses by up to 55.64% and 57.67% for active and reactive losses, respectively, while maintaining voltage levels within safe operational limits. These findings underscore the effectiveness of RKA in addressing complex optimization challenges in power systems, offering a robust tool for planners and engineers aiming to integrate renewable energy sources and EV infrastructure into existing distribution networks. Future work can expand on this approach by incorporating additional renewable energy sources, such as solar PV systems, and evaluating the impacts of varying load profiles and seasonal fluctuations. Furthermore, the integration of real-time data and advanced machine learning techniques could further enhance the adaptability and accuracy of optimization solutions, contributing to more resilient and sustainable power systems.

ACKNOWLEDGMENT

During the preparation of this work the author(s) used ChatGPT 4.o-mini in order to refine the English wording of certain phrases. After using this tool/service, the author reviewed and edited the content as needed and take(s) full responsibility for the content of the publication.

REFERENCES

[1] M. Çıkan and N. Nacar Çıkan, “Elektrikli Araç Şarj İstasyonlarının Enerji Dağıtım Hatlarına Optimum Şekilde Konumlandırılması,” Kahramanmaraş Sütçü İmam Üniversitesi Mühendislik Bilimleri Dergisi, vol. 27, no. 2, pp. 340–363, 2024, doi: 10.17780/ksujes.1365209.

[2] M. Çıkan, “Çita optimizasyon algoritması kullanarak kısmi gölgelenme altındaki fotovoltaik sistemlerde maksimum güç noktası izleyicisinin tasarlanması,” Gazi Üniversitesi Mühendislik Mimarlık Fakültesi Dergisi, vol. 40, no. 1, pp. 555–572, 2024, doi: 10.17341/gazimmfd.1183267.

[3] M. Cikan and K. Dogansahin, “A Comprehensive Evaluation of Up-to-Date Optimization Algorithms on MPPT Application for Photovoltaic Systems,” Energy Sources, Part A: Recovery, Utilization, and Environmental Effects, vol. 45, no. 4, pp. 10381–10407, Oct. 2023, doi: 10.1080/15567036.2023.2245771.

[4] M. Cikan and N. N. Cikan, “Optimum allocation of multiple type and number of DG units based on IEEE 123-bus unbalanced multi-phase power distribution system,” International Journal of Electrical Power & Energy Systems, vol. 144, p. 108564, 2023, doi: https://doi.org/10.1016/j.ijepes.2022.108564.

[5] K. Aygül, M. Cikan, T. Demirdelen, and M. Tumay, “Butterfly optimization algorithm based maximum power point tracking of photovoltaic systems under partial shading condition,” Energy Sources, Part A: Recovery, Utilization, and Environmental Effects, pp. 1–19, Oct. 2019, doi: 10.1080/15567036.2019.1677818.

[6] F. Akın, M. Çıkan, O. Arikan, and B. Kekezoğlu, “Optimizing Distribution Network Reconfiguration for Power Loss and Fault Current Management,” Mühendislik Bilimleri ve Araştırmaları Dergisi, vol. 6, no. 2, pp. 188–197, 2024, doi: 10.46387/bjesr.1501986.

[7] N. Nacar Cikan and M. Cikan, “Reconfiguration of 123-bus unbalanced power distribution network analysis by considering minimization of current & voltage unbalanced indexes and power loss,” International Journal of Electrical Power & Energy Systems, vol. 157, p. 109796, 2024, doi: https://doi.org/10.1016/j.ijepes.2024.109796.

[8] K. Doğanşahin and M. Çikan, “A new line stability index for voltage stability analysis based on line loading,” vol. 1, no. 1, pp. 23–30, 2023, doi: 10.14744/cetj.2023.000.

[9] M. Cikan and B. Kekezoglu, “Comparison of metaheuristic optimization techniques including Equilibrium optimizer algorithm in power distribution network reconfiguration,” Alexandria Engineering Journal, vol. 61, no. 2, pp. 991–1031, 2022, doi: https://doi.org/10.1016/j.aej.2021.06.079.

[10] T. Yuvaraj and K. Ravi, “Multi-objective simultaneous DG and DSTATCOM allocation in radial distribution networks using cuckoo searching algorithm,” Alexandria Engineering Journal, vol. 57, no. 4, pp. 2729–2742, Dec. 2018, doi: 10.1016/j.aej.2018.01.001.

[11] J. R. S. Mantovani, F. Casari, and R. A. Romero, “Reconfiguração De Sıstemas De Dıstrıbuıção Radıaıs Utılızando O Crıtérıo De Queda De Tensão,” 2000.

[12] I. Ahmadianfar, A. A. Heidari, A. H. Gandomi, X. Chu, and H. Chen, “RUN beyond the metaphor: An efficient optimization algorithm based on Runge Kutta method,” Expert Syst Appl, vol. 181, Nov. 2021, doi: 10.1016/j.eswa.2021.115079.

ICENS 10TH INTERNATIONAL CONFERENCE ON ENGINEERING AND NATURAL SCIENCE
October 02-06 2024 Sarajevo (Hybrid Event)

Optimization of PV, Capacitor Bank, and EV Charging Station Allocation in a 33-Bus Power Distribution System Using the Slime Mould Algorithm

***Nisa NACAR ÇIKAN*[1]**

Abstract

This study presents a comprehensive approach to the optimal allocation and sizing of photovoltaic (PV) systems and capacitor banks in a 33-bus power distribution system, focusing on enhancing system performance. Simultaneously, the allocation of PV systems, capacitor banks, and electric vehicle (EV) charging stations is addressed to optimize system efficiency. The primary objectives include minimizing active power losses and improving the voltage profile across the network. To solve this complex optimization problem, the Slime Mould Algorithm (SMA), a cutting-edge metaheuristic technique, is employed as an advanced tool for distributed generation (DG) allocation. SMA's robust search capability and adaptability make it well-suited for addressing the multi-objective nature of this study, delivering optimized results that balance system losses and voltage stability. The proposed method demonstrates significant potential for improving the efficiency and stability of modern power distribution networks.

Keywords: Electrical Vehicle Charging Stations, Slime Mode Algorithm, DG Allocation

1. INTRODUCTION

The growing incorporation of renewable energy sources into power distribution systems has become crucial for improving efficiency and sustainability. Among various renewable technologies, photovoltaic (PV) systems are particularly notable for their capability to capture solar energy, which is plentiful and eco-friendly [1],[2]. However, merely integrating PV systems into current power distribution systems is inadequate; a thoughtful strategy for their placement and sizing is essential to ensure they effectively enhance overall system performance. This research concentrates on a 33-bus power distribution system, analyzing the most effective locations for PV systems and capacitor banks to reduce active power losses and enhance the voltage profile throughout the network.

In addition to PV systems, the allocation of capacitor banks and electric vehicle (EV) charging stations is also critical in modern power distribution [3]. The rise of electric vehicles necessitates the establishment of efficient charging infrastructure, which can significantly influence power demand and network stability. By integrating these components, the overall efficiency of the power distribution system can be maximized [4]. To tackle this multifaceted optimization challenge, this research employs the Slime Mould Algorithm (SMA), a novel metaheuristic technique known for its flexibility and effective search capabilities. The SMA's strength lies in its ability to navigate complex optimization landscapes, allowing it to find optimal solutions that achieve a balance between minimizing losses and enhancing voltage stability.

Moreover, the need for advanced optimization techniques is underscored by the growing complexity of modern power distribution systems, driven by factors such as increased energy consumption and the penetration of distributed generation sources. Traditional methods often fall short in addressing these challenges due to their inability to efficiently explore the solution space and manage the inherent trade-offs between competing objectives [5], [6]. The application of SMA [7] in this study not only addresses the intricacies of optimizing PV and capacitor bank allocations but also highlights its potential as a powerful tool for enhancing the stability and reliability of power distribution networks. By optimizing the interplay between renewable energy sources, energy storage solutions, and infrastructure improvements, this research contributes to a more resilient and sustainable energy future.

[1] *Corresponding author: Cukurova University, Electrical and Electronics Engineering, 01330, Balcali, Sarıçam/Adana, Turkey.*
ncikan@cu.edu.tr

The remainder of the paper is organized as follows: Section 2 introduces the 33-bus Power Distribution Network (PDN) system and outlines the associated constraints. Section 3 delves into the Slime Mould Algorithm (SMA), detailing its methodology. Section 4 presents the results of the study, along with a discussion of their implications. Finally, the paper concludes with a summary of the findings and their significance.

2. 33-BUS TEST SYSTEM

The 33-bus distribution system depicted in Figure 1 serves as an important reference for analyzing power distribution networks. This network consists of one feeder, 33 buses, and 37 branches, along with five tie switches (T.S.) and 32 sectionalizing switches (S.S.). The total active power demand within the system is 3.72 MW, while the reactive power demand is measured at 2.3 MVAR. Under this configuration, the power loss in the distribution network is calculated to be 202.6771 kW for active power and 135.14 kVAR for reactive power. Additionally, the minimum voltage magnitude in this setup is recorded at 0.9131 p.u., occurring at bus 18. These characteristics highlight the essential parameters of the system, providing a foundation for evaluating its efficiency and performance in various operational scenarios.

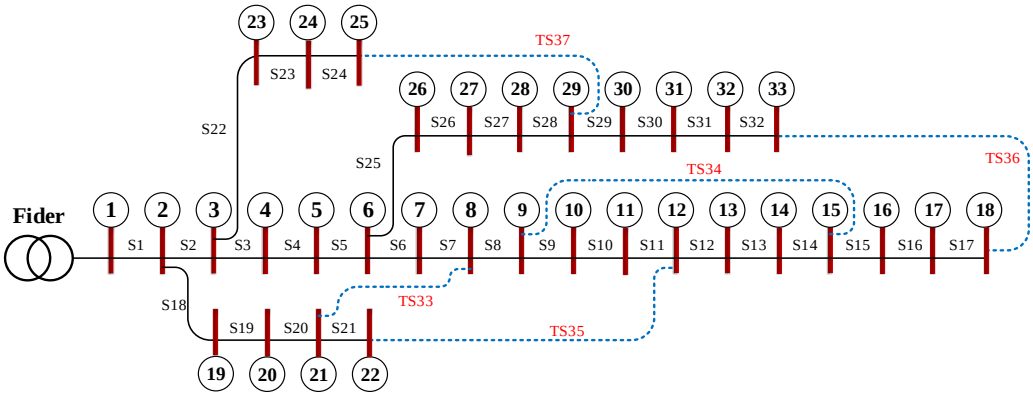

Figure 1. 33-bus test system [5].

2.1. Problem formalization

This study aims to reduce active power loss and improve the voltage stability index. The equation for minimizing power loss is provided in Equation 1. [5].

$$\mathbf{P_{Loss}^{min}} = \left(\sum_{i,k=1,}^{N_{br}} \mathbf{r_{(i,k)}} \cdot \left(\frac{P_k^2+Q_k^2}{V_k^2}\right) . \mathbf{Sw_{(i,k)}}\right) \quad \textbf{(1)}$$

Equation 1 provides the formula for enhancing the voltage stability index [5].

$$\mathbf{VSI} = \frac{4|V_i|^2|C||D||S_k|\cos(\varphi_k+\delta_S).\sin(\delta_i)}{|S_i|^2.\cos^2(\varphi_i+\delta_k)} \leq \mathbf{1} \quad \textbf{(2)}$$

A deeper examination is necessary to assess the voltage stability of systems operating close to their limit thresholds. The literature presents numerous voltage stability indices; however, most are based on certain assumptions or oversights. This study utilizes a newly proposed index that incorporates various line characteristics and is grounded in line loading considerations [2]. It has been observed that the proposed index reliably yields results across different conditions and loading scenarios.

In power systems, voltage fluctuations must be maintained within defined limits, as illustrated in Equation 3. [5].

$$V_{i,\phi}^{min} \leq V_{i,\phi} \leq V_{i,\phi}^{max} \qquad \forall\phi \in \{a,b,c\}, \quad \forall i \in \text{Buses} \quad (3)$$

The cable within the system must not carry current exceeding the limit specified in Equation 4 [5].

$$I_{i,\phi} \leq I_{i,\phi}^{max} \quad \forall\phi \in \{a,b,c\}, \quad \forall i \in \text{Branches} \quad (4)$$

Equation 5 guarantees that the sum of generated power matches the combined total of the load and losses within the system [5].

$$\sum_{i=1}^{N_{Gen}} P_{i,Gen}^{\emptyset} = \sum_{i=1}^{N_{Load}} P_{i,Load}^{\emptyset} + \sum_{i=1}^{N_{Branch}} P_{i,Loss}^{\emptyset} + \sum P_{i,Loss}^{equipment} \qquad \forall \phi \in \{a,b,c\} \tag{5}$$

As outlined in Equation 6, transformers must operate within specified voltage and current limits for each phase to ensure optimal performance and avoid potential damage [5].

$$X_{i,\emptyset}^{trfmin} \leq X_{i,\emptyset,trf} \leq X_{i,\emptyset}^{trfmax} \quad \forall \phi \in \{a,b,c\} \tag{6}$$

Equation 7 shows that to ensure line security, the power flow on a line must remain below a specified limit [5].

$$S_{i,\emptyset,line} \leq S_{i,\emptyset,line}^{max} \qquad \forall \phi \in \{a,b,c\}, \quad \forall i \in Lines \tag{7}$$

3. SLIME MOULD ALGORITHM

The Slime Mould Algorithm is an innovative optimization technique inspired by the foraging behavior of slime moulds, particularly Physarum polycephalum [7]. This metaheuristic method is distinguished by its ability to explore complex solution spaces effectively while balancing exploration and exploitation. SMA operates through a unique mechanism where agents, representing solutions, mimic the nutrient-seeking movement of slime moulds as they search for food sources [7]. This adaptive behavior allows the algorithm to converge on optimal solutions efficiently by dynamically adjusting to the characteristics of the problem at hand. The algorithm's flexibility makes it suitable for tackling a wide range of optimization challenges, from engineering applications to energy management, thus demonstrating its potential as a powerful tool in the field of computational intelligence [7].

4. RESULTS AND DISCUSSION

Table 1 presents three cases. In Case 1, the system is optimized for 1 PV unit, in Case 2 for 2 PV units, and in Case 3 for 3 PV units. In Case 1, the first PV unit is placed at bus 6, and its maximum power output to the grid is found to be 2575.32 kW. Under these conditions, the active power loss decreases from 202.68 kW to 103.97 kW. The minimum bus voltage is improved from 0.91 to 0.95. This reduction in active power loss corresponds to a 49% decrease. The analytical analysis of the study, which was conducted using a metaheuristic approach, is illustrated in the accompanying figures. As can be seen in the figures, the active power loss is calculated as 103.97 kW when a 2.575 MW DG unit is placed at bus 6.

Table 1. Determination of the sizes and locations of PV panels in the 33-bus test system using the SMA algorithm

Case	DG Type	Location (Bus No)	Size of DG (kW)	Total Size of DG (kW)	Power Factor cos(Φ)	P_{Loss}^{Active} (kW)	Q_{Loss}^{Active} (kVar)	Voltage Stability Index	Minimum Voltage (p.u.)	Bus No at V_{min}	P_{Loss}^{Active} Reduction (%)
Initial	w/o PV	-	-	-	-	202.68	135.14	0.0379	0.9131	18	0.00
Case 1	1-PV	6	2575.32	2575.32	1	103.97	74.78	0.1796	0.9511	18	48.7037
Case 2	2-PV	13	846.38	2005.05	1	85.91	58.55	0.28484	0.9685	33	57.6123
		30	1158.67		1						
		14	753.98		1			0.25347			
Case 3	3-PV	24	1099.44	2924.84	1	71.46	49.39		0.9686	33	64.7433
		30	1071.42		1						

As shown in Table 1, the accuracy of the optimization study performed using the metaheuristic algorithm is verified, as similar results are obtained both from the literature and through the analytical approach. When the same study is conducted for Case 2 and Case 3, the active power losses are further reduced to 85.91 kW and 71.46 kW, respectively.

There are three cases presented in Table 2. In Case 1, the system is optimized by adding 1 capacitor bank, in Case 2 by adding 2 capacitor banks, and in Case 3 by adding 3 capacitor banks. In Case 1, the first capacitor bank is placed at bus 30, and its maximum reactive power output is found to be 1257.2 kW. Under these conditions, the active power loss decreases from 202.68 kW to 143.60 kW. The minimum bus voltage is improved from 0.91 to 0.92. This reduction in active power loss corresponds to a decrease of 29.15%. When the same study is conducted for Case 2 and Case 3, the active power losses are further reduced to 135.74 kW and 132.16 kW, respectively.

Table 2. Determination of the sizes and locations of capacitor tanks in the 33-bus test system using the SMA algorithm

Case	DG Type	Location (Bus No)	Size of DG (kW)	P_{Loss}^{Active} (kW)	Q_{Loss}^{Active} (kVar)	Minimum Voltage (p.u.)	Bus No at V_{min}	P_{Loss}^{Active} Reduction (%)
Initial	w/o PV	-	-	202.68	135.14	0.9131	18	0.00
Case 1	1-Capacitor	30	1257.2	143.60	96.30	0.9258	18	29.15%
Case 2	2-Capacitor	12 30	468.87 1057.8	135.74	90.54	0.9362	18	33.03%
Case 3	3-Capacitor	13 24 30	378.69 544.21 1036.7	132.16	88.32	0.9383	18	34.80%

A multi-objective approach was implemented in this study. To demonstrate the effectiveness of the algorithm, three different cases were considered. The peak load value of the electric vehicle (EV) charging stations was set to 500 kW. Assuming that the minimum charging power of a vehicle is 50 kW, approximately 10 vehicles can be charged simultaneously. In Table 3, the PV, capacitor banks, and EV charging stations were optimally located in the 33-bus test system simultaneously. Moreover, the sizes of the PV units and capacitor banks were optimized simultaneously.

Table 3. PV, Capacitor and EV charging stations

Case	DG Type	Location (Bus No)	Size of DG / EV (kW)	P_{Loss}^{Active} (kW)	Q_{Loss}^{Active} (kVar)	Voltage Stability Index	Minimum Voltage (p.u.)	Bus No at V_{min}	P_{Loss}^{Active} Reduction (%)
Initial	w/o PV	-	-	202.68	135.14	37.9e-3	0.9131	18	0.00
Case 1	1st PV 1st Cap 1st EV	6 30 2	2538.89 1251.09 500.00	52.688	40.917	6.35e-3	0.962	18	73.92%.
Case 2	1st PV 1st Cap 1st EV 2nd PV 2nd Cap 2nd EV	12 12 12 30 30 2	1466.29 455.14 500.00 1095.5 1040.3 500.00	29.724	20.957	1.42e-3	0.980	25	85.32%
Case 3	1st PV 1st Cap 1st EV 2nd PV 2nd Cap 2nd EV 3rd PV 3rd Cap 3rd EV	24 14 2 30 3 2 14 30 2	1143.3 335.9 500.00 1065.3 797.46 500.00 755.97 994.17 500.00	15.504	12.08	5.43e-3	0.992	8	93.34%

It was assumed that the PV units can supply power to the system within the range of 0 to 4 MW, and similarly, capacitor banks can provide reactive power within the range of 0 to 4 MVAR. In Case 1, 5 parameters were optimized, which are: PV location and size, capacitor bank location and size, and EV location. As a result, the PV was placed at bus 6, the capacitor bank at bus 30,

and the EV charging station at bus 2. It was observed that these locations were consistent with the results obtained for PV and capacitor banks. The size values also produced similar results. The EV charging station was optimally located near the feeder bus (bus 1) at bus 2. When Cases 2 and 3 were examined, it was found that the optimal location results in the multi-objective study were quite similar to those obtained when PV was optimized individually. The number of optimized parameters in the multi-objective approach was 5 in Case 1, 10 in Case 2, and 15 in Case 3. Despite the presence of renewable energy sources in the system, when considering configurations with minimum power losses, it was observed that the EV charging stations were optimally located near the feeder bus.

5. CONCLUSION

In conclusion, the optimal allocation and sizing of distributed generation sources such as PV units, capacitor banks, and EV charging stations play a crucial role in enhancing the overall performance of distribution networks. The results from the multi-objective optimization cases demonstrated that proper placement of these components significantly reduces active power losses and improves voltage profiles. Furthermore, the findings indicate that EV charging stations are optimally located near the feeder bus to minimize power losses, even when integrated with other DG sources like PV and capacitors. The consistency between the obtained results and analytical analyses confirms the accuracy and robustness of the proposed approach, making it an effective strategy for addressing complex optimization problems in power distribution systems.

REFERENCES

[1]. M. Çıkan, "Çita optimizasyon algoritması kullanarak kısmi gölgelenme altındaki fotovoltaik sistemlerde maksimum güç noktası izleyicisinin tasarlanması," *Gazi Üniversitesi Mühendislik Mimarlık Fakültesi Dergisi*, vol.40, pp.555-572.

[2]. M. Çıkan and K. Dogansahin, "A Comprehensive Evaluation of Up-to-Date Optimization Algorithms on MPPT Application for Photovoltaic Systems*," Energy Sources, Part A: Recovery, Utilization, and Environmental Effects*, vol. 45, pp.10381-10407.

[3]. M. Çıkan and N. Nacar Çıkan, "Optimum allocation of multiple type and number of DG units based on IEEE 123-bus unbalanced multi-phase power distribution system," *International Journal of Electrical Power & Energy Systems*, vol.144, pp.108564

[4]. M. Çıkan and N. Nacar Çıkan, "Elektrikli araç şarj istasyonlarının enerji dağıtim hatlarına optimum şekilde konumlandırılması*," Kahramanmaraş Sütçü İmam Üniversitesi Mühendislik Bilimleri Dergisi,* vol.27, pp.340-363, Jun. 2024.

[5]. M. Çıkan and B. Kekezoglu, "Comparison of metaheuristic optimization techniques including Equilibrium optimizer algorithm in power distribution network reconfiguration," *Alexandria Engineering Journal.*, vol.61, pp.991-1031.

[6]. N. Nacar Çıkan and M. Çıkan, "Reconfiguration of 123-bus unbalanced power distribution network analysis by considering minimization of current & voltage unbalanced indexes and power loss," *International Journal of Electrical Power & Energy Systems*, vol.157, pp.109796.

[7]. S. Li, H. Chen, M. Wang, A.A. Heidari, and S. Mirjalili, "Slime mould algorithm: A new method for stochastic optimization," *Future Generation Computer Systems*, vol.111, pp.300-323.

ICENS 10TH INTERNATIONAL CONFERENCE ON ENGINEERING AND NATURAL SCIENCE
October 02-06 2024 Sarajevo (Hybrid Event)

Maximum Power Point Tracking (MPPT) in Photovoltaic Systems Using the Slime Mould Algorithm Under Uniform and Partial Shading Conditions

Murat ÇIKAN

Abstract

This study explores the application of the Slime Mould Algorithm (SMA), an advanced metaheuristic technique, for maximum power point tracking (MPPT) in photovoltaic (PV) systems. The focus is on a configuration involving three solar panels connected in both series and parallel arrangements, operating under uniform and partial shading conditions. Accurate detection of the maximum power point (MPP) is critical to improving the efficiency of PV systems, especially when subjected to varying irradiance levels. The proposed SMA-based MPPT method is evaluated for its effectiveness in handling the non-linear characteristics and power fluctuations inherent in partial shading. Comparative analysis is performed to assess its performance against traditional MPPT algorithms in terms of convergence speed, accuracy, and robustness. The results highlight the potential of the SMA to optimize energy extraction under diverse shading scenarios, offering a promising approach for enhancing PV system efficiency.

Keywords: Partial Shading, Maximum power point tracker (MPPT), Slime Mould Algorithm, Meta-heuristic optimization

1. INTRODUCTION

In today's world, where the demand for electrical energy is constantly rising, energy production—primarily based on fossil fuels—brings significant environmental challenges. The limited reserves of fossil fuels and the emission of harmful greenhouse gases negatively impact climate change, contributing to ozone depletion and acid rain. In response, countries are turning to renewable energy sources [1], particularly solar energy, to address the energy crisis and protect the environment [2]. Solar energy systems, with their advantages such as large installation areas, low maintenance needs, and low emissions, stand out among renewable sources. Photovoltaic (PV) cells, which form solar energy systems, convert sunlight into electricity, and the increasing popularity of rooftop systems is making solar power more accessible. However, the efficiency of PV cells remains relatively low, ranging from 11-28%, necessitating methods such as Maximum Power Point Tracking (MPPT) to maximize system efficiency [3].

In PV systems, energy losses due to partial shading significantly impact system performance. Partial shading occurs when some modules are shaded while others receive full sunlight, leading to uneven irradiance across the array and resulting in reduced PV module efficiency. Factors such as chimneys, trees, or moving clouds can cause partial shading. To mitigate these effects, bypass diodes are used to optimize energy production by deactivating the shaded cells. However, this can create multiple local maximum power points (LMPP) and a global maximum power point (GMPP) within PV arrays. MPPT algorithms are designed to monitor and control both GMPP and LMPP points, enabling more efficient energy production. [4], [5]

Conventional MPPT algorithms perform effectively in single-power-point conditions but experience performance degradation in complex situations like partial shading. Consequently, meta-heuristic search algorithms have emerged as alternative solutions, and researchers have extensively analysed the effectiveness of these stochastic algorithms in locating the GMPP. Methods such as the slime mould algorithm (SMA) [6], gray wolf algorithm (GWO) [7], equilibrium algorithm (EO) [8], mountain gazelle optimization (MO) [9] and hippopotamus algorithms (HO) [10] have been applied to enhance MPPT performance under partial shading conditions. This study compares the performance of these selected algorithms for optimizing PV arrays affected by partial shading, making an innovative contribution to addressing the MPPT problem.

2. BLOCK DIAGRAM OF PV SYSTEMS

The basic configuration of a photovoltaic (PV) system is shown in Figure 1. As illustrated, PV systems consist of PV panels connected to a DC-DC converter. The power output from PV cells is directly impacted by solar irradiance and the temperature of the panels. Other factors, such as atmospheric conditions, panel arrangement, and load impedance, also affect the power generated by PV arrays.

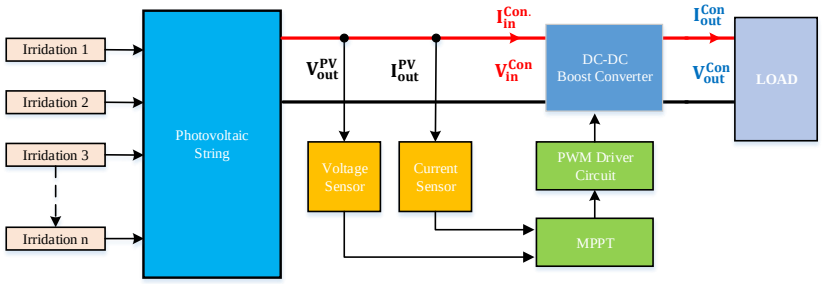

Figure 10. *Block diagram of the PV system [3]*

Maximum Power Point Tracking (MPPT) serves to optimize the impedance on the panel side, enabling the PV panels to deliver maximum power by utilizing a boost converter to match the load impedance. MPPT controllers are designed to ensure PV panels operate at their peak power level under both standard conditions and partial shading. The MPPT device collects current and voltage data from the PV panel output using sensors, and the search algorithm processes this data to generate a duty cycle signal between 0 and 1. This signal activates the converter's switch (typically a MOSFET or transistor) through a PWM driving circuit. As a result, depending on the effectiveness of the search algorithm, power generation occurs at either the Global Maximum Power Point (GMPP) or a Local Maximum Power Point (LMPP) on the PV panel.

2.1. PV Cell Modelling

PV cells display a nonlinear output characteristic, and the configuration of cells in series or parallel directly affects the panel's output current, voltage, and power. PV cells are modelled using different diode arrangements; in this study, a single diode equivalent circuit model, as proposed by [author], is used to represent the PV cell. The electrical schematic of this model is shown in Figure 2.

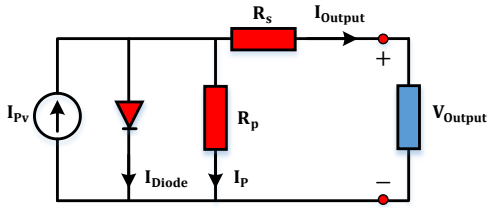

Figure 11 *Single diode equivalent circuit diagram of PV cell* [3], [4]

The output current formula for the PV cell is expressed in Equation 1.

$$I_{Output} = I_{PV} - I_{Diode} - I_p \tag{1}$$

In Equation 1, I_{PV} PV represents the light current of the PV cell, I_{Diode} denotes the current through the diode, I_P: R_P is the shunt current flowing through the resistance R_P, and I_{Output} indicates the output current. The current I_{Diode} can be expressed in relation to the saturation current, as shown in Equation 2.

$$I_{Diode} = I_0 \cdot \left[e^{\left(\frac{(V+I.R_S)}{a}\right)} - 1 \right] \tag{2}$$

For I_P, the expression $\frac{V+I.R_s}{R_p}$ can be substituted. Considering these expressions, Equation 1 can be rearranged as presented in Equation 3.

$$I_{Output} = I_{pv} - I_0.\left[e^{\left(\frac{(V+I.R_S)}{a}\right)} - 1\right] - \frac{V + I.R_S}{R_P} \tag{3}$$

2.2. Mathematical Analysis of the Boost Converter

A boost converter is a DC-DC converter designed to produce an output voltage higher than its input voltage. The output voltage changes based on the duty cycle of the control signal applied to the switching element. The state-space equations for the converter are defined separately for two operational states: when energy is stored in the switching element (closed) and when no energy is stored (open). By reorganizing these equations for the switch's open and closed states, the transient state equations are derived. This process is outlined between Equation 4 and Equation 5. [3]

$$\begin{aligned} A_{avg} &= A_1.d + A_2(1-d)T_s \\ B_{avg} &= B_1.d + B_2(1-d)T_s \\ C_{avg} &= C_1.d + C_2(1-d)T_s \end{aligned} \tag{4}$$

$$A_{avg} = \begin{bmatrix} -\frac{r_L + \frac{R.r_C}{R+r_C}(1-d)}{L} & -\frac{R(1-d)}{L(R+r_C)} \\ \frac{R(1-d)}{C(R+r_C)} & -\frac{1}{C(R+r_C)} \end{bmatrix}, B_{avg} = \begin{bmatrix} \frac{1}{L} \\ 0 \end{bmatrix} \text{ and } C_{avg} = \begin{bmatrix} \frac{R.r_C}{R+r_C}(1-d) & \frac{R}{R+r_C} \end{bmatrix} \tag{5}$$

3. SLIME MOULD ALGORITHM

The Slime Mould Algorithm (SMA) [6] is a population-based metaheuristic inspired by the foraging behaviours of slime moulds, simple organisms that can address complex optimization problems. SMA models the morphological changes of slime moulds as they search their environment, guided by pheromone trails that attract other colony members to efficient paths. In SMA, a virtual population of slime moulds explores a multi-dimensional solution space by following high pheromone concentrations, avoiding obstacles, and expanding into new areas. Communication between neighbouring slime moulds enables cooperative movement, allowing the population to converge on an optimal solution by updating positions and pheromone levels based on solution quality. SMA has proven effective in tasks like vehicle routing, scheduling, and supply chain management, offering adaptability to dynamic conditions through local and global interactions. Although it requires parameter tuning and may occasionally converge on local optima, SMA remains a promising area of research in optimization. Its process includes three main stages: searching, approaching, and enveloping food, modelled in equations (6) through (9) to simulate contraction behaviour.

$$\vec{X}^{t+1} = \begin{cases} \vec{X}_b^{(t)} + \vec{v}_b.\left(\vec{W}.\vec{X_A}^{(t)} - \vec{X_B}^{(t)}\right) & r < p \\ \vec{v}_c.\vec{X}^{(t)} & r \geq p \end{cases} \tag{6}$$

$$p = \tanh|S(i) - DF| \tag{7}$$

$$a = \tanh^{-1}\left(1 - \left(\frac{iter}{max_{iter}}\right)\right) \tag{8}$$

$$\vec{W} = \begin{cases} 1 + r.\log_{10}\left(\frac{Fit_{Best} - S(i)}{Fit_{Best} - Fit_{worst} + \epsilon} + 1\right) & , condition \\ 1 - r.\log_{10}\left(\frac{Fit_{Best} - S(i)}{Fit_{Best} - Fit_{worst} + \epsilon} + 1\right) & , others \end{cases} \tag{9}$$

4. PV SYSTEM ABD CONFIGURATION

In this study, data from the KC200GT PV panel were used as a reference. The parameters used in the modelling, along with the technical specifications of the panel, are presented in Table 1. The results from the code written in the MATLAB environment were compared with real-time measurement results obtained from the KC200GT PV panel and simulation results generated in MATLAB/Simulink. Variations in current and voltage values contribute to a decrease in the maximum generated power (P_{max}). The parameters used in the modeling of the KC200GT PV panel and their associated variables are also provided in Table 1. These parameters are crucial for accurately characterizing the power generation capabilities and overall behaviour of the PV system under varying environmental conditions.

Table 5 *Technical Specifications and Parameters of the KC200GT PV Module*

Variable Name	Symbol	Unit	Value of Variable
Short circuit current	I_{sc}	Amper	8,2099
Open circuit voltage	V_{oc}	Volt	32,990
Number of cells connected in series	N_{Cell}	-	54
Voltage temperature coefficient	K_v	% /deg. C	-0,35502
Current temperature coefficient	K_i	% /deg. C	0,06
Idealization factor	a	-	0,97736
Series resistance value	R_s	Ω	0,34483
Parallel resistance value	R_{sh}	Ω	170,37921

4.1. Determination of Maximum Power Point Under Partial Shading in PV Array)

A PV array configuration with 3 parallel-connected branches, each containing 3 series-connected KC200GT PV modules (a 3x3 configuration), is utilized as shown in Figure 3.

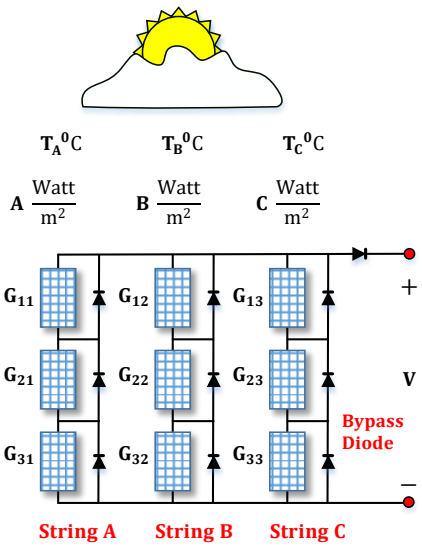

Figure 12 *PV Array Configuration with 3 Parallel Branches of 3 Series-Connected Panels (3x3 Configuration) [5]*

The PV system's performance was analysed across six distinct shading scenarios (Case 0 through Case 5), with each case applying unique irradiance and temperature levels to the PV panels, as detailed in Table 2. Case 0 represents the baseline condition where each panel uniformly receives 1000 W/m² irradiance. In contrast, other cases simulate partial shading conditions. For example, in Case 1, irradiance values on the panels vary (e.g., 500 W/m² on some panels while others maintain 1000 W/m²), effectively modelling realistic shading impacts. Additionally, panel temperatures fluctuate across cases, reflecting typical

environmental variations that affect the maximum power point (MPP) by influencing the current-voltage characteristics of each panel.

Table 6 *Irradiance and Temperature Conditions for PV Panels Across Different Shading Cases (Case 0 to Case 5) [4]*

Panel No	Case 0	Case 1	Case 2	Case 3	Case 4	Case 5	
	NSC (W/m^2)	PSC (W/m^2)	PSC (W/m^2)	PSC (W/m^2)	PSC (W/m^2)	**PSC** (W/m^2)	**Temp.** (°C)
G11	1000	500	250	750	100	750	55
G21	1000	500	1000	300	200	300	25
G31	1000	1000	600	950	300	950	60
G12	1000	500	250	750	400	750	55
G22	1000	500	1000	300	500	300	25
G32	1000	1000	600	950	600	950	60
G13	1000	500	250	750	700	750	55
G23	1000	500	1000	300	800	300	25
G33	1000	1000	600	950	900	950	60

This configuration and experimental design facilitate a comprehensive analysis of maximum power point tracking (MPPT) performance under diverse shading and temperature conditions, which is essential for optimizing the PV system's energy output under real-world scenarios. Figures 4 and 5 present the current-voltage (I-V) and power-voltage (P-V) characteristics of the PV system under different irradiance and temperature conditions.

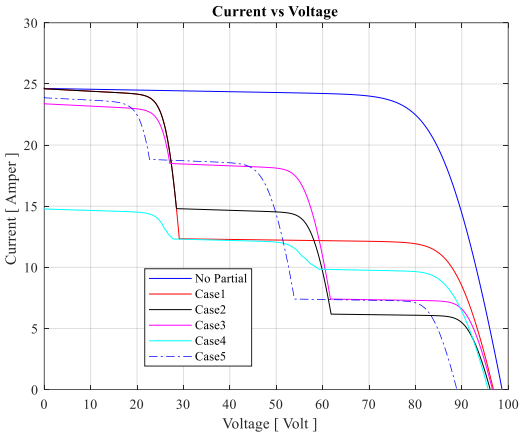

Figure 13 *Current-Voltage (I-V) Characteristics of the PV System Under Various Irradiance and Temperature Conditions*

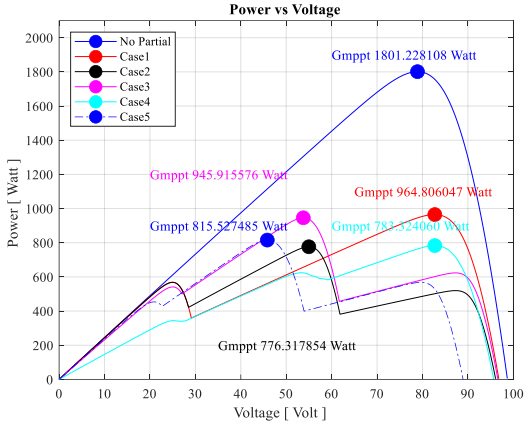

Figure 14 *Power-Voltage (P-V) Characteristics of the PV System Under Various Irradiance and Temperature Conditions*

The data indicate that maximum current and voltage values are achieved at an irradiance of 1000 W/m² and a temperature of 25°C, conditions in which the PV modules reach optimal efficiency. Under these ideal conditions, the output power peaks at approximately 1801.22 Watt, showcasing the system's maximum capacity. These findings highlight the direct effects of irradiance and temperature on PV performance, as higher irradiance and moderate temperature levels support enhanced power generation. This relationship provides valuable insights for system design and optimization to maximize efficiency under variable environmental conditions.

5. RESULTS AND DISCUSSIONS

To track the maximum power point (MPP) under partial shading conditions in PV arrays, five different meta-heuristic algorithms were implemented to optimize power tracking based on the KC200GT PV panel data. The PV panel, boost converter, partial shading scenarios, and optimization algorithms were fully modelled in MATLAB to simulate real-world environmental impacts on power output. The study aimed to maximize power extraction from the PV system using meta-heuristic optimization methods that iteratively solve the MPP problem. According to the "No Free Lunch" (NFL) theorem [11], [12],[13],[14] no single

algorithm can solve all optimization problems most efficiently; each algorithm's performance varies depending on the problem set. Thus, multiple algorithms were evaluated to determine the most effective approach for this specific MPP problem. Among the meta-heuristic algorithms tested, the SMA (Sine Cosine Algorithm), as a recently developed search algorithm, was chosen and benchmarked against 15 other methods.

5.1. Power Production and Capture of Global Values

Table 3 presents the results of power production and global value capture rates across various algorithms under optimal (best) and sub-optimal (worst) switching scenarios. The SMA algorithm yielded the highest average power production of 783.3240532 W with the best global capture rate of 905 out of 1000 runs. This performance aligns with its highest efficiency rate of 99.9999998%, demonstrating SMA's superior consistency in reaching MPP compared to other algorithms. For example, while GWO achieved an average power of 783.3231401 W with an efficiency of 99.9998825%, it fell behind SMA in terms of global capture occurrences (704/1000), highlighting slight performance trade-offs. Conversely, MGO, with an average power production of 780.2738261 W and only 14/1000 global captures, exhibited a lower performance level, indicating its limitations in handling the MPP challenge effectively under partial shading.

Table 7 *Power production and global value capture in best/worst switching scenarios*

Algorithm Name	Power Produced in Best Case	Power Produced in Worst Case	Average Power Produced	Number of Global Value	Efficiency
	$\mathbf{P_{Güç}^{Maks.}}$ **(W)**	$\mathbf{P_{Güç}^{Mini.}}$ **(W)**	$\mathbf{P_{Güç}^{Orta}}$ **(W)**	out of 1000	$\boldsymbol{\eta = \frac{P_{ortalama}}{P_{global}}}$
GWO	783.3240598	783.25719760	783.3231401	704 / 1000	0.999998825
HO	783.3240598	775.69245320	783.2917029	424 / 1000	0.999958692
MGO	783.3240598	751.26493254	780.2738261	14 / 1000	0.996106038
EO	783.3240598	782.28499599	783.3037792	507 / 1000	0.999974109
SMA	783.3240598	783.32125971	783.3240532	905 / 1000	0.999999998

5.2. Statistical Evaluation of Algorithm Performance

To further assess each algorithm's performance reliability, Table 4 provides statistical evaluations, including standard deviation (STD), standard error (SE), mean absolute error (MAE), and root mean square error (RMSE). The SMA algorithm consistently demonstrated the lowest variance (1.01e-08) and error measures (e.g., MAE = 6.14e-06, RMSE = 0.00010), reinforcing its accuracy in power estimation. The GWO algorithm showed similar statistical reliability but with a slightly higher RMSE of 0.00391, while MGO displayed the largest deviations (e.g., STD = 3.9962, RMSE = 5.02578), indicating less stability and higher fluctuation in performance. These findings confirm that SMA and GWO algorithms provide more stable and accurate power tracking under various operational scenarios.

Table 8 *7Statistical evaluation of the performance of each algorithm*

Algorith Name	STD **(σ)**	SE	% RE	MAE	MSE	RMSE	RMSLE	Mode	Variance
GWO	0.0038	0.0001	0.00011	0.00091	1.53e-05	0.00391	2.16e-06	783.32	1.44e-05
HO	0.2686	0.0084	0.00413	0.03235	0.073149	0.27046	0.00015	783.32	0.072174
MGO	3.9962	0.1263	0.39092	3.05021	25.25812	5.02578	0.00280	781.82	15.97543
EO	0.0837	0.0026	0.00258	0.02028	0.007409	0.08608	4.76e-05	783.32	0.00700
SMA	0.0001	3.2e-06	7.84e-07	6.14e-06	1.00e-08	0.00010	5.55e-08	783.32	1.01e-08

5.3. Algorithmic Efficiency and Completion Times

Table 5 summarizes the completion times for each algorithm across multiple runs. The SMA algorithm demonstrated a median completion time of 0.003783 seconds, although it had a higher range of outliers due to its detailed search process, reflecting its thoroughness in finding global maxima. GWO and MGO algorithms, with lower median times of 0.002837 seconds and 0.001692 seconds respectively, were generally faster but had a few additional computational trade-offs, as shown by their larger outlier counts. The elapsed time results indicate that while SMA may take longer per iteration, its superior accuracy justifies the computational cost, especially in applications requiring precise MPP tracking.

Table 9 *Completion times for algorithm iterations*

Algorithm Name	Elapsed Time						
	Maximum	Minimum	Average	median	Upper	Lower	Number of outliers
GWO	0.0049743	0.0024906	0.0028626	0.002837	0.0031974	0.0024976	67
HO	0.0054347	0.0021329	0.0025311	0.002418	0.0031095	0.0021329	57
MGO	0.0051094	0.0015607	0.0017602	0.001692	0.0019121	0.0015607	89
EO	0.0056260	0.0018632	0.0022708	0.002178	0.0028891	0.0018632	58
SMA	0.0066686	0.0032440	0.0039177	0.003783	0.0048393	0.003244	41

6. CONCLUSION

The SMA algorithm excelled across both power capture rate and statistical performance metrics, making it the most effective solution for MPP tracking in PV arrays under partial shading. Its balance between high accuracy, stability, and reliable performance suggests that SMA is well-suited for PV systems facing variable environmental conditions.

ACKNOWLEDGMENT

During the preparation of this work the author(s) used ChatGPT 4.o-mini in order to refine the English wording of certain phrases. After using this tool/service, the author reviewed and edited the content as needed and take(s) full responsibility for the content of the publication.

REFERENCES

[1] K. Doğanşahin and M. Çikan, "A new line stability index for voltage stability analysis based on line loading," vol. 1, no. 1, pp. 23–30, 2023, doi: 10.14744/cetj.2023.000.

[2] M. Çıkan and N. Nacar Çıkan, "Elektrikli Araç Şarj İstasyonlarının Enerji Dağıtım Hatlarına Optimum Şekilde Konumlandırılması," Kahramanmaraş Sütçü İmam Üniversitesi Mühendislik Bilimleri Dergisi, vol. 27, no. 2, pp. 340–363, 2024, doi: 10.17780/ksujes.1365209.

[3] M. Çıkan, "Çita optimizasyon algoritması kullanarak kısmi gölgelenme altındaki fotovoltaik sistemlerde maksimum güç noktası izleyicisinin tasarlanması," Gazi Üniversitesi Mühendislik Mimarlık Fakültesi Dergisi, vol. 40, no. 1, pp. 555–572, 2024, doi: 10.17341/gazimmfd.1183267.

[4] M. Cikan and K. Dogansahin, "A Comprehensive Evaluation of Up-to-Date Optimization Algorithms on MPPT Application for Photovoltaic Systems," Energy Sources, Part A: Recovery, Utilization, and Environmental Effects, vol. 45, no. 4, pp. 10381–10407, Oct. 2023, doi: 10.1080/15567036.2023.2245771.

[5] K. Aygül, M. Cikan, T. Demirdelen, and M. Tumay, "Butterfly optimization algorithm based maximum power point tracking of photovoltaic systems under partial shading condition," Energy Sources, Part A: Recovery, Utilization, and Environmental Effects, pp. 1–19, Oct. 2019, doi: 10.1080/15567036.2019.1677818.

[6] S. Li, H. Chen, M. Wang, A. A. Heidari, and S. Mirjalili, "Slime mould algorithm: A new method for stochastic optimization," Future Generation Computer Systems, vol. 111, pp. 300–323, 2020, doi: https://doi.org/10.1016/j.future.2020.03.055.

[7] S. Mirjalili, S. M. Mirjalili, and A. Lewis, "Grey Wolf Optimizer," Advances in Engineering Software, vol. 69, pp. 46–61, 2014, doi: https://doi.org/10.1016/j.advengsoft.2013.12.007.

[8] A. Faramarzi, M. Heidarinejad, B. Stephens, and S. Mirjalili, "Equilibrium optimizer: A novel optimization algorithm," Knowl Based Syst, vol. 191, p. 105190, 2020, doi: https://doi.org/10.1016/j.knosys.2019.105190.

[9] B. Abdollahzadeh, F. S. Gharehchopogh, N. Khodadadi, and S. Mirjalili, "Mountain Gazelle Optimizer: A new Nature-inspired Metaheuristic Algorithm for Global Optimization Problems," Advances in Engineering Software, vol. 174, p. 103282, 2022, doi: https://doi.org/10.1016/j.advengsoft.2022.103282.

[10] M. H. Amiri, N. Mehrabi Hashjin, M. Montazeri, S. Mirjalili, and N. Khodadadi, "Hippopotamus optimization algorithm: a novel nature-inspired optimization algorithm," Sci Rep, vol. 14, no. 1, p. 5032, 2024, doi: 10.1038/s41598-024-54910-3.

[11] M. Cikan and N. N. Cikan, "Optimum allocation of multiple type and number of DG units based on IEEE 123-bus unbalanced multi-phase power distribution system," International Journal of Electrical Power & Energy Systems, vol. 144, p. 108564, 2023, doi: https://doi.org/10.1016/j.ijepes.2022.108564.

[12] N. Nacar Cikan and M. Cikan, "Reconfiguration of 123-bus unbalanced power distribution network analysis by considering minimization of current & voltage unbalanced indexes and power loss," International Journal of Electrical Power & Energy Systems, vol. 157, p. 109796, 2024, doi: https://doi.org/10.1016/j.ijepes.2024.109796.

[13] M. Cikan and B. Kekezoglu, "Comparison of metaheuristic optimization techniques including Equilibrium optimizer algorithm in power distribution network reconfiguration," Alexandria Engineering Journal, vol. 61, no. 2, pp. 991–1031, 2022, doi: https://doi.org/10.1016/j.aej.2021.06.079.

[14] F. Akın, M. Çıkan, O. Arikan, and B. Kekezoğlu, "Optimizing Distribution Network Reconfiguration for Power Loss and Fault Current Management," Mühendislik Bilimleri ve Araştırmaları Dergisi, vol. 6, no. 2, pp. 188–197, 2024, doi: 10.46387/bjesr.1501986.